SYNTHESIS AND CHARACTERIZATION OF HIERARCHICALLY POROUS METAL, METAL OXIDE, AND CARBON MONOLITHS WITH HIGHLY ORDERED NANOSTRUCTURE

by

AMY JANINE GRANO

MARTIN G. BAKKER, COMMITTEE CHAIR

SHANLIN PAN
SHANE STREET
LAURA BUSENLEHNER
STEPHEN RITCHIE

A DISSERTATION

Submitted in partial fulfillment of the requirements
for the degree of Doctor of Philosophy
in the Department of Chemistry
in the Graduate School of
The University of Alabama

TUSCALOOSA, ALABAMA

2013

ABSTRACT

Hierarchically porous materials are of great interest in such applications as catalysis, separations, fuel cells, and advanced batteries. One such way of producing these materials is through the process of nanocasting, in which a sacrificial template is replicated and then removed to form a monolithic replica. This replica consists of mesopores, which can be ordered or disordered, and bicontinuous macropores, which allow flow throughout the length of the monolith. Hierarchically porous metal oxide and carbon monoliths with an ordered mesopores system are synthesized for the first time via nanocasting. These replicas were used as supports for the deposition of silver particles and the catalytic efficiency was evaluated. The ordered silica template used in producing these monoliths was also used for an in-situ TEM study involving metal nanocasting, and an observation of the destruction of the silica template during nanocasting made. Two new methods of removing the silica template were developed and applied to the synthesis of copper, nickel oxide, and zinc oxide monoliths. Finally, hollow fiber membrane monoliths were examined via x-ray tomography in an attempt to establish the presence of this structure throughout the monolith.

DEDICATION

This dissertation is dedicated to everyone who helped me and guided me through the trials and tribulations of creating this manuscript. I will forever be grateful to my parents, for both their financial and emotional support throughout these past 5 years, and my entire life. They have made me into the person I am today, and given me the strength necessary to survive graduate school and being a single mother. I also wish to thank my son, Dylan, who has been a constant source of motivation throughout graduate school. I strived to be the best I could be in order to make him proud and make a better life for us. Finally, I wish to thank Leslie Gentry Dye. She is my best friend in the world, and has believed in me even when I didn't believe in myself, giving me support and a shoulder to cry on. I am forever grateful for her friendship and support during the completion of this work.

LIST OF ABBREVIATIONS AND SYMBOLS

˚C	degrees Celsius
%	percent
2θ	diffraction angle in degrees
3-D	three-dimensional
AU	absorbance unit or arbitrary unit
BET	Brunauer-Emmett-Teller
BJH	*Barret-Joyner-Halenda*
b.p.	boiling point
$C_{14}TAB$	tetradecyltrimethylammonium bromide
$C_{16}TAB$	hexadecyltrimethylammonium bromide
$C_{18}TAB$	octadecyltrimethylammonium bromide
ca.	circa (around)
cm	centimeter
d	diameter
DSSC	*dye sensitized solar cell*
d_{surf}	surfactant pore diameter
dV(d)	derivative of volume with respect to diameter
EDS	energy dispersive X-ray spectroscopy
e.g.	exempli gratia
et al.	et alia (and others)

etc.	et cetera (and so on)
ETEM	Environmental transmission electron microscopy
FIB	focused ion beam
g	grams
h	hour
i.e.	in est (in other words)
K	Kelvin
keV	kiloelectron volt
kg	kilogram
L	liters
M	molarity
mg	milligram
min	minute
mL	milliliter
mm	millimeter
mol	mole
m.p.	melting point
MW	molecular weight
nm	nanometer
NLDFT	non-local density functional theory
OTAB	octadecyltrimethylammonium bromide

P	pressure
P123	Pluronic 123
P_0	initial pressure
PEG	polyethylene glycol
P/P_o	partial pressure
s	second
SEM	scanning electron microscope
TEM	transmission electron microscope
TEOS	tetraethoxysilane
TMOS	tetramethoxysilane
V	volt
V	volume
V_{macro}	macropore volume
vs.	versus
V_{surf}	surfactant pore volume
V_{text}	textural pore volume
V_{total}	total pore volume
wt%	weight percent
XRD	X-ray diffraction
μL	microliter
μm	micrometer

ACKNOWLEDGEMENTS

I am pleased to have this opportunity to thank the many colleagues, friends, and faculty members who have helped me with this research project. I am most indebted to Dr. Martin Bakker, the chairman of this dissertation, for sharing his research expertise and wisdom. I would also like to thank all of my committee members, Dr. Shanlin Pan, Dr. Shane Street, Dr. Laura Busenlehner, and Dr. Steve Ritchie for their invaluable input, inspiring questions, and support of both the dissertation and my academic progress. I would like to thank Jan-Henrik Smatt for his international collaboration and the chance to spend a month working at Abo Akademi in Turku, Finland, and completing some of my dissertation work in his laboratory.

I would also like to thank Dr. Franchessa Sayler for working with me on this project, and for valuable discussion. My other group members, Dr. Nik Courdes, Chris Redden, and Katrina Staggemeir are gratefully acknowledged.

The Central Analytical Facility has provided valuable resources, such as grants for instrument time and training. The CAF staff, Rich Martens, Johnny Goodwin, and Rob Holler, are gratefully acknowledged for the training and expertise.

Funding for this research was provided by the National Science Foundation grant CHE-0719398(MGB).

CONTENTS

ABSTRACT ii

DEDICATION iii

LIST OF ABBREVIATIONS AND SYMBOLS iv

ACKNOWLEDGEMENTS vii

LIST OF TABLES xii

LIST OF FIGURES xiii

CHAPTER 1 INTRODUCTION 1

1.1 Hierarchically Porous Materials 1

1.2 Applications of Hierarchically Porous Materials 3

1.3 Monolithic Materials 5

1.4 Nanocasting 7

1.5 A Comprehensive Nanocasting Model 9

1.6 References 13

CHAPTER 2 HIERARCHICALLY POROUS MONOLITHS OF CARBON, COBALT OXIDE, AND NICKEL OXIDE WITH HIGHLY ORDERED MESOPORES 19

2.1 Abstract 19

2.2 Introduction 19

2.3 Experimental 21

2.3.1 Silica Monolith Templates 21

2.3.2 Replicas.....21

2.3.3 Ag-loaded monoliths.....22

2.3.4 Characterization.....22

2.4 Results and Discussion.....23

2.4.1 Replicas.....23

2.4.2 Ag loaded monoliths.....32

2.4.3 Catalysis experiments.....35

2.5 Conclusions.....36

2.6 Acknowledgements.....36

2.7 References.....37

CHAPTER 3 IN-SITU OBSERVATION OF NICKEL NANOPARTICLES DURING NANOCASTING INTO MESOPOROUS SILICA.....39

3.1 Abstract.....39

3.2 Introduction.....39

3.3 Experimental.....40

3.3.1 Materials.....40

3.3.2 Preparation of Silica Template.....40

3.3.3 Preparation of nickel/silica composite.....40

3.3.4 Microscopy.....41

3.4 Results and Discussion.....41

3.5 Conclusions.....45

3.6 Acknowledgements....45

3.7 References....46

3.8 Supplemental Figures....47

CHAPTER 4 ALTERNATIVE ETCHING METHODS TO EXPAND NANOCASTING AND THE USE IN THE SYNTHESIS OF HIERARCHICALLY POROUS NICKEL OXIDE, ZINC OXIDE, AND COPPER MONOLITHS....49

4.1 Abstract....49

4.2 Introduction....49

4.3 Experimental....51

4.3.1 Chemicals Used....51

4.3.2 Synthesis of Silica Monolith Template....51

4.3.3 Synthesis of Replicas....52

4.3.4 Etching of Silica....52

4.3.5 Characterization....53

4.4 Results....53

4.4.1 Silica....54

4.4.2 Zinc Oxide....55

4.4.3 Nickel Oxide....57

4.4.3.1 Methanolic Base Etch....57

4.4.3.2 Aqueous Base Etch....57

4.4.4 Copper....58

4.4.4.1 Methanolic Base Etch 59

4.4.4.2 Voltage Stabilized Etch.....59

4.5 Discussion 60

4.5.1 Zinc Oxide 60

4.5.2 Nickel Oxide 60

4.5.3 Copper.....61

4.6 Conclusions.....62

4.7 Acknowledgements.....63

4.8 References.....64

4.9 Supplemental Figures.....67

CHAPTER 5 X-RAY AND FIB TOMOGRAPHY OF EXTREMELY HIGH SURFACE AREA NANOSTRUCTURED HOLLOW FIBER MEMBRANES 69

5.1 Abstract.....69

5.2 Introduction.....69

5.3 Experimental.....71

5.4 Results.....72

5.4.1 Microtomography 72

5.4.2 Nanotomography.....73

5.5 Discussion.....75

5.6 Conclusions.....75

5.7 Acknowledgements....76
5.8 References....77
CHAPTER 6 CONCLUSIONS AND FUTURE WORK....78
6.1 Conclusions....78
6.2 Future Work....79
6.2.1 Ordered Monoliths....79
6.2.2 Environmental TEM....79
6.2.3 Plasma Focused Ion Beam....80
6.2.4 Catalysis....80
6.2.5 Dye Sensitized Solar Cells....81
APPENDIX....83

LIST OF TABLES

2.1 Nitrogen sorption and Scherrer analysis data for parent silica monolith and carbon, cobalt oxide, and nickel oxide replicas 24

4.1 Nitrogen physisorption data from parent silica monolith and replicas.....55

LIST OF FIGURES

1.1 Pictoral Representation of a hierarchically porous material 1

1.2 Structural Differences between particulate vs.
monolithic chromatography columns 6

1.3 Nanocasting variables 9

2.1 Photograph and SEM images of a) parent silica monolith,
b) carbon replica, c)cobalt oxide replica, and
d) nickel oxide replica.....23

2.2 XRD diffractograms of cobalt oxide and nickel oxide replicas.....24

2.3 TEM images of a) parent silica monolith, b) carbon replica,
c) cobalt oxide replica, and d) nickel oxide replica 25

2.4 HR SEM and TEM images of a,b) cobalt oxide and
c,d) nickel oxide.....26

2.5 SAXS patterns for silica template and replica 27

2.6 Isotherm and pore size distribution of parent silica
monolith and carbon replica.....29

2.7 Isotherms and pore size distribution of cobalt oxide and
Nickel oxide replica and composite.....31

2.8 SEM images and EDS maps of Ag loaded monoliths 33

2.9 Isotherms of Ag loaded monoliths.....34

2.10 Pore size distributions of Ag loaded monoliths.....34

2.11 UV-Vis data from monoliths and Ag loaded monoliths.....36

3.1 Top, nitrogen sorption isotherms and bottom, BJH pore size distribution for silica-nickel composite and nickel replica 42

3.2 a,b)SEM image of etched nickel replica, c) representative TEM image of etched sample, and d) TEM of silica-nickel composite 43

3.3 TEM images of silica-nickel sample during heating at a) 150 °C, b) 200 °C, and c) 250 °C 44

3.S1 Nitrogen Sorption isotherm and BJH pore size distribution for silica template 47

3.S2 Left, SEM, and right, TEM, of silica monolith template 48

3.S3 XRD Diffractogram of Nickel Replica 48

4.1 SEM images of (a,b) parent silica monolith, (c,d) ZnO replica, and (e,f) NiO replica 54

4.2 XRD diffractograms of NiO, ZnO, Cu-m, and Cu-v 56

4.3 Top) Nitrogen physisorption isotherms and bottom) BJH pore size distribution of replicas 56

4.4 Raman spectra of nickel oxide standard, precipitate from aqueous etch, and monolith piece from aqueous etch 58

4.5 SEM images of (a,b) Cu-v and (c,d) Cu-m 59

4.S1 Parent silica monolith nitrogen physisorption isotherm and BJH pore size distribution 67

4.S2 a) SEM image of Cu-e copper b) EDS spectra of Cu-e, c) SEM image of Cu-m, and d) EDS of Cu-m 68

5.1 SEM images of a) Co_3O_4 and b) Nickel/nickel oxide showing macropore network 70

5.2 X-ray tomography images of cobalt oxide monolith
a) reconstructed slice and b) full 3D rendering.....72

5.3 (a) left: rendering of one sub-region with solid interfaces
selected. (b) right: plot of solid volume fractions for
different regions of the dataset.....73

5.4 Higher resolution synchrotron x-ray CT of hollow
nickel/nickel oxide.....74

CHAPTER 1
INTRODUCTION

1.1 Hierarchically Porous Materials

Hierarchically porous materials (HPM's) can be described as materials that have porosity across several length scales, including micropores (<2 nm), mesopores (2-50 nm), and/or macropores (> 50 nm). Several types of metal and metal oxide HPM's can be found in the literature, which include such forms as aerogels, xerogels, metal foams, metal organic frameworks, and silica materials from sol-gel synthesis utilizing spinodal decomposition[1]. They come in various forms, including monolithic[2], particulate[3], or granular[4]. One of the most widely published HPM's is silica, which can be monolithic or particulate. This silica can be used as is or with surface functionalization for chromatography[5], or as a support for deposition of nanoparticles for catalysis[6].

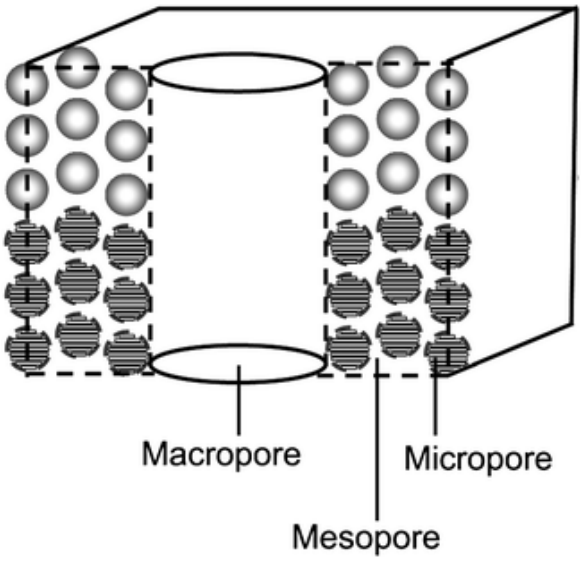

Figure 1.1. Pictoral Representation of a Hierarchically Porous Material[1]

The first report of the synthesis of a mesoporous silica was in 1992 by the Mobil Research Corporation[7]. They reported a synthesis of a family of mesoporous silicas, which includes MCM-41 and MCM-48. These are mesoporous silica particles with a 2-D hexagonal and ordered cubic pore geometry, respectively. Since then, there have been reports of silica particles with a number of different pore geometries, including hexagonal, gyroid, and lamellar. Nakanishi developed a synthesis for hierarchically porous, monolithic silica with a bicontinuous macropore system and a disordered mesopore structure in 1997[8]. Since then, a number of silica monolith syntheses which yield an ordered mesoporous system have also been developed[9,10].

Aerogels[11] and xerogels[12] are closely related classes of materials, with their porosity being a combination of micropores and mesopores. They are both synthesized by sol-gel methods, with the difference between aerogels and xerogels being in the drying step. Aerogels undergo supercritical drying, which results in a lower density material. Xerogels undergo drying by evaporation; this allows some of the pore volume to collapse, resulting in a higher density material. They can be synthesized in several forms, including monolithic, particulate, and granular. Although the materials produced by this synthesis are fairly robust, their shortcoming is that synthesis takes about two weeks, and the supercritical drying necessary requires specific and relatively expensive equipment[13].

Metal foams[14] can consist of a variety of pores, including macropores, mesopores, and micropores. They are most commonly synthesized through bubbling of gas through molten metal, electroless deposition onto a hard template, or self assembly of metal nanoparticles. Although these techniques are capable of producing hierarchically porous materials with length scales that are comparable to that of other hierarchically porous materials, these synthesis methods can take far longer to develop, as they are often material specific[15]. Metal organic

frameworks have pore sizes predominately on the micropore scale, with only some incorporating mesopores to make them a hierarchically porous material[16].

There are also direct synthesis methods which result in hierarchically porous metal oxide monoliths. Zajickova et. al.[17] developed an in-situ direct sol-gel synthesis to produce alumina monoliths for use in chromatography. They made a solution of aluminum nitrate, acetonitrile, and N-methylformamide, followed by addition of propylene oxide. This solution was then poured into a capillary tube for gelation, and the result was a macroporous/mesoporous alumina. Hoa et al.[18] synthesized a hierarchically porous tungsten oxide monolith with a plate like structure from a solution of tungsten hexachloride, oxalic acid, ethanol, and cetyltrimethylammonium bromide (CTAB). These tungsten oxide monoliths were evaluated for their performance in gas sensors.

1.2 Applications of Hierarchically Porous Materials

Hierarchially porous materials have found utility in a wide variety of applications, including energy storage and conversion, catalysis, and separations. The application determines which geometry will be employed, with thin films being used in solar cells, and monoliths being used in chromatography, supercapacitors, and flow-thru catalysis.

In energy applications, hierarchically porous materials have proven to be more efficient in photocatalysis, dye sensitized solar cells, and fuel cells. In photocatalysis, scientists have taken lessons from nature and the structure of leaves as inspiration to design a hierarchically porous photocatalyst[19]. TiO_2 was used to produce the "leaf", and Pt nanoparticles served as the "photosynthetic pigments" to drive water splitting. These hierarchically porous leaves have much greater photocatalytic activity than TiO_2 nanoparticles. The particles with the combination of porosity showed about 50% higher activity than commercially bought P25 TiO_2.

In dye sensitized solar cells (DSSC), hierarchically porous metal oxide films with adsorbed dye molecules are being used as the anode. These DSSC are much cheaper and easier to produce in bulk, and therefore have attracted a large amount of research attention. The two most predominate oxides being utilized are titanium dioxide (TiO_2) and zinc oxide (ZnO). Hierarchically porous TiO_2 thin films are being synthesized via sol-gel methods, atomic layer deposition, or dual-templating. In one study done by Kim et al.[20], hierarchically structured TiO_2 shows improvement of about 5% in conversion efficiency vs. that of sintered TiO_2 nanoparticles. Hierarchically porous ZnO is produced through aggregation of nanocrystals, and self-assembly of nanoparticles and nanodisks[21].

In catalysis, the hierarchically porous nature of a catalyst can lessen the diffusion limitations found in strictly microporous catalysts. These catalysts offer advantages particularly in diffusion limited gas phase or liquid phase reactions. In the gas phase, hierarchically structured bismuth subcarbonate and bismuth tungstate, which possess flower morphology, have proven efficient in the photocatalytic degradation of nitrous oxide under ultraviolet and visible light, respectively. In the liquid phase, mixed oxides of zinc and ceria have been shown to be catalytically active for the degradation of rhodamine B under both ultraviolet and visible light. Hierarchically porous iron (III) oxide cores combined with tungsten (VI) oxide needles, in a sea urchin type structure, have proven to be about 30% more efficient than lower surface area iron oxide or tungsten oxide commercial catalysts[22].

These catalysts are important in processes in the petrochemical industry. Fischer-Tropsch reactions, the conversion of syngas to hydrocarbons, have been proven to be more efficient with a hierarchically porous catalyst vs. the traditional mesoporous alumina catalysts[22]. Hierarchically porous catalysts of cobalt and ruthenium doped alumina, and cobalt deposition on

a hierarchically porous colloidal silica have both shown promise as replacements. There are also examples on the smaller scale of the organic laboratory in which there is a benefit with hierarchical porosity. Mesoporous/macroporous copper oxide sea urchin particles have catalytic activity in epoxidation reactions, and palladium on a mesoporous/macroporous silicon carbide are active in hydrogenation reactions. Others have been used in isomerisation, Friedyl-crafts alkylation, and esterification reactions[22].

In separations, hierarchically porous monoliths of silica and titania have made major advances in the field. These monoliths have been applied to the separation of biomolecules[5], benzene derivatives[9], organophosphates[17], and food ingredients[23]. Both silica and titania monoliths are synthesized via a sol gel process. The resulting materials have a combination of micropores, mesopores, and macropores, and have surface areas from 218 m^2/g for titania up to 800 m^2/g for silica. Although the surface area of the titania monolith isn't as high as that of silica, it has the advantage of being base stable, and can therefore be used over a wider pH range. Our group has recently evaluated cobalt oxide, zinc oxide, and sterling silver monolithic columns, and both the cobalt oxide and zinc oxide showed retention of nitrogen heterocycles[24].

1.3 Monolithic Materials

Another landmark in the development of mesoporous silica was the report by Nakinishi in 1997[8]. He reported the development of a silica monolith synthesis with a disordered pore system. This revolutionized high pressure liquid chromatography (HPLC), allowing for faster flow rates and enhanced solute/stationary phase interactions. This also provided a monolithic template that has been used for nanocasting to form monolithic replicas[2]. To date, a variety of carbon syntheses[25] have been developed, using precursors such as furfuryl alcohol and sucrose. A wide range of metal oxide monoliths have been nanocast, including manganese oxide, cobalt

oxide, and tin oxide. Our group has also recently synthesized metal monolith replicas, which include cobalt, nickel, and silver[26].

Monolithic materials are advantageous over particulate materials in several ways, as is depicted in Figure 1.2. In the case of a flow through system, such as chromatography or a catalytic reactor, the macropores within the monolith give faster flow rates and minimize problems due to clogging. A monolithic column also alleviates the time needed to pack a column, allowing a replacement to simply be dropped in. In the case of a monolithic metal oxide electrode, in a system such as a fuel cell or battery, the material allows for faster mass transport throughout the electrode. A monolithic catalyst also allows for easy removal after the reaction, instead of requiring filtration to remove the catalyst. The research presented within this dissertation deals with the synthesis of monolithic, hierarchically porous materials via nanocasting.

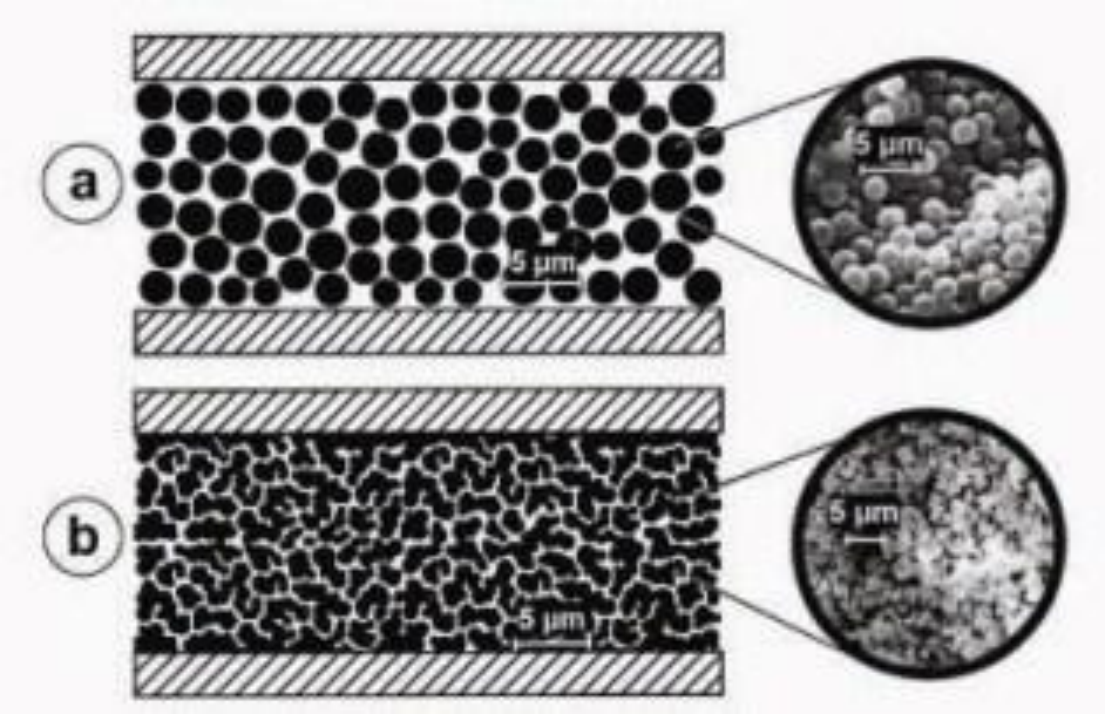

Figure 1.2. Structural differences between particulate vs. monolithic chromatograhpy columns[27]

1.4 Nanocasting

Casting is a thousands of years old process which involves pouring molten metal or other fluid into a mold, allowing the liquid to harden, then removing the mold to leave a replica of the original mold. Nanocasting is an extension of the traditional casting process down to the nanometer scale. During the nanocasting process, a liquid precursor is introduced into the micrometer or nanometer size pores. The liquid precursor then undergoes a chemical conversion to the desired end product. With the exception of the carbon nanocasting process, there is normally a drastic volume reduction during this conversion, with the final product only occupying 6-12% of that of the precursor solution. Due to this volume reduction, repeated infiltrations with the precursor solution are required if complete pore filling is desired[28].

One of the first examples of the nanocasting process was shown by Rodriguez and coworkers[29] in 1997. They used a mesoporous zeolite as a template to form a mesoporous and microporous carbon. The term nanocasting was first introduced by Goltner and Beibenberger[30] in 1998. Their work used a two step nanocasting process to form an organic polymer monolith. Since then, there have been many reports of nanocasting into mesoporous silica templates[28]. In the case of nanocasting metal or metal oxides, the amount of precursor solution used results in smaller mesoporous particles or nanowires. The replication of silica monoliths utilizes multiple infiltration cycles, resulting in metal and metal oxide monoliths.

Nanocast carbons have been synthesized in a variety of different silica precursors, including MCM-41[31], MCM-48[32], SBA-1[33], SBA-15[34], KIT-6[35], and MSU[25b] type silica. This work has predominately been done in silica particles, which results in a mesoporous-microporous carbon particulate replica. Carbon sources can also vary, including sucrose[36], furfuryl alcohol[37], phenol resin[38], and acetylene[39]. The resulting carbons are so popular they have been given their own

naming scheme, CMK-n, with n depending on the precursor silica used. The first report of a monolithic nanocast carbon came in 2003[40], which replicated a monolith with a disordered pore system.

In the case of metal oxides, particles of SBA-15, MCM-48, and KIT-6 are the predominate types of mesoporous silica used to form replicas. This is because these types of silica contain smaller micropore channels which connect the mesopores, giving the precursor solution an efficient route to fill the entire pore network. This three dimensional network also leads to a replica that consists of particles rather than individual nanowires or nanoparticles. The most common precursor used is the nitrate salt due to its high solubility. To date, ordered metal oxide arrays of chromium oxide[41], manganese oxide[42], iron oxide[43], cobalt oxide[44], nickel oxide[42], copper oxide[45], tungsten oxide[46], indium oxide[47], and cerium oxide[45] have been synthesized from particulate SBA-15 silica. There have also been oxide composites, such as LaMnO[48], CoNiO[49], and MnNiO[50] produced. Metal oxide monoliths with a disordered pore structure have been produced in cobalt oxide[51], manganese oxide[52], zirconia[53], and tin oxide[52].

Other metal oxides have also been synthesized using a repeat nanocasting procedure. One example is that of magnesium oxide synthesized by Tiemann[54] and group. Starting with a SBA-15 silica particles, they first replicated these form CMK-3 carbon. After removing the silica template, the carbon replica was infiltrated with magnesium nitrate and converted to magnesium oxide. The carbon template is then removed by heating under air. This resulted in mesoporous magnesium oxide particles, but the final product did have some structural irregularities. Other metal oxides prepared by this repeat templating method include aluminum oxide[55], cerium oxide[56], zinc oxide[57], and copper oxide[58].

In the case of metals, there has been less work done. The mesoporous metal particles produced by nanocasting use a salt precursor, but undergo reduction by hydrogen or hydrazine to reduce the salt to the metal. Mesoporous metals that have been successfully produced include platinum[59] and osmium[60]. Nickel can also be formed by electroless deposition[61]. Silver has been synthesized from SBA-15 silica using an alternative method. Silica template and silver nitrate powder were ground together, and then heated to form mesoporous silver particles[62]. Monolithic metals that have recently been produced include nickel, silver, and sterling silver[63].

1.5 A Comprehensive Nanocasting Model

During the past several years, a detailed model of nanocasting has been developed by Bakker, Smatt, Sayler, and the author[64]. This model, seen in Figure 1.3, breaks down the process of nanocasting into several steps, providing a basis for exploring each one of those steps individually. In this introduction, work will be presented that gives an overview for the conditions used in the subsequent experimental chapters.

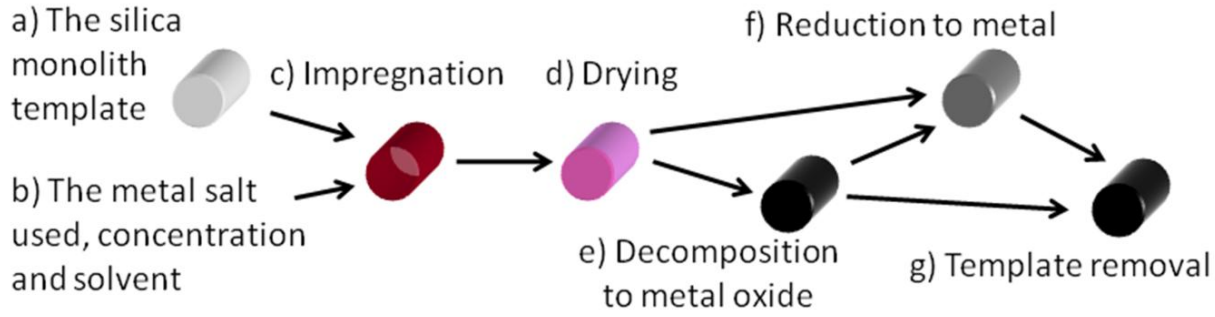

Figure 1.3. Nanocasting Variables

The first variable in the nanocasting process is selection of the silica template to be used. In order to form a nanocast monolith, the replica must be well connected. For this study, hierarchically porous silica monoliths with a trimodal pore structure were synthesized. These monoliths included surfactant templated mesopores, and the alkyl chain length of the surfactant

was varied between tetradecyltrimethylammonium bromide (C_{14} tab), hexadecyltrimethylammonium bromide (C_{16} tab), and octadecyltrimethylammonium bromide (C_{18} tab). The weight percent of surfactant was also varied from 3-9 weight percent (wt. %). By using a combination of conductivity measurements, water sorption, and nitrogen sorption, it was determined that the most highly connected silica monolith was the 7% C_{18} tab, and therefore this has been the silica template used for the majority of our studies[65].

The next set of variables concerns the metal salt solution used, specifically the nature of the metal salt, the concentration, and the solvent. The formation of nickel oxide replicas reported in this work utilized nickel nitrate as the precursor. Earlier work used nickel acetate[64]. The benefit of using the nitrate salt over the acetate salt is that it is considerably more soluble. With nickel acetate, a saturated solution is only 0.7 M, and with nickel nitrate, concentrations of 4.0 M are attainable. When the nickel nitrate salt is used, a complete nickel oxide replica can be formed in 3 cycles of impregnation vs. the 7 cycles that are required when the nickel acetate salt is used. If pure cobalt nitrate hexahydrate is heated to its melting point, this melt can be used to impregnate the monoliths, and only requires two cycles to build up a complete replica. Using the cobalt nitrate melt also allows different geometries to be formed. The melt takes longer to infiltrate throughout the ligaments, and can lead to a "hollow fiber" structure being formed. With this, material is built up on the macropore walls, and leaves a second network within the macropore ligaments as well as the first present in the silica.

The impregnation method also has a tremendous effect on the surface area of the final replica. Incipient wetness is the technique that has been previously used[2], in which drops of solution are added to the monolith. This is repeated until the monolith appears translucent, indicating that all the macropore volume has been filled with solution. In the case of cobalt

oxide, this yields a replica with a surface area of 30-70 m^2/g. With the vacuum infiltration method, a vacuum is first applied to the monolith to empty the pores of all air and water. Then, the solution is introduced under vacuum to help facilitate mesopore filling. Using this vacuum infiltration technique has helped achieve a surface area of 140 m^2/g[26].

Temperature of decomposition/reduction can have an effect on the final structure of the replica. When dealing with nanostructure, one has to consider the Hüttig and Tamman temperatures of a material. The Hüttig temperature is the temperature at which the nanostructure can begin sintering, and is approximately one third of the melting temperature of the bulk material in Kelvin. The Tamman temperature is the temperature at which the nanostructure can begin melting, and is approximately one half of the bulk melting temperature in Kelvin[66]. In light of these considerations, to produce the highest surface area replicas, it is desirable to carry out all processing at temperatures below the Tamman and Hüttig temperatures. When the material is heated above these temperatures, the material can sinter to form large particles, and/or can become sufficiently mobile for migration out of the mesopores into the macropores.

The atmosphere under which the decomposition process is done impacts the oxidation state of the compound. Decomposition under air, nitrogen, or argon typically results in formation of a metal oxide as the product. Decomposition under 5%H_2/N_2, methanol vapor, or ethylene glycol vapor results in a metal product. When comparing a cobalt oxide replica which has been synthesized under different atmospheres, decomposition under nitrogen yields the smallest feature sizes, therefore allowing the nanostructure of the replica to most closely resemble that of the template[64].

The final step in the nanocasting process is template removal. This removes the silica monolith from the composite and leaves a free standing metal oxide, metal, or carbon replica.

This replica is a positive replica of the macrostructure, and a negative replica of the mesostructure. Template removal is done either by aqueous base or hydrofluoric acid etch. This places a limitation on the materials that can be synthesized by nanocasting. Hydrofluoric acid is dangerous and dissolves many metals, which limits its utility. Base etch is safe and effective, but does not work for amphoteric metal oxides.

1.6 References

1. Yang, X.-Y.; Leonard, A.; Lemaire, A.; Tian, G.; Su, B.-L., Self-formation phenomenon to hierarchically structured porous materials: design, synthesis, formation mechanism and applications. *Chem. Commun. (Cambridge, U. K.)* **2011,** *47*, 2763-2786.

2. Smatt, J.-H.; Weidenthaler, C.; Rosenholm, J. B.; Linden, M., Hierarchically Porous Metal Oxide Monoliths Prepared by the Nanocasting Route. *Chem. Mater.* **2006,** *18*, 1443-1450.

3. Carroll, N. J.; Crowder, P. F.; Pylypenko, S.; Patterson, W.; Ratnaweera, D. R.; Perahia, D.; Atanassov, P.; Petsev, D. N., Microfluidic Synthesis of Monodisperse Nanoporous Oxide Particles and Control of Hierarchical Pore Structure. *ACS Appl. Mater. Interfaces* **2013,** *5*, 3524-3529.

4. Jhun, J.-S.; Yun, H.-S.; Park, E.-K.; Shin, H.-I., Bone repair efficiency by various round granular bone substitutes. *Key Eng. Mater.* **2012,** *493-494*, 143-146.

5. Nagase, K.; Kobayashi, J.; Kikuchi, A.; Akiyama, Y.; Kanazawa, H.; Okano, T., Thermally Modulated Cationic Copolymer Brush on Monolithic Silica Rods for High-Speed Separation of Acidic Biomolecules. *ACS Appl. Mater. Interfaces* **2013,** *5*, 1442-1452.

6. Jiang, Z.-J.; Liu, C.-Y.; Sun, L.-W., Catalytic Properties of Silver Nanoparticles Supported on Silica Spheres. *J. Phys. Chem. B* **2005,** *109*, 1730-1735.

7. Beck, J. S.; Vartuli, J. C.; Roth, W. J.; Leonowicz, M. E.; Kresge, C. T.; Schmitt, K. D.; Chu, C. T. W.; Olson, D. H.; Sheppard, E. W.; et, a., A new family of mesoporous molecular sieves prepared with liquid crystal templates. *J. Am. Chem. Soc.* **1992,** *114*, 10834-43.

8. Nakanishi, K., Pore structure control of silica gels based on phase separation. *J. Porous Mater.* **1997,** *4*, 67-112.

9. Zhong, H.; Zhu, G.; Wang, P.; Liu, J.; Yang, J.; Yang, Q., Direct synthesis of hierarchical monolithic silica for high performance liquid chromatography. *J. Chromatogr. A* **2008,** *1190*, 232-240.

10. Nakanishi, K.; Kobayashi, Y.; Amatani, T.; Hirao, K.; Kodaira, T., Spontaneous Formation of Hierarchical Macro−Mesoporous Ethane−Silica Monolith. *Chemistry of Materials* **2004,** *16* (19), 3652-3658.

11. Lecloux, A. J.; Pirard, J. P., High-temperature catalysts through sol–gel synthesis. *Journal of Non-Crystalline Solids* **1998,** *225* (0), 146-152.

12. Meixner, D. L.; Dyer, P., Influence of Sol-Gel Synthesis Parameters on the Microstructure of Particulate Silica Xerogels. *Journal of Sol-Gel Science and Technology* **1999,** *14* (3), 223-232.

13. Phalippou, J. Sol-gel: A low temperature process for the materials of the new millenium. http://www.solgel.com/articles/june00/phalip/introsolgel.htm.

14. Lefebvre, L.-P.; Banhart, J.; Dunand, D. C., Porous metals and metallic foams: current status and recent developments. *Adv. Eng. Mater.* **2008,** *10*, 775-787.

15. Tappan, B. C.; Steiner, S. A.; Luther, E. P., Nanoporous Metal Foams. *Angewandte Chemie International Edition* **2010,** *49* (27), 4544-4565.

16. Sudik, A. C.; Côté, A. P.; Wong-Foy, A. G.; O'Keeffe, M.; Yaghi, O. M., A Metal–Organic Framework with a Hierarchical System of Pores and Tetrahedral Building Blocks. *Angewandte Chemie* **2006,** *118* (16), 2590-2595.

17. Zajickova, Z.; Rubi, E.; Svec, F., In situ sol-gel preparation of porous alumina monoliths for chromatographic separations of adenosine phosphates. *J. Chromatogr. A* **2011,** *1218*, 3555-3558.

18. Hoa, N. D.; Duy, N. V.; Hieu, N. V., Crystalline mesoporous tungsten oxide nanoplate monoliths synthesized by directed soft template method for highly sensitive NO2 gas sensor applications. *Mater. Res. Bull.* **2013,** *48*, 440-448.

19. Zhou, H.; Li, X.; Fan, T.; Osterloh, F. E.; Ding, J.; Sabio, E. M.; Zhang, D.; Guo, Q., Artificial Inorganic Leaves for Efficient Photochemical Hydrogen Production Inspired by Natural Photosynthesis. *Adv. Mater. (Weinheim, Ger.)* **2010,** *22*, 951-956.

20. Kim, Y. J.; Lee, M. H.; Kim, H. J.; Lim, G.; Choi, Y. S.; Park, N.-G.; Kim, K.; Lee, W. I., Formation of Highly Efficient Dye-Sensitized Solar Cells by Hierarchical Pore Generation with Nanoporous TiO2 Spheres. *Adv. Mater. (Weinheim, Ger.)* **2009,** *21*, 3668-3673.

21. Li, Y.; Fu, Z.-Y.; Su, B.-L., Hierarchically Structured Porous Materials for Energy Conversion and Storage. *Adv. Funct. Mater.* **2012,** *22*, 4634-4667.

22. Parlett, C. M. A.; Wilson, K.; Lee, A. F., Hierarchical porous materials: catalytic applications. *Chem. Soc. Rev.* **2013,** *42*, 3876-3893.

23. Brady, R.; Woonton, B.; Gee, M. L.; O'Connor, A. J., Hierarchical mesoporous silica materials for separation of functional food ingredients — A review. *Innovative Food Science & Emerging Technologies* **2008,** *9* (2), 243-248.

24. Sayler, F. M.; Grano, A.; Wiedmer, S.; Smatt, J.-H.; Bakker, M. G., Application of 3-D hierarchically porous silver, cobalt oxide, and zinc oxide monoliths to chromatographic separations. *MRS Online Proc. Libr.* **2011,** *1389*,1-5.

25. (a) Parmentier, J.; Saadhallah, S.; Reda, M.; Gibot, P.; Roux, M.; Vidal, L.; Vix-Guterl, C.; Patarin, J., New carbons with controlled nanoporosity obtained by nanocasting using a SBA-15 mesoporous silica host matrix and different preparation routes. *J. Phys. Chem. Solids* **2004,** *65*, 139-146; (b) Kim, C. H.; Lee, D.-K.; Pinnavaia, T. J., Graphitic Mesostructured Carbon Prepared from Aromatic Precursors. *Langmuir* **2004,** *20*, 5157-5159.

26. Sayler, F. M. Synthesis and Application of Hierarchically Porous Metal and Metal Oxide Monolithic Materials. The University of Alabama, Tuscaloosa, AL, 2013.

27. Oberacher, H.; Huber, C. G., Capillary monoliths for the analysis of nucleic acids by high-performance liquid chromatography–electrospray ionization mass spectrometry. *TrAC Trends in Analytical Chemistry* **2002,** *21* (3), 166-174.

28. Lu, A.-H.; Zhao, D.; Wan, Y.; Editors, *Nanocasting: A Versatile Strategy for Creating Nanostructured Porous Materials*. Royal Society of Chemistry Publishing: 2009; p 265 pp.

29. Rodriguez-Mirasol, J.; Cordero, T.; Radovic, L. R.; Rodriguez, J. J., Structural and Textural Properties of Pyrolytic Carbon Formed within a Microporous Zeolite Template. *Chem. Mater.* **1998,** *10*, 550-558.

30. Goeltner, C. G.; Weissenberger, M. C., Mesoporous organic polymers obtained by two-step nanocasting. *Acta Polym.* **1998,** *49*, 704-709.

31. Freire, R. M.; Batista, A. H. D.; Souza, A. G.; Mendes, J.; Saraiva, G. D.; Oliveira, A. C., High Catalytic Activity of Nitrogen-Containing Carbon from Molecular Sieves in Fine Chemistry. *Catal Lett* **2009,** *131* (1-2), 135-145.

32. Ryoo, R.; Joo, S. H.; Jun, S., Synthesis of Highly Ordered Carbon Molecular Sieves via Template-Mediated Structural Transformation. *The Journal of Physical Chemistry B* **1999,** *103* (37), 7743-7746.

33. R. Ryoo, S. H. J., S. Jun, T. Tsubakiyama, and O. Terasaki, *Stud. Surf. Sci. Catal.* 2001; Vol. 135.

34. Xia, Y.; Yang, Z.; Mokaya, R., Simultaneous Control of Morphology and Porosity in Nanoporous Carbon: Graphitic Mesoporous Carbon Nanorods and Nanotubules with Tunable Pore Size. *Chem. Mater.* **2006,** *18*, 140-148.

35. Kleitz, F.; Choi, S. H.; Ryoo, R., Cubic Ia3d large mesoporous silica: synthesis and replication to platinum nanowires, carbon nanorods and carbon nanotubes. *Chem. Commun. (Cambridge, U. K.)* **2003,** 2136-2137.

36. Orooji, Y.; Kazemzad, M.; Ganjkhanlou, Y.; Youzbashi, A. A.; Khanlarkhani, A., Easy and economical nanocasting method for preparation of carbon adsorbent using low-cost precursors in the presence of a natural zeolite as template. *Micro Nano Lett.* **2012,** *7*, 1136-1139.

37. Joo, S. H.; Choi, S. J.; Oh, I.; Kwak, J.; Liu, Z.; Terasaki, O.; Ryoo, R., Ordered nanoporous arrays of carbon supporting high dispersions of platinum nanoparticles. *Nature (London, U. K.)* **2001,** *412*, 169-172.

38. Lee, J.; Yoon, S.; Hyeon, T.; Oh, S. M.; Kim, K. B., Synthesis of a new mesoporous carbon and its application to electrochemical double-layer capacitors. *Chem. Commun. (Cambridge)* **1999,** 2177-2178.

39. Chen, F.; Xu, X.-J.; Shen, S.; Kawi, S.; Hidajat, K., Microporosity of SBA-3 mesoporous molecular sieves. *Microporous Mesoporous Mater.* **2004,** *75*, 231-235.

40. Lu, A.-H.; Smatt, J.-H.; Linden, M.; Schueth, F., Synthesis of carbon monoliths with a multi-modal pore system by a one step impregnation technique. *Xinxing Tan Cailiao* **2003,** *18*, 265-270.

41. Jiao, K.; Zhang, B.; Yue, B.; Ren, Y.; Liu, S.; Yan, S.; Dickinson, C.; Zhou, W.; He, H., Growth of porous single-crystal Cr2O3 in a 3-D mesopore system. *Chem. Commun. (Cambridge, U. K.)* **2005,** 5618-5620.

42. Tian, B.; Liu, X.; Yang, H.; Xie, S.; Yu, C.; Tu, B.; Zhao, D., General synthesis of ordered crystallized metal oxide nanoarrays replicated by microwave-digested mesoporous silica. *Adv. Mater. (Weinheim, Ger.)* **2003,** *15*, 1370-1374.

43. Tueysuez, H.; Salabas, E. L.; Weidenthaler, C.; Schueth, F., Synthesis and Magnetic Investigation of Ordered Mesoporous Two-Line Ferrihydrite. *J. Am. Chem. Soc.* **2008,** *130*, 280-287.

44. Tuysuz, H.; Lehmann, C. W.; Bongard, H.; Tesche, B.; Schmidt, R.; Schuth, F., Direct Imaging of Surface Topology and Pore System of Ordered Mesoporous Silica (MCM-41, SBA-15, and KIT-6) and Nanocast Metal Oxides by High Resolution Scanning Electron Microscopy. *J. Am. Chem. Soc.* **2008,** *130*, 11510-11517.

45. Laha, S. C.; Ryoo, R., Synthesis of thermally stable mesoporous cerium oxide with nanocrystalline frameworks using mesoporous silica templates. *Chem. Commun. (Cambridge, U. K.)* **2003,** 2138-2139.

46. Bordoloi, A.; Halligudi, S. B., Studies in structural characterization and correlation with the catalytic activity of an efficient and stable WOx/SBA-15 nanocomposite catalyst. *J. Catal.* **2008,** *257*, 283-290.

47. Yang, H.; Shi, Q.; Tian, B.; Lu, Q.; Gao, F.; Xie, S.; Fan, J.; Yu, C.; Tu, B.; Zhao, D., One-Step Nanocasting Synthesis of Highly Ordered Single Crystalline Indium Oxide Nanowire Arrays from Mesostructured Frameworks. *J. Am. Chem. Soc.* **2003,** *125*, 4724-4725.

48. Sarshar, Z.; Kleitz, F.; Kaliaguine, S., Novel oxygen carriers for chemical looping combustion: La1-xCexBO3 (B = Co, Mn) perovskites synthesized by reactive grinding and nanocasting. *Energy Environ. Sci.* **2011,** *4*, 4258-4269.

49. Cabo, M.; Pellicer, E.; Rossinyol, E.; Estrader, M.; Lopez-Ortega, A.; Nogues, J.; Castell, O.; Surinach, S.; Baro, M. D., Synthesis of compositionally graded nanocast NiO/NiCo2O4/Co3O4 mesoporous composites with tunable magnetic properties. *J. Mater. Chem.* **2010,** *20*, 7021-7028.

50. Zhu, J.; Gao, Q., Mesoporous MCo2O4 (M=Cu, Mn and Ni) spinels: Structural replication, characterization and catalytic application in CO oxidation. *Microporous Mesoporous Mater.* **2009,** *124*, 144-152.

51. Smatt, J.-H.; Spliethoff, B.; Rosenholm, J. B.; Linden, M., Hierachically porous nanocrystalline cobalt oxide monoliths through nanocasting. *Chemical Communications* **2004,** *0* (19), 2188-2189.

52. Smtt, J.-H.; Weidenthaler, C.; Rosenholm, J. B.; Linden, M., Hierarchically Porous Metal Oxide Monoliths Prepared by the Nanocasting Route. *Chem. Mater.* **2006,** *18*, 1443-1450.

53. Smått, J.-H.; Sayler, F. M.; Grano, A. J.; Bakker, M. G., Formation of Hierarchically Porous Metal Oxide and Metal Monoliths by Nanocasting into Silica Monoliths. *Advanced Engineering Materials* **2012,** *14*, 1059-1073.

54. Roggenbuck, J.; Tiemann, M., Ordered Mesoporous Magnesium Oxide with High Thermal Stability Synthesized by Exotemplating Using CMK-3 Carbon. *J. Am. Chem. Soc.* **2005,** *127*, 1096-1097.

55. Liu, Q.; Wang, A.; Wang, X.; Zhang, T., Ordered crystalline alumina molecular sieves synthesized via a nanocasting route. *Chem. Mater.* **2006,** *18*, 5153-5155.

56. Roggenbuck, J.; Schaefer, H.; Tsoncheva, T.; Minchev, C.; Hanss, J.; Tiemann, M., Mesoporous CeO2: Synthesis by nanocasting, characterisation and catalytic properties. *Microporous Mesoporous Mater.* **2007,** *101*, 335-341.

57. Wagner, T.; Waitz, T.; Roggenbuck, J.; Froeba, M.; Kohl, C. D.; Tiemann, M., Ordered mesoporous ZnO for gas sensing. *Thin Solid Films* **2007,** *515*, 8360-8363.

58. Lai, X.; Li, X.; Geng, W.; Tu, J.; Li, J.; Qiu, S., Ordered mesoporous copper oxide with crystalline walls. *Angew. Chem., Int. Ed.* **2007,** *46*, 738-74.

59. Shin, H. J.; Ryoo, R.; Liu, Z.; Terasaki, O., Template Synthesis of Asymmetrically Mesostructured Platinum Networks. *J. Am. Chem. Soc.* **2001,** *123*, 1246-1247.

60. Lee, K.; Kim, Y.-H.; Han, S. B.; Kang, H.; Park, S.; Seo, W. S.; Park, J. T.; Kim, B.; Chang, S., Osmium Replica of Mesoporous Silicate MCM-48: Efficient and Reusable Catalyst for Oxidative Cleavage and Dihydroxylation Reactions. *J. Am. Chem. Soc.* **2003,** *125*, 6844-6845.

61. Li, H.; Lin, H.; Xie, S.; Dai, W.; Qiao, M.; Lu, Y.; Li, H., Ordered Mesoporous Ni Nanowires with Enhanced Hydrogenation Activity Prepared by Electroless Plating on Functionalized SBA-15. *Chem. Mater.* **2008,** *20*, 3936-3943.

62. Worboys, L. M.; Edwards, P. P.; Anderson, P. A., Silver nanowires. Inclusion in and extrusion from a mesoporous template. *Chem. Commun. (Cambridge, U. K.)* **2002,** 2894-2895.

63. Sayler, F. M.; Grano, A. J.; Scogin, W.; Sanders, P.; Smått, J.-H.; Shaughnessy, K. H.; Bakker, M. G., Formation and Applications of Hierarchically Porous Carbon, Metals and Metal Oxides Formed by Nanocasting. *MRS Online Proceedings Library* **2012,** *1389*, 1-5.

64. Smatt, J.-H.; Sayler, F. M.; Grano, A. J.; Bakker, M. G., Formation of Hierarchically Porous Metal Oxide and Metal Monoliths by Nanocasting into Silica Monoliths. *Adv. Eng. Mater.* **2012,** *14*, 1059-1073.

65. Maddox Sayler, F.; Bakker, M. G.; Smått, J.-H.; Lindén, M., Correlation between Electrical Conductivity, Relative Humidity, and Pore Connectivity in Mesoporous Silica Monoliths. *The Journal of Physical Chemistry C* **2010,** *114* (19), 8710-8716.

66. Moulijn, J. A.; van Diepen, A. E.; Kapteijn, F., Catalyst deactivation: is it predictable?: What to do? *Applied Catalysis A: General* **2001,** *212* (1–2), 3-16.

CHAPTER 2
HIERARCHICALLY POROUS MONOLITHS OF CARBON, COBALT OXIDE, AND NICKEL OXIDE WITH HIGHLY ORDERED MESOPORES

2.1 Abstract

Hierarchically porous materials are of great interest in the fields of separations, catalysis, and energy storage. Nanocasting of carbon, nickel oxide, and cobalt oxide into SBA-15 type monoliths results in monolithic replicas with ordered mesopore structures. However, the monoliths vary in their degree of ordering, with carbon being the most ordered, followed by cobalt oxide, and finally nickel oxide. These silica, cobalt oxide, and nickel oxide monoliths have also been utilized as supports for silver particles and proven catalytically active in the reduction of methyl orange.

2.2 Introduction

Nanostructured materials have attracted considerable attention because of the interesting and useful properties that come from the high surface/volume ratios and the quantum effects seen in these materials. Nanoparticles and nanowires have attracted the most effort because of the ease of synthesis. However, many important applications, particularly those involving energy storage and utilization, require macroscopic single pieces with continuous structure, combined with precise control of the structure at multiple length scales. Such materials are often referred to as "monoliths". For example, fuel cells, advanced batteries, and supercapacitors all require fast interfacial kinetics, coupled with efficient transport of electrons and ions[1]. Fuel cells also require efficient transport of reactants and products. One strategy that has been widely used is to synthesize zero or one dimensional nanomaterials and then develop methods for

controlling the assembly into or onto 3-dimensional materials. A less explored strategy is to form 3-dimensionally porous materials and then use these materials as templates to direct the synthesis of the desired nanomaterials. An outstanding example of the power of this approach is recent work by Zhang et al.[2], who used colloidal liquid crystal templating to form a nickel hydroxide/manganese dioxide-based battery with both high energy density and extremely fast charge and discharge characteristics. We[3] and others[4] have demonstrated a somewhat different approach using sol-gel syntheses of silica to make hierarchically porous silica monoliths, which are then used as templates for nanocasting.[5] Nanocasting has been more widely applied to mesoporous silica particles.[6] Application to hierarchically porous silica monoliths results in materials with extremely high surface areas coupled with superior flow characteristics. Such materials are particularly advantageous for catalytic applications, as illustrated by their recent use as microreactors.[7] Metal oxide and silica materials are also being used as catalyst supports. Our materials show these catalytic properties, but have superior real-world possibilities due to the monolithic nature of the materials.

One limitation of this sol-gel based approach has been that the materials produced are not ordered at the nanoscale. This lack of order produces materials with a distribution of lengths which could result in a broader than desired range of physical and chemical properties, and the loss of the co-operative physical properties potentially available from ordered nanostructured arrays in e.g. plasmonics. In this contribution, the first examples of hierarchically porous monoliths, consisting of highly ordered nanowire arrays of cobalt oxide, nickel oxide and carbon are presented. Also included is the use of these monoliths as catalyst supports, which show excellent catalytic activity in the reduction of methyl orange. The approach utilizes a sol-gel synthesis that gives highly ordered arrays of mesopores in the silica monoliths which also

incorporate a macropore network.[8] Controlled addition of solution phase precursors to the silica monoliths, followed by heating, produces the metal oxide or carbon monoliths which form an inverse replica of the mesopore structure while retaining the macropore network structure.

2.3 Experimental

2.3.1 Silica Monolith Templates

Silica monolith templates with macropores and highly ordered hexagonal mesopores were synthesized using a previously reported method.[15] 6.25 g of Pluronic 123 block copolymer (P123) is added to 20 mL 0.02 M CH_3COOH, and the solution is stirred until the block copolymer is completely dissolved. The solution is then put on ice and 8 g of tetramethylorthosilicate (TMOS) is added. The solution is stirred for thirty minutes, and then poured into molds. Molds are place in a 40 °C oven for 24 h and then a 60 °C oven for 24 h. The formed monoliths then undergo a steam treatment for 12 h at 100 °C followed by a water treatment for 12 h at 100 °C. The resulting monoliths are dried at 60 °C for 12 h, and then calcined at 550 °C for 5 h with a heating ramp of 1 °C/min.

2.3.2 Replicas

For carbon replicas, parent silica monoliths are impregnated with a solution of 0.0324 g oxalic acid, 3.2 mL furfuryl alcohol, and 4.8 mL mesitylene[9]. The impregnated monoliths are then heated for 24 h at 60 °C and 24 h at 80 °C. They are then heated under nitrogen to 150 °C for three hours, followed by heating to 300 °C at a ramp rate of 1 °C/min, and lastly heating to 800 °C at a ramp rate of 2 °C/min and holding for 4 h. For cobalt and nickel oxides, parent silica monoliths are vacuum impregnated with a saturated nitrate salt solution consisting of 4.6 M and 4.5 M for cobalt and nickel nitrates respectively. The impregnated monoliths are then heated at 150 °C for 10 h under nitrogen atmosphere for drying of the monolith. The cobalt nitrate-

infiltrated monoliths are then taken to 250 °C to insure conversion to Co_3O_4. The nickel nitrate-infiltrated monoliths are heated to 600 °C in air to convert the salt to NiO. The infiltration and decomposition steps are repeated two more times to build up a complete replica. All composites are then etched in a solution of 3 M KOH for 24 h and then rinsed till pH of the rinse is neutral. After silica template removal, a free-standing monolithic replica remains, which is about 5 mm in diameter and 1.5 cm in length.

2.3.3 Ag-loaded Monoliths

To prepare Ag-loaded monoliths for catalysis experiments, a 2 M aqueous solution of $AgNO_3$ was vacuum impregnated into SiO_2, Co_3O_4, and NiO monoliths. The impregnated monoliths were then dried at 90 °C, after which the silver nitrate was reduced to silver under ethylene glycol vapor at 165 °C. For reduction of methyl orange, 0.05 g of bare monolith or Ag-loaded monolith and 0.2 g $NaBH_4$ were added to 200 mL of 2.0×10^{-5} M methyl orange solution under stirring. Aliquots of 3 mL were taken out at each time increment and the absorbance at 463 nm reported.

2.3.4 Characterization

The images of macropore structure were taken on a JEOL 7000 scanning electron microscope (SEM). The images of mesopore structure were taken on a FEI TECNAI F-20 transmission electron microscope (TEM). Nitrogen physisorption measurements were carried out on a Quantichrome Nova 2200e surface area and pore size analyzer. Isotherms were analyzed with Quantachrome NovaWin software version 10.01, and the fitting errors between the NLDFT model used and our measured samples were less than 1%. X-ray Diffraction (XRD) was performed with a Bruker D8 Discover with GADDS X-ray diffractometer (wavelength Co K_α). Small angle X-ray scattering (SAXS) was performed on a Kratky compact small-angle

system (Hecus, Austria). UV/Vis spectroscopy was performed on a Varian Cary UV/Vis spectrophotometer.

2.4 Results and Discussion

2.4.1 Replicas

The photograph in Figure 2.1 (top) shows the original silica and etched monoliths. All

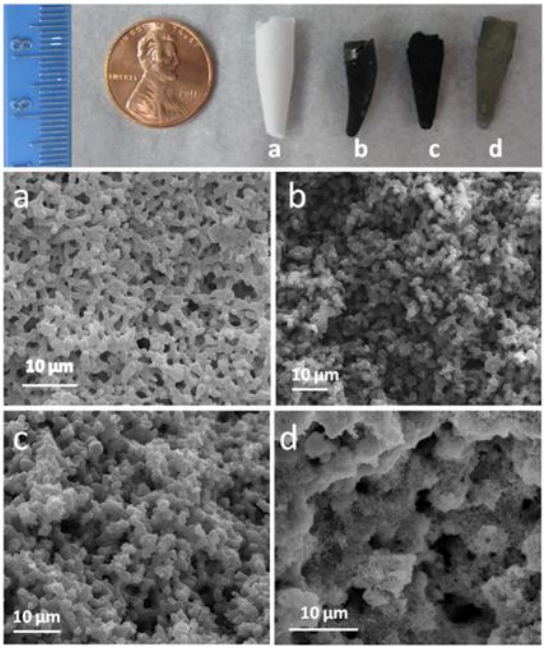

Figure 2.1. Photograph and SEM images of a)parent silica monolith, b)carbon replica, c)cobalt oxide replica, and d) nickel oxide replica

replicas remained intact after the template was removed. A slight shrinkage in the carbon monolith can be observed (b), but the cobalt (c) and nickel (d) oxide replicas show little to no shrinkage. SEM images (Figure 2.1a) shows the macropore network of the parent silica monolith. SEM images of the carbon and cobalt oxide replicas after removal of the silica can be seen in Fig. 2.1b & 2.1c, which show that the surface topologies of the macropore walls are similar to that of the parent silica monolith. The nickel oxide replica (Fig. 2.1d) shows signs of coarsening of the structure of the macropore walls. XRD (Figure 2.2) confirms the formation of only Co_3O_4 and NiO. All peaks present in the diffractograms can be assigned to Co_3O_4 and NiO.

Scherrer analysis was performed to determine crystallite size, and the results can be seen in Table 1.

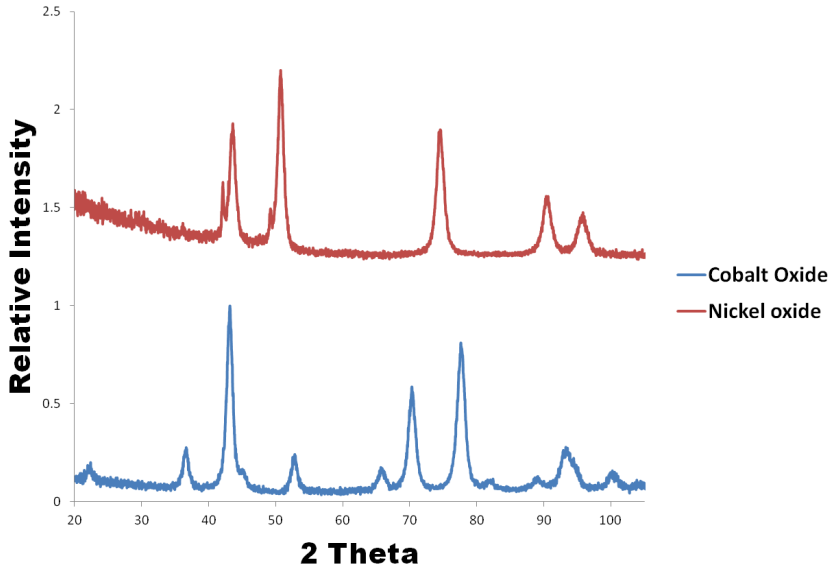

Figure 2.2. XRD diffractogram of cobalt oxide and nickel oxide. All peaks can be assigned to the respective material

Table 2.1. Nitrogen sorption and Scherrer analysis data for parent silica monolith and carbon, cobalt oxide, and nickel oxide replicas

	BET Surface Area		Mesopore Diameter (nm)	Mesopore Volume		Crystallite Size(nm)
Sample	m^2/g	m^2/mL	DFT	(mL/g)	(mL/mL)	
SiO_2	782	1720	7.6	1.27	2.8	-
Carbon	680	1541	3.5	0.18	0.41	-
Co_3O_4	122	745	3.7	0.06	0.37	8.5 ± 0.7
NiO	15	100	5.6	0.006	0.04	8.4 ± 0.8
SiO_2-Ag	93.9	-	-	0.617	-	-
Co_3O_4-Ag	60.1	-	-	0.1	-	-
NiO-Ag	40.1	-	-	0.082	-	-

The TEM image, seen in Figure 2.3a, shows the highly ordered network of mesopores, which are present within the macropore wall of the parent silica monolith. Upon infiltration and decomposition, these hexagonally ordered pores are inverted to become a hexagonally ordered nanowire array in the replicas. The TEM images (Figure 2.3 b-d) show that the carbon, cobalt oxide, and nickel oxide all display replication of the mesopores. High resolution SEM (Figure 2.4a & 2.4c) images of both the cobalt oxide and nickel oxide show these nanowires arrays seen in the TEM images are 3-dimensional ordered networks that are present within the walls of the macropores. High-resolution TEM images (Figure 2.4b & 2.4d) show the "bridges" that are present between the nanowires for these two samples. These bridges are formed from replication of the micropores and/or small mesopores that form the connections between the mesopores in the parent silica. Their replication is important in forming a stable replica[5].

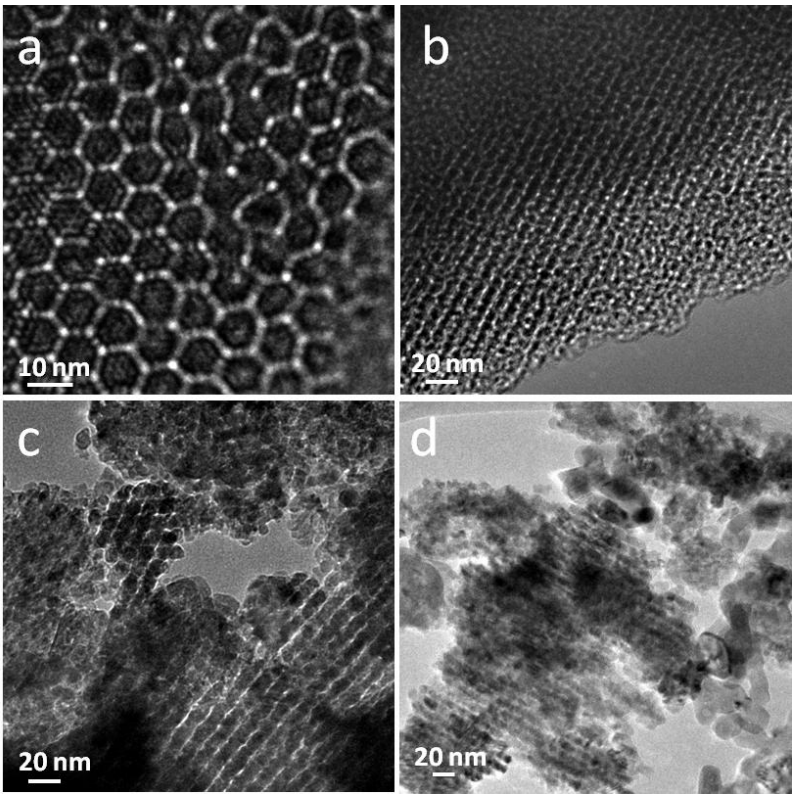

Figure 2.3. TEM images of a)parent silica monolith, b)carbon replica, c) cobalt oxide replica, and d) nickel oxide replica

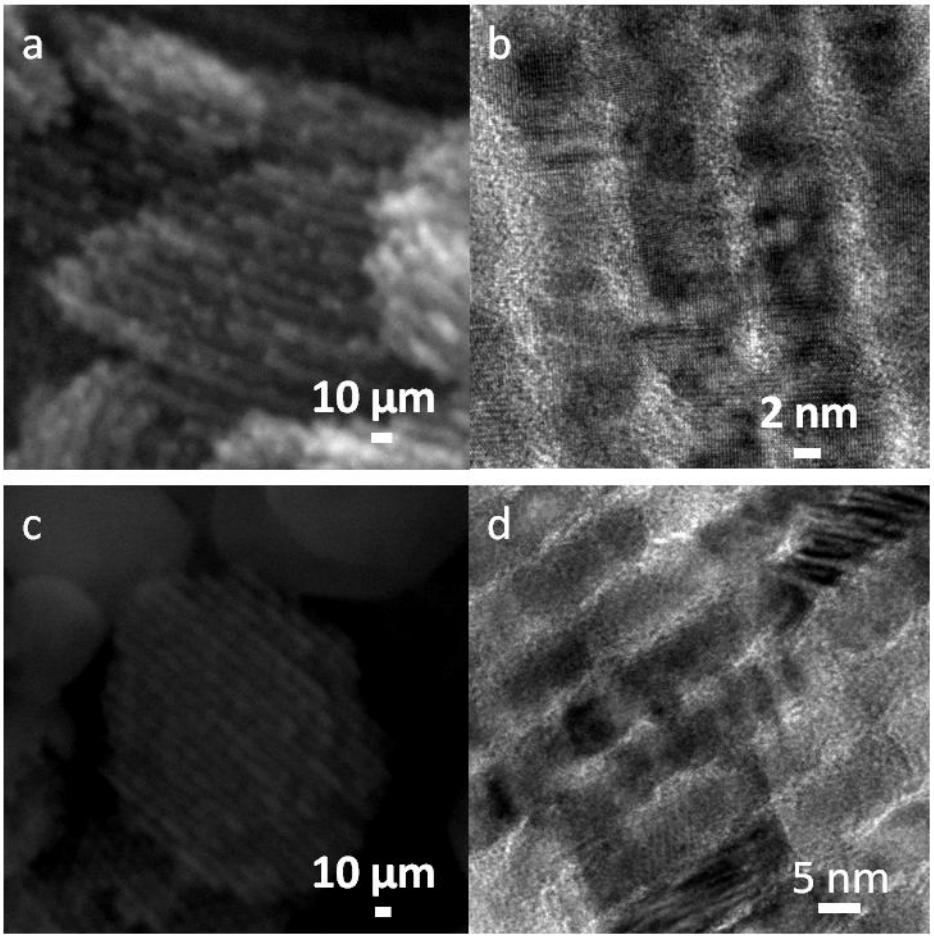

Figure 2.4. HR SEM and TEM images of a,b) cobalt oxide replica and c,d) nickel oxide replica

Since electron microscopy can only image a small portion of the entire monolith, small angle X-ray scattering (SAXS) and nitrogen physisorption were used to determine whether ordering was seen throughout the entire monolith. SAXS (Figure 2.5) of the parent silica monolith show (100), (110), and (200) reflections, indicating that the highly ordered network, as seen in the TEM images, is present throughout the entire monolith. The *a* value as calculated from the (100) SAXS peak, is 10.7 nm. SAXS of the carbon shows (100), (110), and (200) reflections, which indicates that the carbon replica has the same long range ordering as is seen in the silica template. Analysis of the (100) peak yields a smaller *a* value of 9.3 nm, which is in accordance with the bulk shrinkage seen in the photograph. For the cobalt oxide and nickel

oxide replicas, only the (100) reflection can be seen, which indicates there is a lower degree of order in the cobalt oxide monolith than in the carbon, and an even lower degree in the nickel oxide replica. The *a* values for the cobalt oxide and nickel oxide are close to the value of the silica template. This is consistent with the TEM images of the materials. The carbon TEM image shows nanowire arrays throughout all images taken of the sample. The cobalt oxide TEM images show a majority of nanowire arrays with a few interdispersed particles, while nickel oxide TEM images show a combination of nanowire arrays and disordered particles.

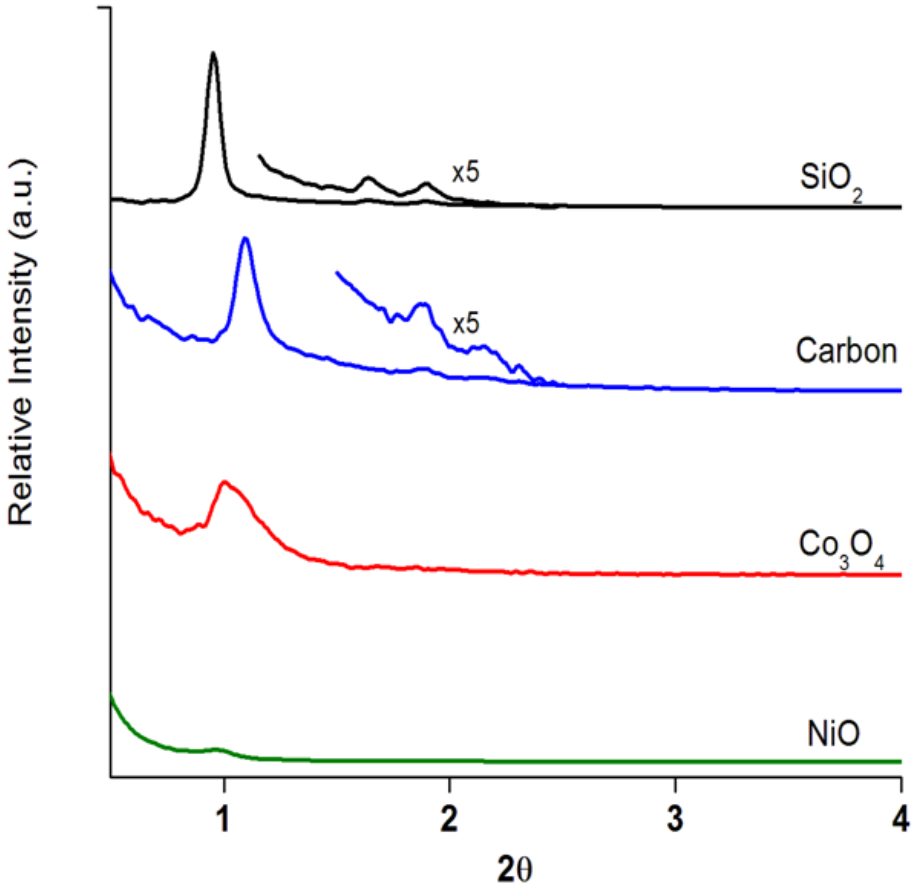

Figure 2.5. SAXS patterns for silica template and replicas

Where SAXS gives qualitative confirmation of the formation of significant amounts of ordered nanowires, nitrogen adsorption can give quantitative information. The nitrogen physisorption isotherm of the parent silica monolith (Figure 2.6) shows a sharp condensation step

at relative pressures between 0.6 and 0.8, indicating a uniform mesopore size distribution. This pore size distribution is confirmed with the non-local density functional theory calculation (NLDFT) of the pore size distribution, which shows a sharp peak at a pore size of 7.6 nm. Taking the *a* value and subtracting the pore size gives a wall thickness of about 3.1 nm. This value is consistent with other reported wall thicknesses, which are in the range 3-6 nm[10], depending on synthesis conditions. The nitrogen physisorption isotherm of the carbon replica (Figure 2.6) shows the intrinsic microporosity present in the carbon replica, as well as an uptake around a relative pressure of 0.3 from the replication of the surfactant mesopores. The NLDFT pore size distribution shows a main sharp peak at 3.5 nm, which is close to the wall thickness of the parent silica monolith. We[9] and others[11] have previously shown that the carbon replication process results in a low density material with micropores (< 1 nm) throughout out the material, therefore giving an accurate replica of the template structure. The surface area of the carbon replica is 680 m^2/g, or 1540 m^2/mL. The total pore volume in the range between 3.5 and 5 nm, which represents the complete inversion of the walls, is 0.18 mL/g, or 0.41 mL/mL. This will be considered the total mesopore volume that should be present in replicas exhibiting complete replication.[6a, 12]

Nitrogen physisorption isotherms were obtained for both the cobalt oxide and nickel oxide composites to give insight into degree of pore filling, as well as the replicas to evaluate the degree of replication (Figure 2.7). The Co_3O_4-SiO_2 composite isotherm shows a much smaller condensation step between 0.6 and 0.8 relative pressure, indicating that there is filling of the surfactant mesopores with cobalt oxide; this coincides with the pore size distribution of the composite, which shows a greatly reduced volume of mesopores around 7.6 nm. The NiO-SiO_2 composite still has a slightly larger condensation step between the relative pressures of 0.6 and

0.8, indicating the degree of metal oxide pore filling in the nickel oxide-silica composite is less than that of the cobalt oxide-silica composite.

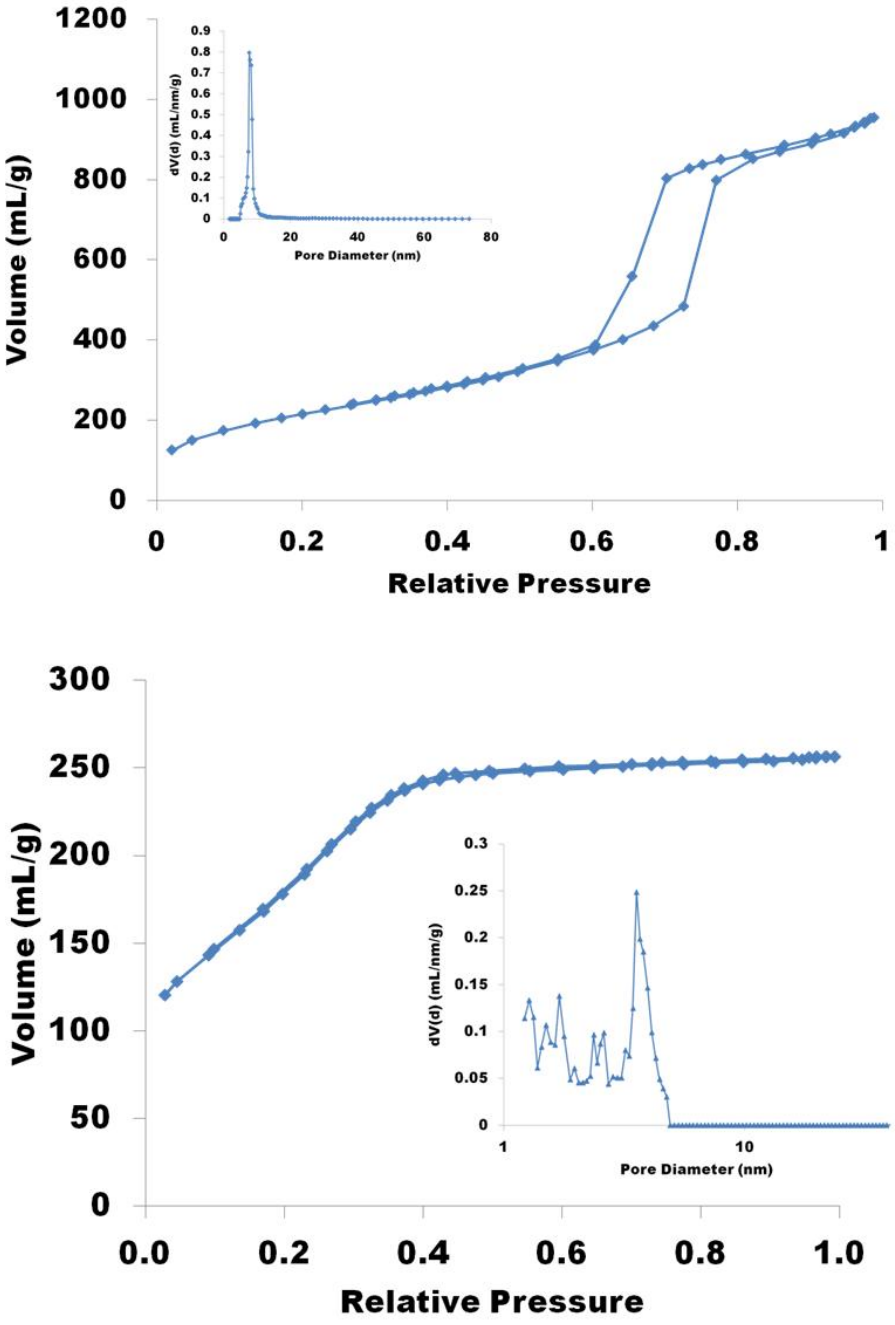

Figure 2.6. Isotherms and pore size distribution (inset) of top) parent silica monolith and bottom) carbon replica

The isotherm of the cobalt oxide replica (Figure 2.7) shows an inflection just below a relative pressure of 0.4, which is representative of the surfactant mesopore replication. The surface area of the cobalt oxide replica is 122 m^2/g, or 745 m^2/mL. The NLDFT shows a peak centered around 3.5 nm, which is slightly larger than the parent silica wall thickness. The total mesopore volume of the replica between 3 and 5 nm is 0.06 mL/g, or 0.37 mL/mL, which represents 90% replication by cobalt oxide. This indicates almost complete filling of all the surfactant templated mesopores with cobalt oxide. The isotherm of the nickel oxide replica (Figure 2.7) shows little evidence of replication of the surfactant mesopores, but instead formation of textural pores between nickel oxide particles. The surface area of the nickel oxide replica is 15 m^2/g, or 100 m^2/mL. The NLDFT pore size distribution shows a major peak at about 6.5 nm, and the volume of these mesopores is much smaller than in either the carbon or cobalt oxide replicas. The increase in pore size is likely due to incomplete filling of the mesopores before template removal, resulting in thinner walls. The sample also contains pores with larger pore diameters.

All nanocasting processes resulted in monolithic replicas of the parent silica, but the degree of ordering in each varies significantly. The nitrogen sorption results, supported by the SAXS, TEM, and SEM data, indicate that carbon shows the highest degree of ordering, followed by cobalt oxide, and lastly nickel oxide. The stability of the replicas also varies, with the carbon and cobalt oxide being mechanically robust, and the nickel oxide being much more fragile. There are a number of factors that could contribute to these differences in degree of replication, including the migration of cobalt and nickel nitrate salts into the pores during the infiltration process,[5] differences in the decomposition pathways of the precursors, and differences in migration of the decomposition intermediates and final product.

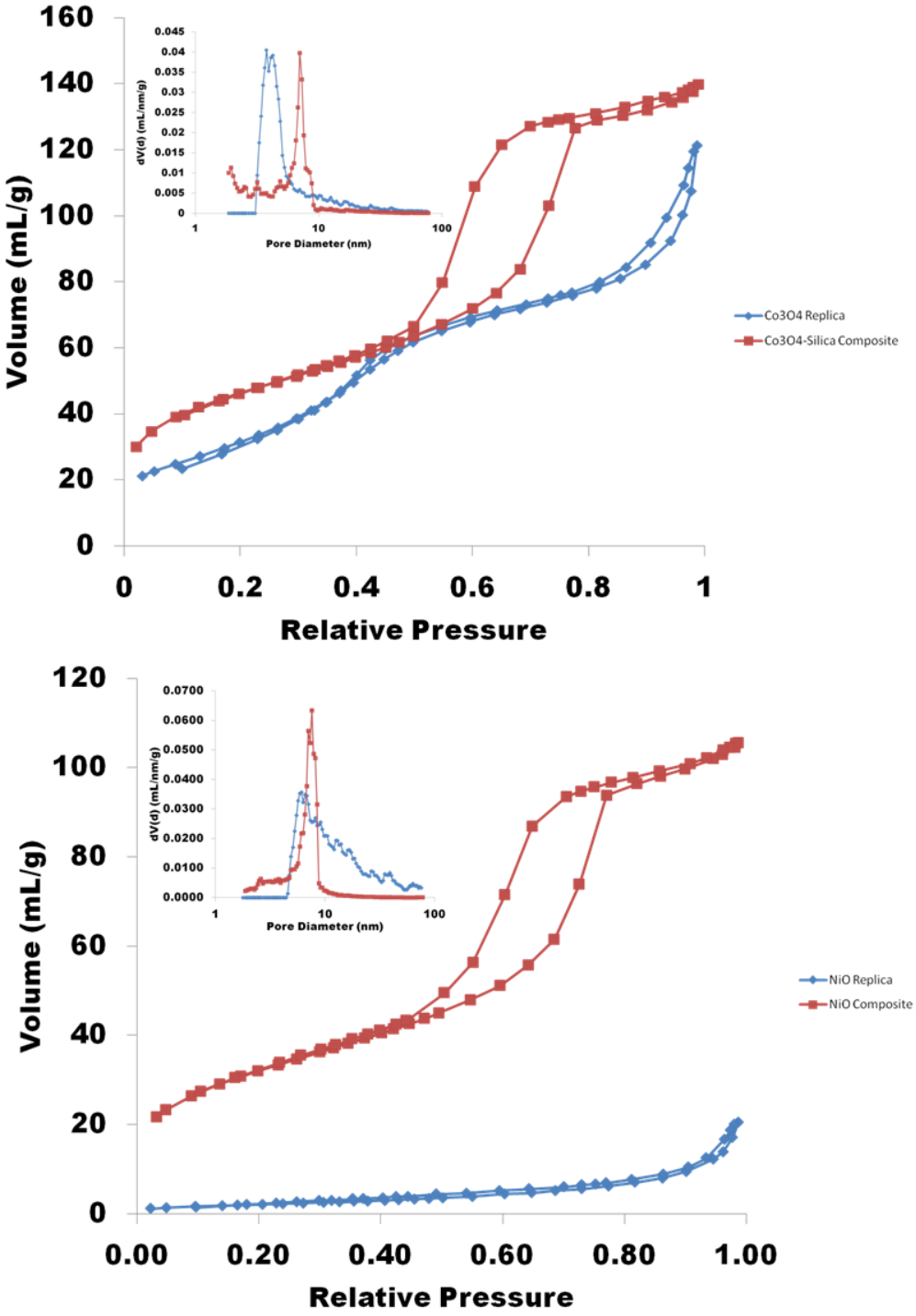

Figure 2.7. Isotherms and pore size distribution (inset) of top) cobalt oxide replica and bottom) nickel oxide replica

The replication by carbon can be accomplished in one infiltration cycle, whereas the metal oxide replicas require multiple cycles of infiltration to achieve a stable replica due to the change in volume during the transition from metal nitrate salt to metal oxide. This volume contraction can be detrimental to the final structure due to the fact that the successive infiltration steps require heating of the already deposited metal oxide above the Hüttig (the point where atoms become mobile) and Tammann (the melting point of the nanostructure) temperatures. It should also be pointed out that the nickel oxide requires heating to a much higher temperature to convert from the non-stoichiometric black nickel oxide to the stoichiometric green nickel oxide (600 °C). The high temperatures and different atmosphere used could also have an influence on the sintering of the nickel oxide nanostructure. We are currently investigating this phenomena is more detail in work elsewhere[13].

2.4.2 Ag loaded monoliths

SEM images and energy dispersive spectroscopy (EDS) maps for the parent silica monolith, cobalt oxide replica, and nickel oxide replica can be seen in Figure 2.8. SEM images were taken at a low magnification to get an EDS spectra representative of the monolith as a whole. Although individual silver particles could not be located, the EDS map shows homogeneous distribution of silver throughout the entire monolith.

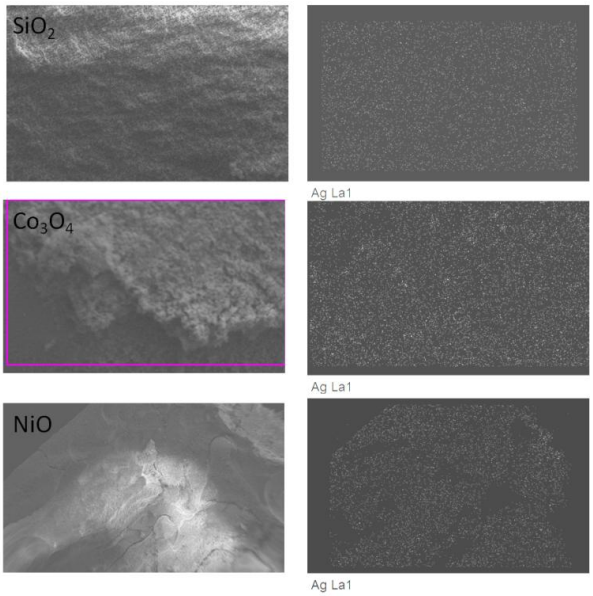

Figure 2.8. SEM images and corresponding EDS maps showing silver distribution

Nitrogen sorption data on the parent silica monolith and cobalt and nickel oxide replicas after silver deposition are shown in Figure 2.9. For the parent silica monolith/silver sample, the condensation step in the isotherm shifts to higher relative pressures, which indicates the silver has filled in some of the surfactant mesopores. The surface area has decreased to 93 m^2/g, which is a tremendous decrease. NL-DFT pore size distribution shows that the distribution has become much broader than in the parent silica. The isotherm for the cobalt oxide/silver sample has the same shape as that of the replica alone, with smaller volume of nitrogen adsorbed. This indicates that the silver has filled in some of the mesopores. The NL-DFT plot also shows a wider pore size distribution. The surface area of the nickel oxide-silver sample actually increases. The nickel oxide sample had a relatively low surface area to begin with at 15 m^2/g, so this increase is due to the silver particles. The NL-DFT plot (Figure 2.10) shows a much wider pore size distribution as with the other samples.

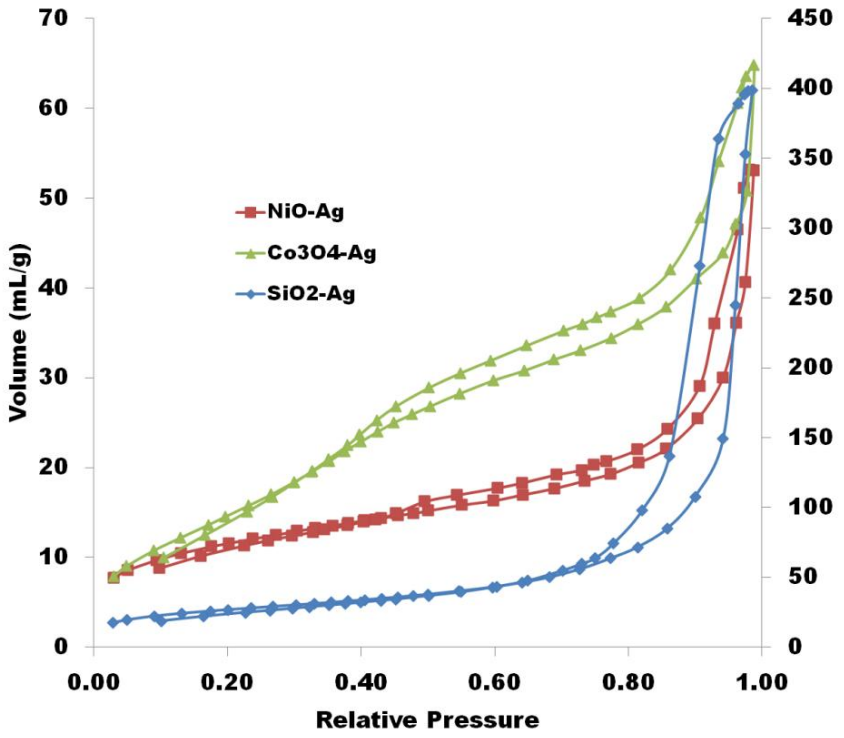

Figure 2.9. Isotherm of Ag loaded monoliths (SiO_2 is on secondary axis)

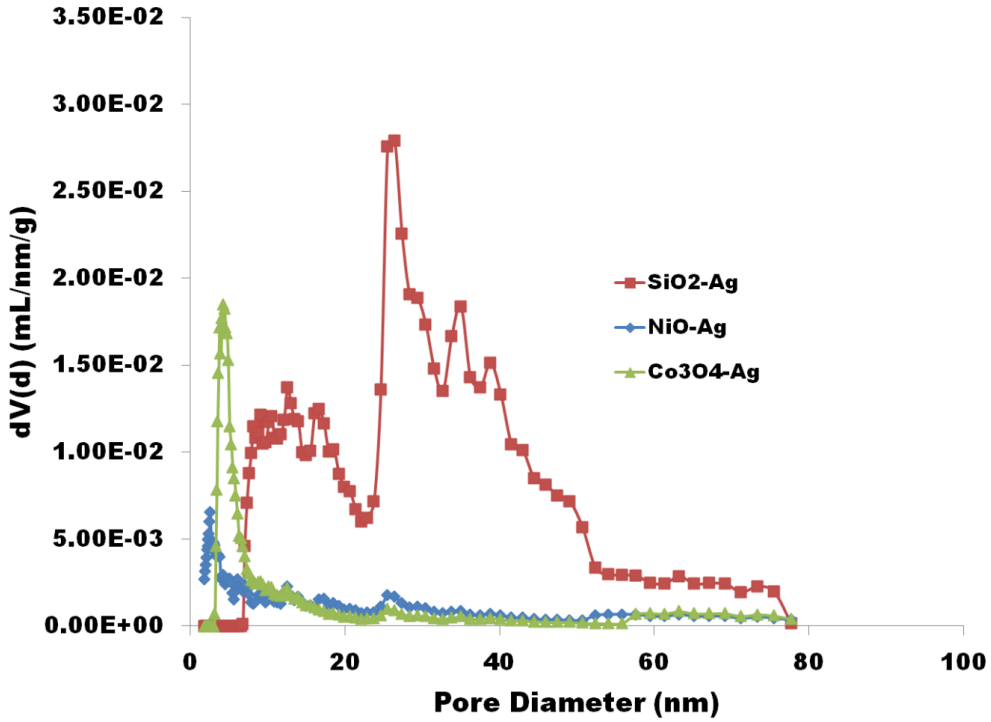

Figure 2.10. NL-DFT pore size distribution of Ag loaded monoliths

2.4.3 Catalysis Experiments

The parent silica monolith, cobalt oxide replica, and nickel oxide replica were evaluated for their catalytic activity by tracking the reduction of methyl orange in the presence of sodium borohydride. The parent silica monlith, cobalt oxide replica, and nickel oxide replica were run both without and with the addition of silver structure. Without the presence of the silver structure, the methyl orange is reduced, but at a much slower rate. Figure 2.11 shows the reduction in absorbance intensity at 463 nm. With the bare silica, nickel oxide, and cobalt oxide, it takes about an hour for the methyl orange to be reduced. In the case of the samples with the addition of silver structure, the methyl orange is reduced in a matter of minutes.

It has previously been show that silver nanoparticles are catalytically active in the reduction of several organic dyes, such as methyl orange, methylene blue, and rose bengal[14]. With time, aggregation of the unsupported nanoparticles leads to a reduction in the overall surface area of the particles, which then leads to decreased catalytic activity. Previous work has been done on silver nanoparticles on mesoporous particulate supports[15]. This helps eliminate the aggregation of the nanoparticles, but still leaves the task of separation after the reaction is done by filtration or centrifugation. The use of a monolithic support offers the same benefit of reduction of aggregation of nanoparticles and high catalytic activity with a much simpler means of removal of the catalyst after the reaction is finished. There has been a previous report of silver nanoparticle infiltrated silica monoliths[16], but our synthesis method for addition of the silver particles takes hours instead of several days.

The silica, cobalt oxide, and nickel oxide were all evaluated in an effort to see if there was any difference in catalytic activity between the silica and the metal oxides. In our preliminary experiments, only minor difference between the tested materials can be seen.

However, slowing down the rate of the reaction would allow us to better evaluate subtle differences if there are any. The results of catalysis experiments can be seen in Figure 2.11.

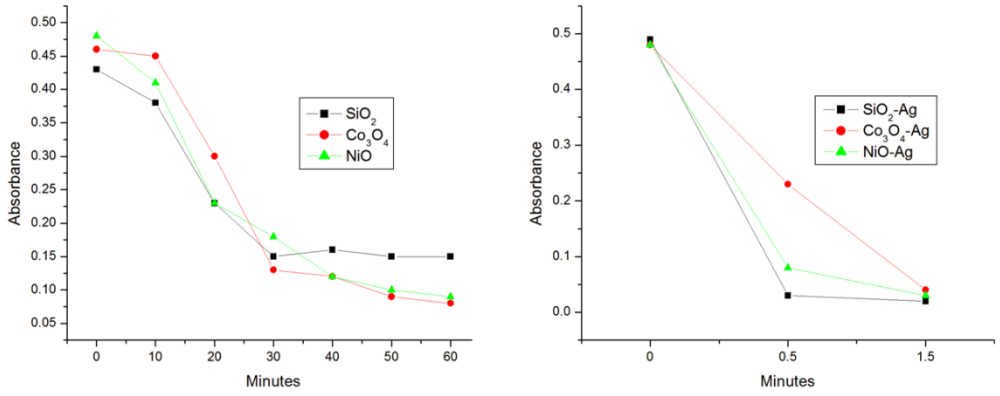

Figure 2.11. UV-Vis data from monolith and Ag loaded monoliths

2.5 Conclusions

In conclusion, we have successfully applied the nanocasting technique to synthesize hierarchically porous monoliths of carbon, cobalt oxide, and nickel oxide with ordered mesopore structures. To the best of our knowledge, this is the first report of nanocasting being used to form ordered monolithic structures. This method should be applicable to formation of a wide range of other monolithic oxides and alloys with ordered pore structures. We have also used these metal oxide replicas as catalyst supports for silver particles and proven them catalytically active for the reduction of methyl orange.

2.6 Acknowledgements

Primary support for this work was provided by NSF grant CHE-0719398 (MGB) and Academy of Finland grant 259310. The use of the microscopy facilities in the University of Alabama Central Analytical Facility is also gratefully acknowledged.

2.7 References

1. Rolison, D. R.; Long, J. W.; Lytle, J. C.; Fischer, A. E.; Rhodes, C. P.; McEvoy, T. M.; Bourg, M. E.; Lubers, A. M., Multifunctional 3D nanoarchitectures for energy storage and conversion. *Chem. Soc. Rev.* **2009,** *38*, 226–252.

2. Zhang, H.; Yu, X.; Braun, P. V., Three-dimensional bicontinuous ultrafast-charge and -discharge bulk battery electrodes. *Nature Nano.* **2011,** *6*, 277-281.

3. (a) Smått, J.-H.; Schunk, S.; Lindén, M., Versatile Double-Templating Synthesis Route to Silica Monoliths Exhibiting a Multimodal Hierarchical Porosity. *Chem. Mater.* **2003,** *15*, 2354-2361; (b) Smått, J.-H.; Weidenthaler, C.; Rosenholm, J. B.; Lindén, M., Hierarchically Porous Metal Oxide Monoliths Prepared by the Nanocasting Route. *Chem. Mater.* **2006,** *18*, 1443-1450.

4. Nakanishi, K., Pore Structure Control of Silica Gels Based on Phase Separation. *J. Porous. Mat.* **1997,** *4*, 67-112.

5. Lu, A.-H.; Zhao, D.; Wan, Y., *Nanocasting: A Versatile Strategy for Creating Nanostructured Porous Materials*. Royal Society of Chemistry: Cambridge, 2010; Vol. 11, p 265.

6. (a) Ryoo, R.; Joo, S. H.; Kryk, M.; Jaroniec, M., Ordered Mesoporous Carbons. *Adv. Mat.* **2001,** *13* (9), 677-681; (b) Yang, H.; Zhao, D., Synthesis of replica mesostructures by the nanocasting strategy. *J. Mater. Chem.* **2005,** *15*, 1217-1231; (c) Jiao, F.; Shaju, K. M.; Bruce, P. G., Synthesis of Nanowire and Mesoporous Low-Temperature LiCoO2 by a Post-Templating Reaction. *Angew. Chem. Int. Ed.* **2005,** *44*, 6550-6553; (d) Zheng, M.; Cao, J.; Liao, S.; Liu, J.; Chen, H.-q.; Zhao, Y.; Dai, W.; Ji, G.; Cao, J.; Tao, J., Preparation of Mesoporous Co_3O_4 Nanoparticles via Solid-Liquid Route and Effects of Calcination Temperature and Textural Parameters on Their Electrochemical Capacitive Behaviors. *J. Phys. Chem. C* **2009,** *113*, 3887-3894; (e) Sun, X.; Shi, Y.; Zhang, P.; Zheng, C.; Zheng, X.; Zhang, F.; Zhang, Y.; Guan, N.; Zhao, D.; Stucky, G. D., Container Effect in Nanocasting Synthesis of Mesoporous Metal Oxides. *J. Am. Chem. Soc.* **2011,** *133* (37), 14542-14545; (f) Yen, H.; Seo, Y.; Guillet-Nicolas, R.; Kaliaguinec, S.; Kleitz, F., One-step-impregnation hard templating synthesis of high-surface-area nanostructured mixed metal oxides ($NiFe_2O_4$, $CuFe_2O_4$ and Cu/CeO_2). *Chem. Comm.* **2011,** *47*, 10473–10475.

7. El Kadib, A.; Chimenton, R.; Sachse, A.; Fajula, F.; Galarneau, A.; Coq, B., Functionalized Inorganic Monolithic Microreactors for High Productivity in Fine Chemicals Catalytic Synthesis. *Angew. Chem. Int. Ed.* **2009,** *121*, 5069 –5072.

8. (a) Amatani, T.; Nakanishi, K.; Hirao, K.; Kodaira, T., Monolithic Periodic Mesoporous Silica with Well-Defined Macropores. *Chem. Mater.* **2005,** *17*, 2114-2119; (b) Zhong, H.; Zhu, G.; Wang, P.; Liu, J.; Yang, J.; Yang, Q., Direct synthesis of hierarchical monolithic silica for high performance liquid chromatography. *J. Chromatogr. A* **2008,** *1190*, 232–240.

9. Lu, A.-H.; Smatt, J.-H.; Linden, M.; Schueth, F., Synthesis of carbon monoliths with a multi-modal pore system by a one step impregnation technique. *New Carbon Materials,* **2003,** *18*, 265-270.

10. Meynen, V.; Cool, P.; Vansant, E. F., Verified syntheses of mesoporous materials. *Micro. Meso. Mater.* **2009,** *125*, 170-223.

11. Parmentier, J.; Saadhallah, S.; Reda, M.; Gibot, P.; Roux, M.; Vidal, L.; Vix-Guterl, C.; Patarin, J., New carbons with controlled nanoporosity obtained by nanocasting using a SBA-15 mesoporous silica host matrix and different preparation routes. *J. Phys. Chem. Solids* **2004,** *65*, 139-146.

12. Lu, A.-H.; Li, W.-C.; Schmidt, W.; Kiefer, W.; Schüth, F., Easy synthesis of an ordered mesoporous carbon with a hexagonally packed tubular structure. *Carbon* **2004,** *42*, 2939-2948.

13. Sayler, F. M. Synthesis and Application of Hierarchically Porous Metal and Metal Oxide Monolithic Materials. The University of Alabama, Tuscaloosa, AL, 2013.

14. Sietsma, J. R. A.; Meeldijk, J. D.; den Breejen, J. P.; Versluijs-Helder, M.; van Dillen, A. J.; de Jongh, P. E.; de Jong, K. P., The Preparation of Supported NiO and Co3O4 Nanoparticles by the Nitric Oxide Controlled Thermal Decomposition of Nitrates. *Angewandte Chemie* **2007,** *119* (24), 4631-4633.

15. Jiang, Z.-J.; Liu, C.-Y.; Sun, L.-W., Catalytic Properties of Silver Nanoparticles Supported on Silica Spheres. *J. Phys. Chem. B* **2005,** *109*, 1730-1735.

16. Zhu, Y.; Morisato, K.; Li, W.; Kanamori, K.; Nakanishi, K., Synthesis of Silver Nanoparticles Confined in Hierarchically Porous Monolithic Silica: A New Function in Aromatic Hydrocarbon Separations. *ACS Applied Materials & Interfaces* **2013,** *5* (6), 2118-2125.

CHAPTER 3
IN-SITU OBSERVATION OF NICKEL NANOPARTICLES DURING NANOCASTING INTO MESOPOROUS SILICA

3.1 Abstract

Hierarchically porous metals are of interest in several application fields, including heterogeneous catalysis. Here, we report the nanocasting of nickel metal into hierarchically porous SBA-15 type monoliths containing ordered arrays of mesopores. Upon removal of the silica template, nickel replicas showed no evidence of an ordered mesopore structure. TEM images of the nickel-silica composite and and XRD measurements of the nickel replica show that nickel nanoparticles larger than the silica mesopores have formed. Heated stage TEM measurements indicate that sintering of nickel nanoparticles occurs, which leads to rapid disruption of the silica template in vacuum. This disruption appears to occur more rapidly in vacuum than under hydrogen atmosphere.

3.2 Introduction

Porous metals have a variety of potential application fields, including catalysis, electrochemical chromatography, and separation[1]. Current syntheses of porous metals include metal foams[2], aerogels[3], and sintering of metal nanoparticles[4], but many of these processes lead to poor control over the final structure and wide pore size distributions are usually obtained. The process of nanocasting has recently been applied to several metals, such as gold[5] and platinum[6], in mesoporous silica particles, as well as some in monolithic form, such as nickel[7]. These nickel metal monoliths have been found to be similar to Rainey nickel in catalytic efficiency[8], but higher surface area and better control over pore size are still desired.

To reach these goals, the underlying process of the nanocasting of metal must be better understood. Herein, we report the use of in-situ transmission electron microscopy to follow the evolution of nickel in ordered mesoporous silica monoliths as a function of temperature. At elevated temperatures, sintering of the nickel metal crystallites disrupts the mesoporous silica template, leading to loss of order in the nickel replica.

3.3 Experimental

3.3.1 Materials

Tetramethyl orthosilicate (TMOS) was purchased from Alfa Aesar. Pluronic 123 (P123) surfactant was provided by BASF Corporation. Acetic acid, nickel nitrate, and potassium hydroxide were purchased from VWR. All materials were used as received.

3.3.2 Preparation of silica template

The SBA-15 monolithic silica template was prepared as previously reported[9]. For a typical synthesis, 6.25 g of P123 was dissolved in 20 mL 0.02 M acetic acid. After fully dissolved, the solution was cooled to 0 °C and 8 g TMOS was added and stirring continued for 30 minutes. The solution was then transferred into molds, gelled at 40 °C for 24 hours, and then 60 °C for 24 hours. The monoliths then underwent a steam treatment in an autoclave for 12 hours at 100 °C, followed by a water treatment at 100 °C. The surfactant was removed by calcination up to 600 °C at a ramp rate of 1 °C/minute.

3.3.3 Preparation of nickel/silica composites

A solution of 4.2 M nickel nitrate was used. Silica monoliths were vacuum infiltrated with solution, followed by heating under 5% H_2/N_2 at 150 °C for 10 h, then heating up to 300 °C at a ramp rate of 1 °C/min, and held for 4 h before being cooled down to room temperature. For

the replica, this process was repeated 4 additional times, followed by removal of the silica in 3M KOH. For heated stage experiments, only one cycle of infiltration/heating was performed.

3.3.4 Microscopy

SEM images were taken on a JEOL 7000 FE-SEM. TEM images were taken on an FEI Tecnai F-20 transmission electron microscope (TEM). Heated stage experiments utilized a Gatan double-tilt holder with heated stage and Gatan Smart Set Model 901 hot stage controller. Sample preparation consisted of grinding the monoliths, sonicating the resulting powder in ethanol, and then dispersing the slurry onto the TEM grid. The heating experiments were performed under vacuum. Nitrogen sorption measurements were taken on a Quantachrome Autosorb 2200 in helium mode.

3.4 Results and Discussion

The parent silica monolith used for nanocasting has a surface area of 760 m^2/g. The isotherm (Figure 3.S1) shows a steep uptake between relative pressures of 0.6 and 0.8, which indicates a uniform pore size. BJH pore distribution reveals a sharp peak at about 8 nm, which is consistent with previous reports of SBA-15 type silica pores. SEM and TEM images of the parent silica can be seen in Figure 3.S2.

The isotherm for the nickel-silica composite (Figure 3.1), shows nitrogen uptake between 0.15 and 0.6 in relative pressure. This is shifted to a lower pressure range than for the parent silica, indicating that there is some pore blockage by the deposited nickel (evidenced by the wide hysteresis), and/or that the silica template has not remained intact. The surface area of the composite is 124 m^2/g. The pore size distribution shows a much broader peak than the parent silica template. After etching, the surface area of the nickel monolith is 77 m^2/g, which is substantially higher than our previous work[10]. X-ray diffraction (XRD) was performed on the

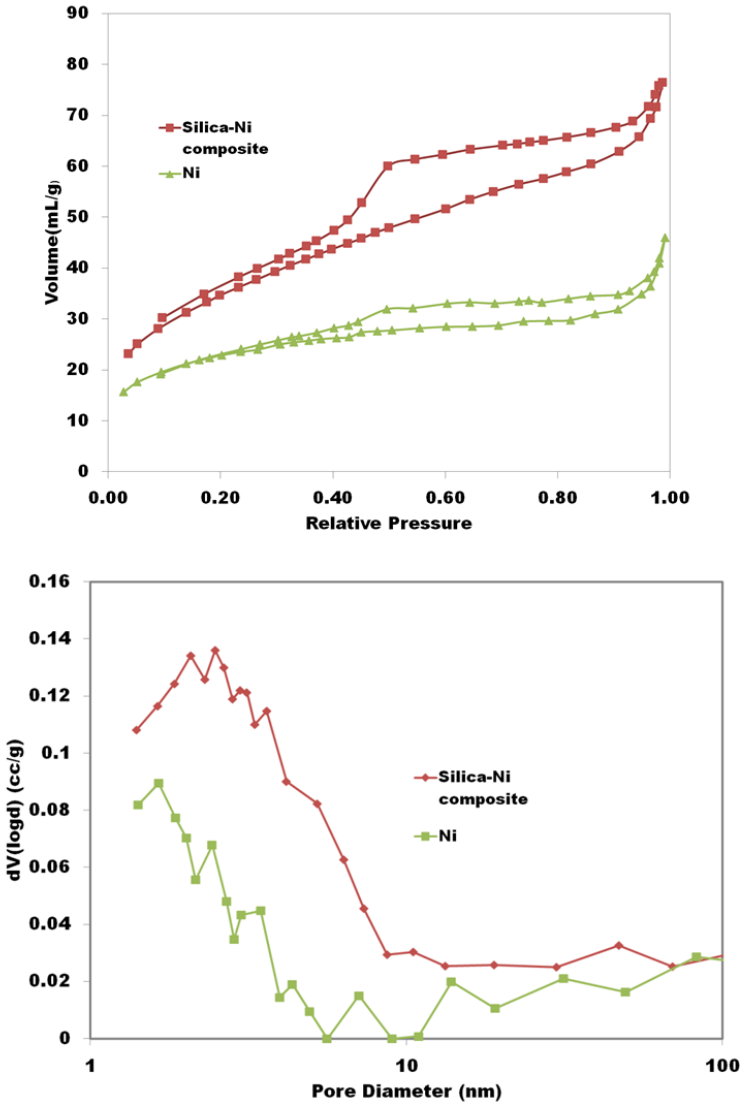

Figure 3.1. Top, nitrogen sorption isotherms, and bottom, BJH pore size distribution for Silica-Nickel composite and nickel replica

replica, and confirmed that it is nickel and not nickel oxide. All peaks can be assigned to metallic nickel (Figure 3.S3). Scherrer analysis yields a crystallite size of 16.8±3.6 nm, showing that there are particles present that are larger than the pores of the silica template.

SEM images (Figure 3.2a) of the nickel replica show macropore dimensions similar to the of the parent silica monolith. However, the macropore walls in the parent silica monolith (Figure 3.S2a) appear smoother than those in the nickel replica (Figure 3.2b). TEM images of etched replica (Figure 3.2c) show that there is no clear replication of the ordered mesopore

system of the silica template. To gain insight into the absence of ordered nickel nanostructure, we have imaged the mesoporous silica-nickel composite. The TEM image (Figure 3.2d) of the composite shows the widespread occurrence of nickel nanoparticles with diameters exceeding that of the parent silica mesopores, accompanied by an overall loss of mesoscopic ordering. This is not surprising since the mean nickel particle size obtained from the XRD measurements was clearly larger than the silica pores. There have been previous suggestions of breakage of silica pore walls from sintering of metal nanoparticles[11] that could explain this loss of ordering.

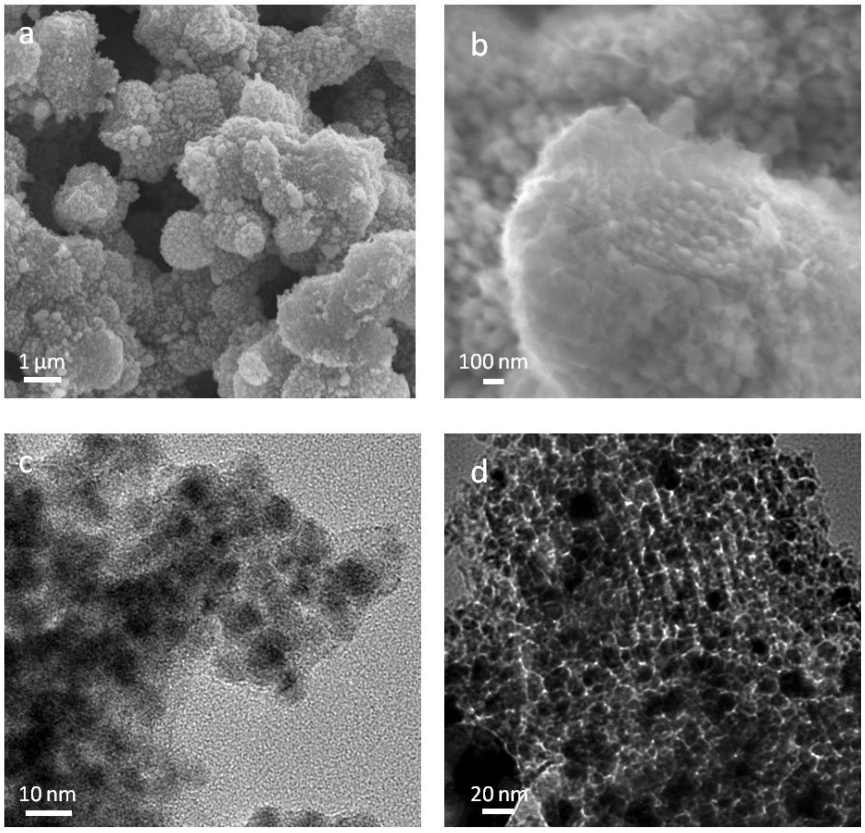

Figure 3.2. a,b)SEM image of etched nickel replica, c) Representative TEM image of etched sample, and d) TEM of silica-nickel composite

The temperature at which nickel nitrate is reduced to nickel under hydrogen was sufficiently high that it is believed that nickel particle growth could have occurred. To investigate this possibility, heated stage TEM experiments were performed on composite

samples that had only one round of infiltration and reduction to metal. The imaging location (Figure 3.3) was chosen where metal nanoparticles could clearly be resolved inside the silica mesopores. First, the sample was heated to 150 °C and held at this temperature for 20 minutes. Subsequent heating steps were done in increments of 25 °C, and each temperature was held for 20 minutes. In the image at 150 °C, the ordered pores of the silica matrix can clearly be seen, along with the nickel nanoparticles inside them. As the heating progresses, the silica matrix appears to become less ordered. In the final image, the majority of the nanoparticles are clearly larger than the silica pores, and the ordering seen before heating of the sample has all but disappeared.

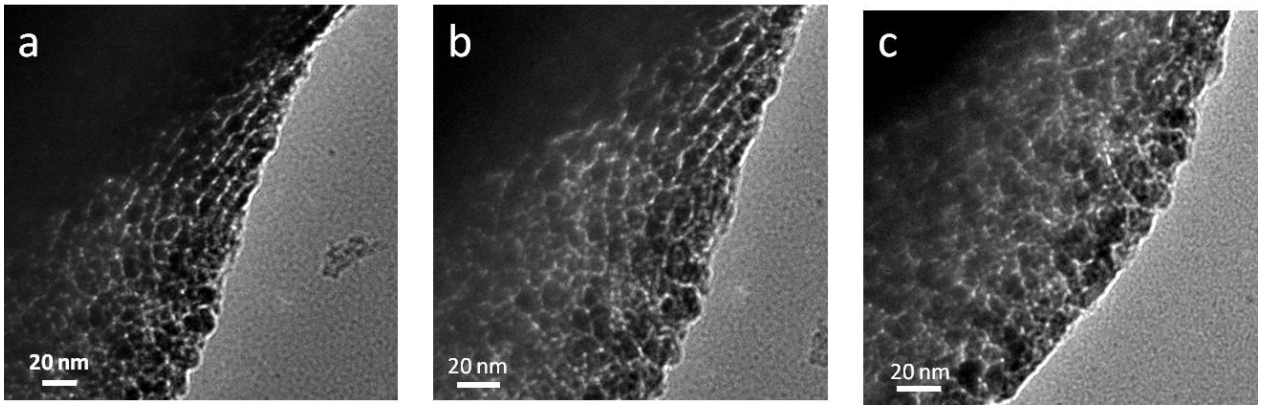

Figure 3.3. TEM images of silica-nickel sample during heating at a) 150 °C, b) 200 °C, and c) 250 °C

The observation of nickel particle growth appears to be consistent with the temperatures at which nickel nanostructures are believed to become mobile, so that sintering of nanoparticles can occur. This is known as the Hüttig temperature, which is about 245 °C for nickel metal[12]. The sintering of the nickel nanoparticles is most evident in the final image, which is slightly above the Hüttig temperature. A consequence of this sintering and growth of nickel nanoparticles is the disruption of the silica template. This disruption under vacuum is consistent with changes in the isotherm observed in the replication under hydrogen. However, it must be

pointed out that the sample in Figure 3.3a is made by decomposing the nickel nitrate precursor under hydrogen gas at 300 °C for three hours. This produces less sintering than is observed for eighty minutes at temperatures between 150 °C and 250 °C under vacuum. As we have previously reported[10], the presence and nature of a gaseous atmosphere can significantly impact the fidelity of replication. From Figures 3.2 and 3.3, we conclude that sintering of the nickel nanoparticles and disruption of the silica lattice occurs both under hydrogen and in vacuum, although slower under hydrogen, and that this process has a negative impact on the fidelity of replication for nickel.

We believe that grain growth and template disruption is important in metal replication generally, as evidenced by the reports of gold disrupting silica templates[11], and our own work on cobalt nanocasting[7].

3.5 Conclusions

We have observed the *in situ* destruction of a silica matrix during the nanocasting process. This has been observed for nickel metal nanocast into SBA-15 silica under hydrogen. From heated stage TEM experiments, we conclude that sintering of the nickel nanoparticles leads to disruption of the template, and occurs more rapidly under vacuum than under hydrogen. Successful production of a metal replica may be possible, but it would require the use of a reductant that is sufficiently efficient below 245 °C.

3.6 Acknowledgements

Primary support for this work was provided by NSF grant CHE-0719398 (MGB) and Academy of Finland grant 259310 (JHS). The use of the microscopy facilities in the University of Alabama Central Analytical Facility is also gratefully acknowledged.

3.7 References

[1] Zhang H, Cooper AI. Synthesis and applications of emulsion-templated porous materials. Soft Matter. 2005;1:107-13.

[2] Tappan BC, Steiner SA, Luther EP. Nanoporous Metal Foams. Angewandte Chemie International Edition. 2010;49:4544-65.

[3] Gash AE, Satcher Jr JH, Simpson RL. Monolithic nickel(II)-based aerogels using an organic epoxide: the importance of the counterion. Journal of Non-Crystalline Solids. 2004;350:145-51.

[4] Lee MN, Mohraz A. Hierarchically Porous Silver Monoliths from Colloidal Bicontinuous Interfacially Jammed Emulsion Gels. Journal of the American Chemical Society. 2011;133:6945-7.

[5] Han Y-J, Kim JM, Stucky GD. Preparation of Noble Metal Nanowires Using Hexagonal Mesoporous Silica SBA-15. Chem Mater. 2000;12:2068-9.

[6] Kleitz F, Choi SH, Ryoo R. Cubic Ia3d large mesoporous silica: synthesis and replication to platinum nanowires, carbon nanorods and carbon nanotubes. Chem Commun (Cambridge, U K). 2003:2136-7.

[7] Sayler FM. Synthesis and Application of Hierarchically Porous Metal and Metal Oxide Monolithic Materials. Tuscaloosa, AL: The University of Alabama; 2013.

[8] Sayler FM, Grano AJ, Scogin W, Sanders P, Smått J-H, Shaughnessy KH, et al. Formation and Applications of Hierarchically Porous Carbon, Metals and Metal Oxides Formed by Nanocasting. MRS Online Proceedings Library. 2012;1389:null-null.

[9] Zhong H, Zhu G, Wang P, Liu J, Yang J, Yang Q. Direct synthesis of hierarchical monolithic silica for high performance liquid chromatography. J Chromatogr A. 2008;1190:232-40.

[10] Smått J-H, Sayler FM, Grano AJ, Bakker MG. Formation of Hierarchically Porous Metal Oxide and Metal Monoliths by Nanocasting into Silica Monoliths. Advanced Engineering Materials. 2012;14:1059-73.

[11] Perez-Cabero M, El HJ, Solsona B, Vazquez I, Dejoz A, Garcia T, et al. Stable anchoring of dispersed gold nanoparticles on hierarchic porous silica-based materials. J Mater Chem. 2010;20:6780-8.

[12] Moulijn JA, van Diepen AE, Kapteijn F. Catalyst deactivation: is it predictable?: What to do? Applied Catalysis A: General. 2001;212:3-16.

3.8 Supplemental Figures

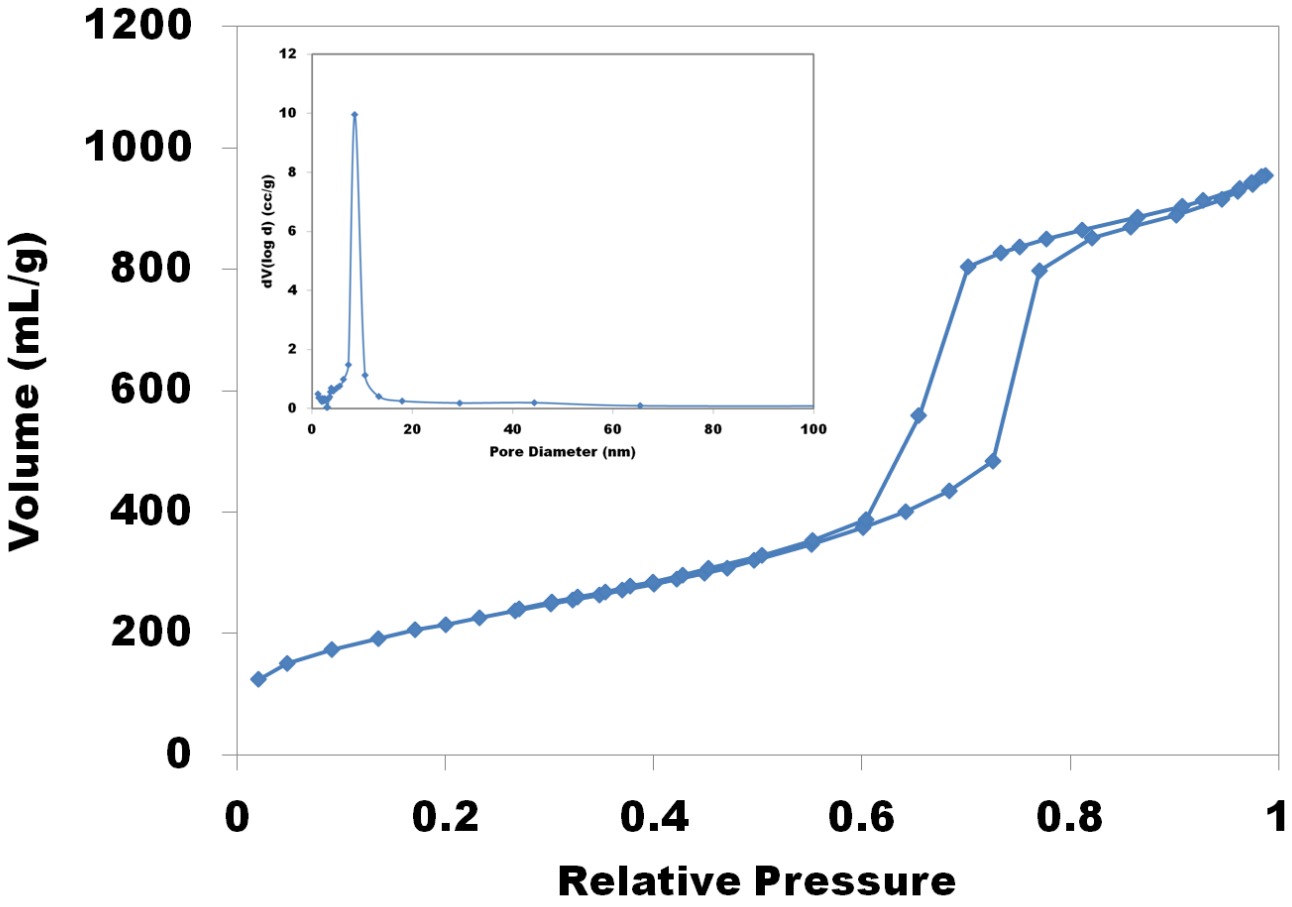

Figure 3.S1. Nitrogen Sorption isotherm and BJH pore size distribution for silica template

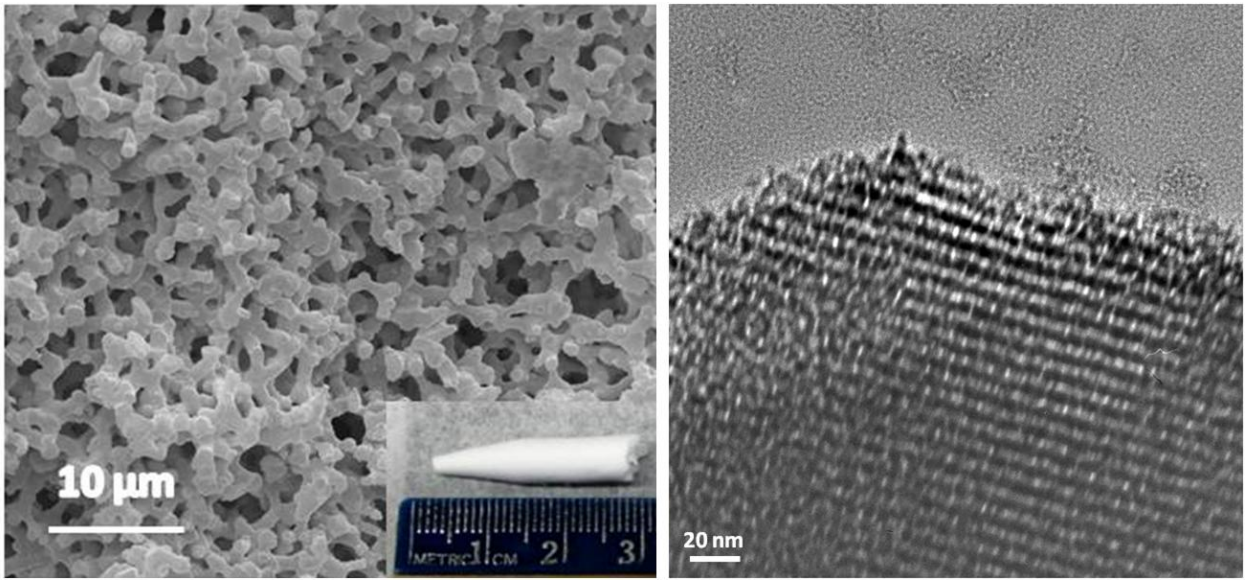

Figure 3.S2. Left, SEM, and right, TEM, of silica monolith template

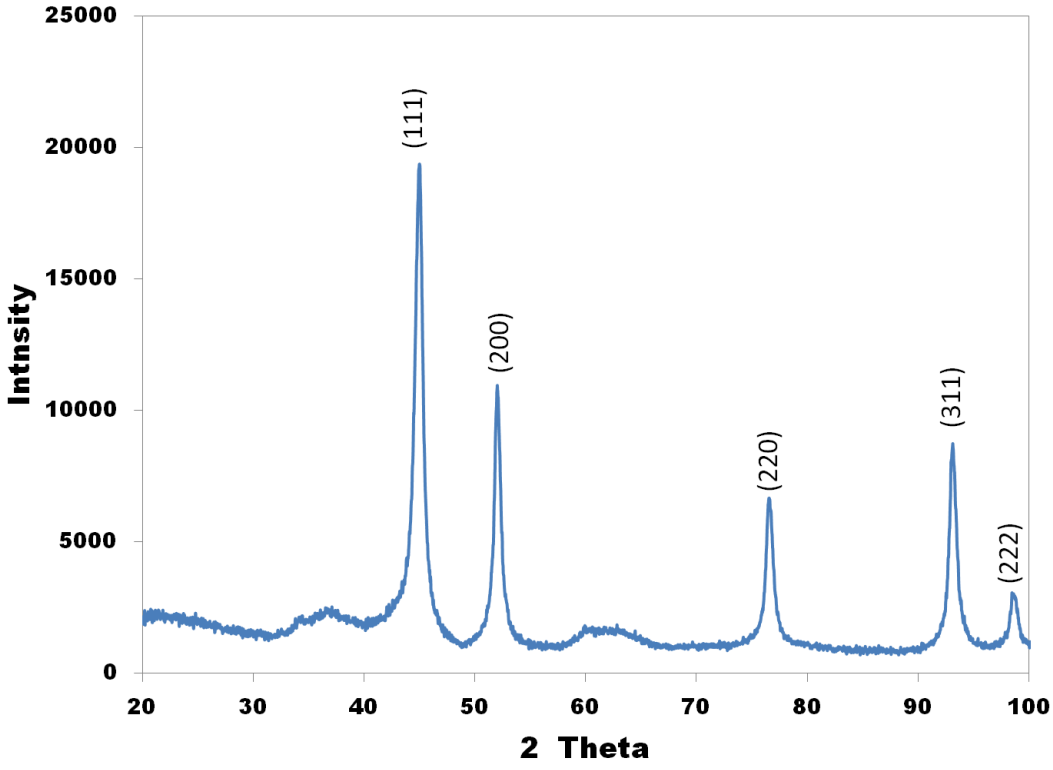

Figure 3.S3. XRD Diffractogram of Nickel Replica

CHAPTER 4
ALTERNATIVE ETCHING METHODS TO EXPAND NANOCASTING, AND USE IN THE SYNTHESIS OF HIERARCHICALLY POROUS NICKEL OXIDE, ZINC OXIDE AND COPPER MONOLITHS

4.1 Abstract

Nanocasting into silica templates for preparation of mesoporous materials has up to now been limited to those metal oxides and metals that can withstand the harsh silica etching processes currently used. Here we demonstrate two new methods of removing the silica template, either by dissolving the silica in methanolic base or by dissolution in aqueous base under an external potential. The utility of these methods is demonstrated in the synthesis of hierarchically porous zinc oxide, nickel oxide and copper monoliths which would dissolve or react using other template removal methods. The successful etching of monolithic zinc oxide using methanolic base etching can be explained by the reduced solubility of zinc oxide in methanol compared to aqueous base, while it also reduces the formation of hydroxides when etching the nickel oxide and copper monoliths. Alternatively, the formation of highly soluble copper oxide/hydroxide can be avoided by holding the copper monolith at a sufficiently negative potential while kept in aqueous etch solution.

4.2 Introduction

Hierarchically porous materials are of great interest for various applications such as catalysis, advanced batteries, and solar cells.[1, 2] Currently, there are several classes of these materials available, such as metal foams,[3] aerogels, xerogels,[4] and a variety of materials produced by spinodal decomposition.[5] These materials are produced by direct synthesis from

precursors. For many materials for which no direct templating method is available, it is often possible to produce them by nanocasting.[6-13] Nanocasting uses a hard template, usually either silica or carbon, as a mold for another material. The mold is then removed leaving a replica. For hierarchically porous materials it is possible to replicate only the mesoscale structure, giving a negative replica at the mesopore level and positive replica at the macropore level of the original structure.

Typical synthesis methods for hierarchically porous materials yield powders. However, a monolithic form consisting of a macroscopic single piece is advantageous in some applications. In catalysis, a monolithic form allows for easy separations of products from the catalyst[14] and in separations, hierarchically porous stationary phases are significantly faster than traditional packed columns.[15, 16] We have demonstrated the use of nanocasting to produce hierarchically porous monoliths of carbon,[17] metal oxides[18] and most recently some metals.[12]

A significant limitation in the field of nanocasting is the ability to remove the silica template after formation of the silica-material composite. Currently, aqueous base or hydrofluoric acid is used to remove the silica. This means that for amphoteric materials, such as zinc oxide, it is difficult to remove the silica template without losing the nanostructure of the replica[19, 20]. One method that has been successfully used to produce these materials has been a double templating method.[21] In this method, the silica is first replicated into carbon, and then the resulting carbon replica is used as a template in a second nanocasting step to give the desired end product. Although cumbersome, this approach has proven to be effective for some materials, but can lead to lower surface areas and destruction of nanostructure due to the high temperatures required to burn off carbon and the amount of energy that is released from the process. A mild (pH 12) basic etch has been successfully used on zinc oxide nanocast into thin silica films,[22] but

the slow rate of etching and limited hydroxide ion concentration mean that this method is unlikely to be suitable for etching of bulk materials such as powders or monoliths. Hydrofluoric acid can be used to etch some metal oxide/silica composites, but is dangerous to use, and is also not compatible with most metals.

In this work we report a new alcoholic base etch that allows silica to be used as the template for synthesis by nanocasting of hierarchically porous zinc oxide, nickel oxide and copper monoliths. In addition, we also show that voltage stabilization while etching in aqueous base solution can be used to produce stable copper monoliths. The demonstration in monoliths is generally a much more rigorous test than application to nanocasting of particles, since any short comings of the procedure would result in the fragmentation of a monolith, where such short comings would only decrease the size of nanocast particles.

4.3 Experimental

4.3.1 Chemicals

All chemicals used are commercially available and used as received. Polyethylene glycol 35000 (PEG 35000), tetraethylorthosilicate (TEOS), zinc nitrate hexahydrate ($Zn(NO_3)_2 \cdot 6H_2O$), nickel nitrate hexahydrate ($Ni(NO_3)_2 \cdot 6H_2O$), copper nitrate ($Cu(NO_3)_2 \cdot 3H_2O$)) and potassium hydroxide (KOH) were all obtained from VWR. Octadecyltrimethylammonium bromide (C_{18}TAB) was obtained from Genscript.

4.3.2 Synthesis of Silica Monolith Templates

Silica monolith templates were synthesized using a previously reported method.[23] In a typical synthesis, the PEG is dissolved in a dilute nitric acid solution, and then TEOS is added. The solution is stirred until no longer cloudy; C_{18}TAB is then added and stirred until dissolved. The resulting sol is poured into molds and undergoes gelation for 24 hours, removed, and then

treated in 1 M ammonium hydroxide at 90 °C for 12 hours. The monoliths are then rinsed and neutralized in HNO_3 and acetone, dried for 3 days at 40 °C, and calcined at 550 °C for 5 hours with a ramp rate of 1 °C/minute.

4.3.3 Synthesis of Replicas

A precursor solution of the metal nitrate salt was introduced into the silica template through vacuum infiltration. The solution concentrations used were 4.6 M for nickel (II) nitrate, 6 M for zinc nitrate, and 5.7 M for copper(I) nitrate. All infiltrated templates were heated at 150 °C for 12 hours under nitrogen flow. If nickel oxide or zinc oxide were the desired end product, the infiltration and heating steps were performed a total of 3 times, with a final heating at 400 °C, with a ramp rate of 1°C/min, under nitrogen flow. If the desired end product was copper, the infiltrated monoliths were heated at 150 °C for a total of 12 hours under nitrogen flow, followed by heating at 310 °C under nitrogen flow for 1 hour to produce copper (II) oxide. This process was performed a total of 4 times and produced a copper oxide-silica composite. Reduction of the copper oxide to copper metal was done under methanol vapor for one hour at 310 °C. This procedure was used for the samples used in both the methanolic base and voltage stabilized etch procedures described below.

4.3.4 Etching of Silica

A 3 M methanolic potassium hydroxide solution (methanol dried by vacuum distillation) was used to chemically dissolve the silica template, releasing nickel oxide, zinc oxide and copper monoliths. Etching was carried out twice for 24 hours at 60 °C, followed by rinsing with methanol until any residual hydroxide was removed. In the case of the copper monolith, a second method was also used; this method will be referred to as a voltage stabilized etch. For this, the copper-silica composite was attached to a piece of copper tape to provide a point of

electrical contact. A potential of negative 3 volts vs. a platinum basket counter-electrode was applied to the copper-silica composite. The composite, while the potential was applied, was then placed in an aqueous 3 M KOH solution and allowed to sit for 2 hours. Subsequent rinsing with water until a neutral pH was reached was also carried out with the potential applied.

4.3.5 Characterization

Scanning electron microscope images (SEM) were taken on a JEOL 7000 FE-SEM. Nitrogen physisorption measurements were taken on a Quantachrome Nova 2200e surface area and pore size analyzer. Isotherms were analyzed with Quantachrome NovaWin software version 10.01, and the Barrett-Joyner-Halenda method was applied to the adsorption branch to determine the pore size distribution. X-ray diffraction (XRD) measurements were performed on a Bruker D8 Discover with GADDS and a Hi-Star area detector. Nickel oxide diffractograms were taken with a cobalt source, and copper and zinc oxide diffractograms taken with a copper source. Raman spectra of nickel hydroxide compounds were obtained on a Horiba Jobin Yvon HR800 Raman spectrometer with an Olympus BX41 microscope.

4.4 Results

Upon etching, all replicas produced free-standing monoliths. SEM and XRD measurements were performed on cross-sections taken from the core of the monoliths. Upon visual inspection, the cross-section of all monoliths appeared homogeneous in color and consistency. The SEM images presented represent the typical morphology observed within the cross-section of the sample. Some variations were observed in the replicas near the outermost edges of the replicas, and this can be attributed to incomplete removal of excess solution before heating and decomposition steps. This was not typical behavior for every sample and therefore was not shown.

4.4.1 Silica

SEM images of the parent silica monolith can be seen in Figure 4.1. The silica monolith template consists of a network of macropores. Inside the walls of these macropores are textural mesopores, which line the walls, and surfactant templates mesopores, which are within the walls. The SEM image shown here is only representative in scale of the macropore size. Variations in the replica macropore size can be due to replication of different batches of the same synthesis of the silica template. The nitrogen adsorption isotherm and pore size distribution can be seen in Figure 4.S1. The isotherm shows two regions of capillary condensation. The one in the lower pressure range is due to the surfactant templated mesopores and the one in the higher range is due to the textural mesopores. The resulting surface of the parent silica is 641 m^2/g, or 1667 m^2/cm^3. This is consistent with what has previously been reported for this material.[23]

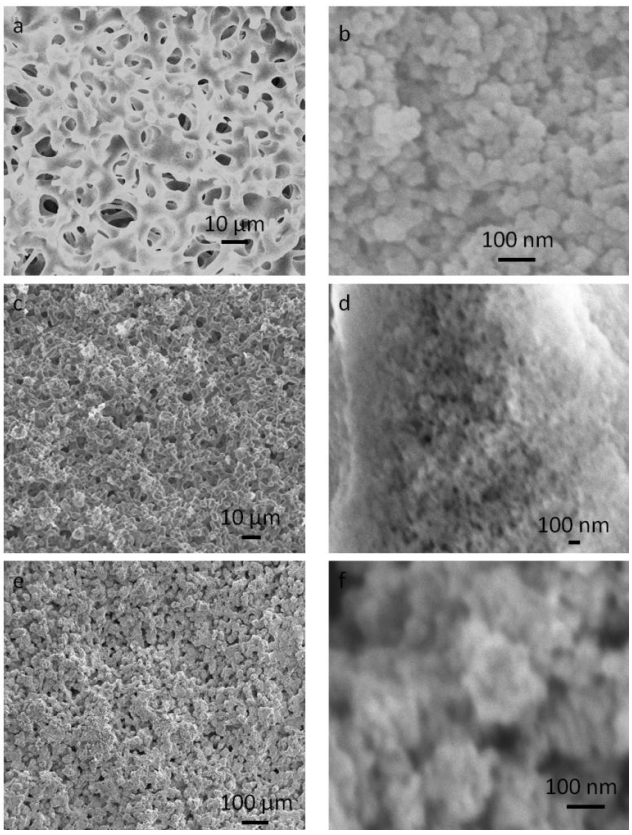

Figure 4.1. SEM images of (a, b) parent silica monolith, (c, d) ZnO replica, and (e, f) NiO replica

The surface areas and total pore volumes for the silica monoliths and for the metal oxide replicas are summarized in Table 4.1.

Table 4.1. Nitrogen Physisorption Data from parent silica monolith and replicas

	Surface Area (m^2/g)	Surface Area (m^2/cm^3)	Total Pore Volume (cc/g)
SiO_2	641	1667	1.12
ZnO	28	157	0.257
NiO	41	273	0.064
Cu-m	2.6	23.3	0.007
Cu-v	1.3	11.7	0.005

4.4.2 Zinc Oxide

SEM images of the zinc oxide replica can be seen in Figure 4.1. The morphology of the macropores is very similar to that of the parent silica monolith. There appears to be fine structure within the walls of the macropores, but higher magnification images are difficult to obtain due to charging of the sample. XRD (Figure 4.2) confirms the formation of zinc oxide in the hexagonal wurtzite structure. The nitrogen adsorption isotherm (Figure 4.3) shows one region of capillary condensation at higher relative pressures, with a fairly narrow hysteresis loop consistent with an open pore structure. The BJH pore size distribution indicates that the sample has pores in the range of 25–100 nm. This broadness and the location of the peak in the pore size distribution would indicate that mainly the textural mesopores were filled instead of the surfactant templated mesopores. The resulting surface area is 28 m^2/g, or 157 m^2/cm^3.

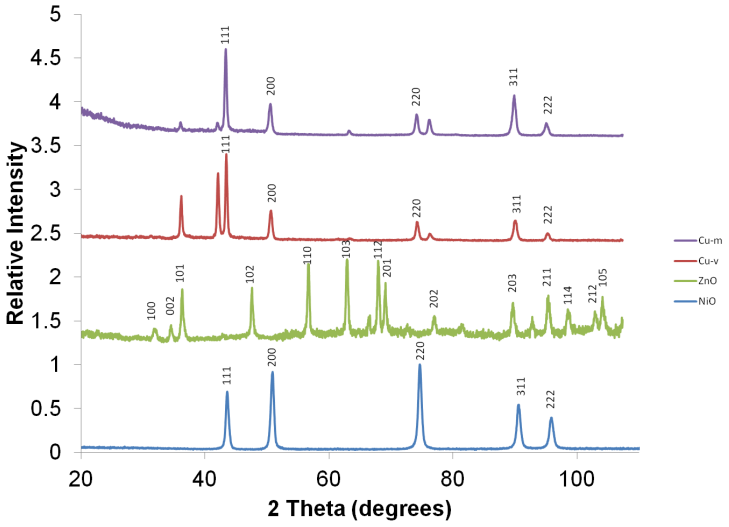

Figure 4.2. XRD diffractograms of NiO, ZnO, CU-m, and Cu-v

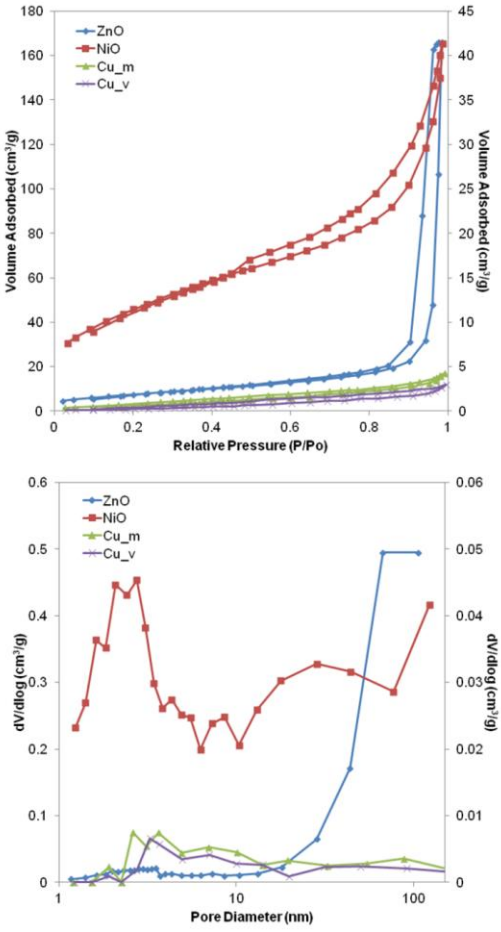

Figure 4.3. Top) Nitrogen physisorption isotherms and bottom) BJH pore size distributions of replicas. ZnO and NiO plots correspond to primary axis and Cu-m and Cu-v to secondary axis

4.4.3 Nickel Oxide

4.4.3.1 Methanolic Base Etch

SEM images of the nickel oxide replica can be seen in Figure 4.1. The topology of the macropore walls is much coarser than that of the parent silica monolith. XRD, Figure 4.2, shows that the resulting monolith is nickel oxide, NiO. Nitrogen sorption isotherm (Figure 4.3) shows a small region of capillary condensation at higher relative pressures. This would indicate that most of the porosity detected by the nitrogen sorption corresponds to replication of the textural mesopores or agglomerates on the macropore walls, which agrees with the SEM images. The broad hysteresis loop is consistent with an interconnected pore structure, suggesting some "ink bottle" type pores. The resulting surface area is 41 m^2/g, or 273 m^2/cm^3. From the BJH pore size distribution plot, it is evident that the NiO sample has a very broad pore size distribution consistent with some replication of the surfactant templated silica mesopores, as it shows a small peak in the pore size distribution in the 3-7 nm range. This peak is similar to what has been observed in earlier studies on nanocasting into monoliths, but is significantly smaller.[12, 24]

4.4.3.2 Aqueous Base Etch

Attempts using 1 M aqueous sodium hydroxide solution to remove the silica template were unsuccessful. This method resulted in the monoliths breaking into smaller pieces (mm sized or larger) accompanied by the formation of a precipitate. Raman spectroscopy (Figure 4.4) showed the presence of nickel hydroxide on both the precipitate and pieces. This is evidenced by the peaks between 3550 cm^{-1} and 3680 cm^{-1}, which have previously been observed in spectra of nickel hydroxide.[25]

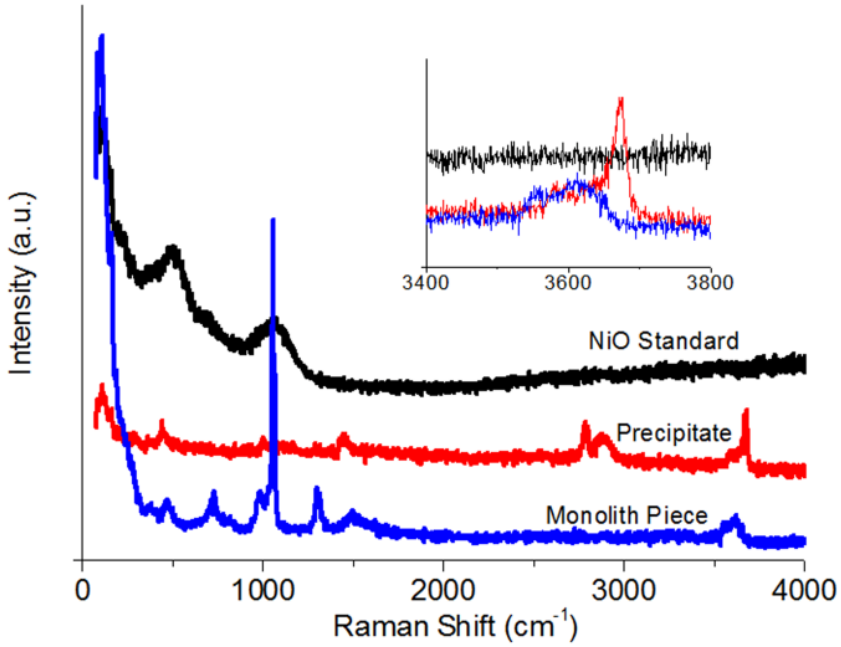

Figure 4.4. Raman spectra of nickel oxide standard, precipitate from aqueous etch, and monolith piece from aqueous etch

4.4.4 Copper

4.4.4.1 Methanolic Base Etch

SEM images of the copper replica etched with basic methanol (Cu-m, Figure 4.5c) show a macropore structure that is much coarser than that present in the parent silica monolith. Within the macropore walls (Figure 4.5d), there are smaller particles of 100 nm or less in diameter which seem to be agglomerates from smaller particles. XRD (Figure 4.2) and EDS (Figure 4.S2) confirm that the monolith is copper in a face centered cubic packing. The nitrogen sorption isotherm shows a small nitrogen uptake over the whole pressure range, and gives a surface area of 2.6 m^2/g, or 23.3 m^2/cm^3. This is indicative that the copper synthesis method would need to be optimized for future samples, but demonstrates that the methanol etch works and can successfully leave a copper monolith.

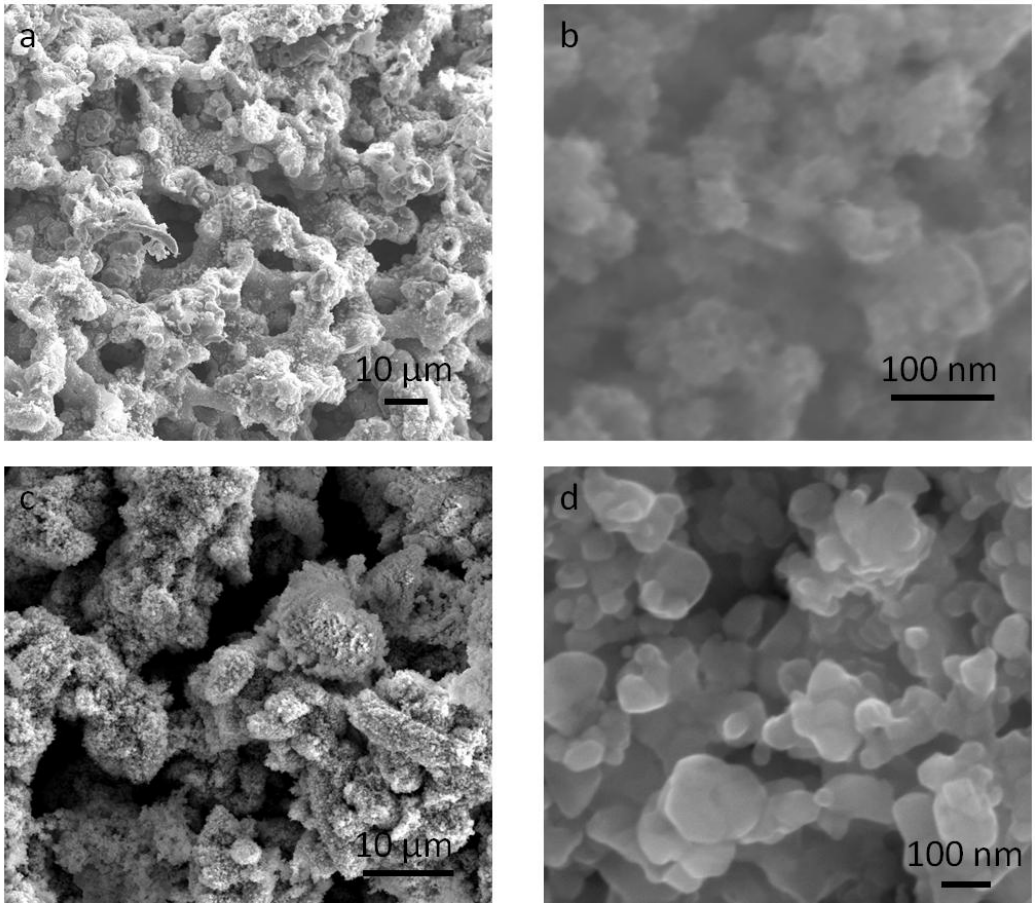

Figure 4.5. SEM images of (a, b) Cu-v and (c, d) Cu-m

4.4.4.2 Voltage Stabilized Etch

After etching as outlined in the experimental section the voltage was removed, and the monolith removed from the copper tape. The monolith held together very well and was observed to have a metallic copper color. SEM images of the copper replica produced by the voltage stabilized etching method (Cu-v, Figure 4.5a) show a macropore structure similar to that of the parent silica monolith. Higher magnification SEM images (Figure 4.5b) show that there are some smaller structures located within the macropores. Both energy dispersive spectroscopy (EDS) (Figure 4.S2) and XRD (Figure 4.2) show that the material produced is copper, face centered cubic packing. Nitrogen sorption again indicates a small uptake in the entire pressure range, and gives a surface area of 1.3 m^2/g or 11.7 m^2/cm^3.

4.5 Discussion

For all four monoliths synthesized, the surface areas are significantly lower than those of the parent silica template. As we have discussed at length elsewhere,[12] nanocasting involves a series of steps: infiltration, drying, decomposition, reduction (for metals), and template removal. The first two steps are similar to materials already reported and so will not be dealt with in detail here. Decomposition is carried out at elevated temperatures where the zinc oxide, nickel oxide or copper oxide being formed may become mobile if the temperature exceeds the Tammann or Hüttig temperatures where particles become mobile and can sinter.[12, 26, 27] These temperatures are respectively one half and one third of the melting point of the solid. This would give Hüttig temperatures of 474 ^{o}C for zinc oxide, 395 ^{o}C for nickel oxide, 260 ^{o}C for copper oxide, and 180 ^{o}C for copper.[28, 29] The nickel oxide and copper oxide samples were heated above their Hüttig temperatures and so may be mobile, depending upon the strength of the interactions with the silica walls. Another possibility is raised by Yue et al. [30] who suggest that the growing nanoparticles can disrupt the silica matrix.

4.5.1 Zinc Oxide

The successful etching of monolithic zinc oxide using the methanolic base etching method presumably reflects the differences in solubility of zinc oxide in methanol compared with that in aqueous base. In general, inorganic salts are less soluble in alcohol than in aqueous media, and our success with removing silica while leaving the complete zinc oxide monoliths indicates that there must be a considerable difference in solubility in basic methanol between silica and zinc oxide. As is discussed below for nickel oxide it, is clear that even a relatively low solubility can be sufficient to cause a monolith to fragment.

4.5.2 Nickel Oxide

Nanocasting of nickel oxide in particles has been reported by a number of groups.[30-35] However, it has not previously been reported by nanocasting into monolithic silica templates. The prime difficulty has been in the aqueous etch which leads to formation of nickel hydroxide and fragmentation of the monoliths. One explanation for the formation of nickel hydroxide is that the nickel oxide was simply reacting with the hydroxide in solution and forming nickel hydroxide on the surface of the monolith. This nickel hydroxide is slightly soluble at room temperature in basic solutions[36], and therefore can be inferred to be more soluble at the elevated temperatures at the hydroxide etch is performed. This conversion to hydroxide during the dissolution process would cause cracking in the monoliths, resulting in them fragmenting.

4.5.3 Copper

Copper in the pure form can not be produced by the nanocasting approach with current etching methods. There are two examples of where nanocast materials containing copper have been successfully removed from a silica template using an aqueous base etch. We have prepared porous monoliths of Sterling silver, an alloy which is 90% silver mixed with 10% copper, by nanocasting into monolithic silica templates.[37] The alloy consists of micrometer sized regions of pure silver and pure copper. We were able to use a standard aqueous base etch, to prepare 10 cm long 4 mm monoliths, which did not show any indications of copper hydroxide formation. Similarly Yen et al.[38] report nanocasting of a mixture of copper and cerium nitrates into mesoporous silica powders to give a mixture of mesoporous copper and cerium oxide. These authors did not report any indications of formation of copper hydroxide. For monoliths in a standard aqueous base etch, any oxidized part of the copper surface would react with hydroxide to form copper hydroxide. This hydroxide would result in weakening of the copper structure due

to this conversion. In a methanolic base etch, it is believed that the methanol is acting as a reducing agent to keep the copper from being oxidized to the hydroxide via the oxide.

The alternative etching method explored in this work, voltage stabilized etching, is one that is particularly applicable to metal monoliths. The basis for this method can be seen by referring to the Pourbaix diagram[39], which shows that copper in an aqueous solution with a high pH can be converted to copper (II) oxide or copper hydroxide. From the diagram it can also be seen that it should be possible to prevent these reactions by holding the copper monolith at a sufficiently negative potential, 3 volts, while in the aqueous etch solution. Our observations certainly are in accord with this expectation. This method speaks to the connectivity of the replica. If the replica did not have good connectivity, then pieces that were not electrically connected would have been converted to copper hydroxide and dissolved during the etching process.

Formation of copper monoliths is more difficult because of the need to carry out a number (four) of infiltration cycles. The nitrate salts are used because they have much higher solubility than other copper salts and therefore can build up enough material to make a complete replica in fewer cycles. The decomposition of the copper nitrate salt under methanol vapor does lead to copper formation. However, a second infiltration cycle with copper nitrate solution is observed to give copious evolution of brown gas which is sufficiently violent to lead to fragmentation of the silica template. It was therefore necessary to decompose the copper nitrate to the copper (II) oxide after each infiltration, with a final reduction to metallic copper.

4.6 Conclusions

We have developed new methods of removing the silica template used in nanocasting, and successfully demonstrated these methods by synthesizing hierarchically porous monoliths of

zinc oxide, nickel oxide (free of nickel hydroxide), and copper metal. The use of methanolic base etch should also be applicable to etching the silica template widely used in nanocasting into mesoporous silica particles. The voltage stabilized etch can also be applicable to other monolithic metal samples.

4.7 Acknowledgements

The use of Central Analytical Facility instruments (SEM, XRD) is greatly acknowledged. This work was partially supported by NSF under grant number CHE-0719398 (MGB) and by the Academy of Finland through the project number 259310 (JHS). The technical assistance of Ms. Kate Price in the development of the voltage stabilized etch, Mr. Jake Mims for sample preparation, and Mr. Clifton Watkins for running Raman spectroscopy is also much appreciated.

4.8 References

1. B.-L. Su, C. Sanchez and X.-Y. Yang (editors): Hierarchically Structured Porous Materials (Wiley-VCH Verlag, City, 2012).

2. Y. Li, Z.-Y. Fu and B.-L. Su: Hierarchically Structured Porous Materials for Energy Conversion and Storage *Adv. Func. Mater.*, 1 (2012).

3. J. Banhart: Metal Foams: Production and Stability *Adv. Eng. Mat.* **8**(9), 781 (2006).

4. J. Biener, M. Stadermann, M. Suss, M.A. Worsley, M.M. Biener, K.A. Rose and T.F. Baumann: Advanced carbon aerogels for energy applications *Energy Environ. Sci.* **4**, 656 (2011).

5. K. Nakanishi: Hierarchically Porous Materials by Phase Separation: Monoliths, in Hierarchically Structured Porous Materials: From Nanoscience to Catalysis, Separation, Optic, Energy, and Life Science., edited by S. Bao-Lian, C. Sanchez and Y. Xiao-Yu (Wiley-VCH Verlag, City, 2012), pp. 241.

6. C.H. Ko and R. Ryoo: Imaging the channels in mesoporous molecular sieves with platinum *Chem. Comm.*, 2467 (1996).

7. R. Ryoo, S.H. Joo and S. Jun: Synthesis of Highly Ordered Carbon Molecular Sieves via Template-Mediated Structural Transformation *J. Phys. Chem. B.* **103**, 7743 (1999).

8. H. Yang, Q. Shi, X. Liu, S. Xie, D. Jiang, F. Zhang, C. Yu, B. Tu and D. Zhao: Synthesis of ordered mesoporous carbon monoliths with bicontinuous cubic pore structure of Ia3d symmetry *Chem. Comm.*, 2842 (2002).

9. F. Dao, Q. Lu and D. Zhao: Synthesis of Crystalline Mesoporous CdS Semiconductor Nanoarrays Through a Mesoporous SBA-15 Silica Template Technique *Adv. Mat.* **15**(9), 739 (2003).

10. A.-H. Lu, D. Zhao and Y. Wan: Nanocasting: A Versatile Strategy for Creating Nanostructured Porous Materials (Royal Society of Chemistry, City, 2010).

11. A.-H. Lu and F. Schüth: Nanocasting: a Versatile Strategy for Creating Nanostructured Porous Materials *Adv. Mat.* **18**, 1793 (2006).

12. J.-H. Smått, F.M. Sayler, A. Grano and M.G. Bakker: Formation of Hierarchically Porous Metal Oxide and Metal Monoliths by Nanocasting into Silica Monoliths *Adv. Eng. Mat.* **14**(12), 1059 (2012).

13. Y. Ren, Z. Ma and P.G. Bruce: Ordered mesoporous metal oxides: synthesis and applications *Chem. Soc. Rev.* **41**, 4909 (2012).

14. N. Linares, S. Hartmann, A. Galarneau and P. Barbaro: Continuous Partial Hydrogenation Reactions by Pd@unconventional Bimodal Porous Titania Monolith Catalysts *ACS Catal.* **2**, 2194 (2012).

15. K. Cabrera, D. Lubda, H.-M. Eggenweiler, H. Minakuchi and K. Nakanishi: A New Monolithic-Type HPLC Column For Fast Separations *J. High Resol. Chromatogr.* **23**(1), 93 (2000).

16. N. Tanaka, H. Nagayama, H. Kobayashi, T. Ikegami, K. Hosoya, N. Ishizuka, H. Minakuchi, K. Nakanishi, K. Cabrera and D. Lubda: Monolithic Silica Columns for HPLC, Micro-HPLC, and CEC *J. High Resol. Chromatogr.* **23**(1), 111 (2000).

17. A. Taguchi, J.-H. Smått and M. Lindén: Carbon Monoliths Possessing a Hierarchical, Fully Interconnected Porosity *Adv. Mat.* **15**(14), 1209 (2003).

18. J.-H. Smått, C. Weidenthaler, J.B. Rosenholm and M. Lindén: Hierarchically Porous Metal Oxide Monoliths Prepared by the Nanocasting Route *Chem. Mater.* **18**, 1443 (2006).

19. S. Polarz, A.V. Orlov, F. Schüth and A.-H. Lu: Preparation of High-Surface-Area Zinc Oxide with Ordered Porosity, Different Pore Sizes, and Nanocrystalline Walls *Chem. Euro. J.* **13**, 592 (2007).

20. T. Waitz, M. Tiemann, P.J. Klar, J. Sann, J. Stehr and B.K. Meyer: Crystalline ZnO with an enhanced surface area obtained by nanocasting *Appl. Phys. Lett.* **90**, 123108 (2007).

21. M. Tiemann: Repeated Templating *Chem. Mater.* **20**, 961 (2008).

22. S. Lepoutre, B. Julián-López, C. Sanchez, H. Amenitsch, M. Linden and D. Grosso: Nanocasted mesoporous nanocrystalline ZnO thin films *J. Mater. Chem.* **20**, 537 (2010).

23. J.-H. Smått, S.A. Schunk and M. Lindén: Versatile Double-Templating Synthesis Route to Silica Monoliths Exhibiting a Multimodal Hierarchical Porosity *Chem. Mater.* **15**, 2354 (2003).

24. A.-H. Lu, J.-H. Smått, S. Backlund and M. Lindén: Easy and flexible preparation of nanocasted carbon monoliths exhibiting a multimodal hierarchical porosity *Micropor. Mesopor. Mater.* **72**, 59 (2004).

25. C. Liu and Y. Li: Synthesis and characterization of amorphous α-nickel hydroxide *J. Alloy Comp.* **478**, 415 (2009).

26. J.A. Moulijn, A.E. van Diepen and F. Kapteijn: Catalyst deactivation: is it predictable? What to do? *App. Catal. A.* **212**, 3 (2001).

27. A. Cao, R. Lu and G. Veser: Stabilizing metal nanoparticles for heterogeneous catalysis *Phys. Chem. Chem. Phys.* **12**, 13499 (2010).

28. R.H. Lamoreaux, D.L. Hildenbrand and L. Brewer: High-Temperature Vaporization Behavior of Oxides II. Oxides of Be, Mg, Ca, Sr, Ba, B, Al, Ga, Tl, Si, Ge, Sn, Pb, Zn, Cd, and Hg *J. Phys. Chem. Ref. Data.* **16**, 419 (1987).

29. D.R. Lide: CRC Handbook of Chemistry and Physics: A Ready-reference Book of Chemical and Physical Data, 85 ed. (CRC Press, City, 2004).

30. W. Yue and W. Zhou: Porous crystals of cubic metal oxides templated by cage-containing mesoporous silica *J. Mater. Chem.* **17**, 4947 (2007).

31. M.e. Cabo, E. Pellicer, E. Rossinyol, O. Castell, S. Surinach and M.D. Baro: Mesoporous $NiCo_2O_4$ Spinel: Influence of Calcination Temperature over Phase Purity and Thermal Stability *Crystal Growth and Design.* **9**, 4814 (2009).

32. Hao Liu, Guoxiu Wang, Jian Liu, Shizhang Qiao and H. Ahn: Highly ordered mesoporous NiO anode material for lithium ion batteries with an excellent electrochemical performance *J. Mater. Chem.* **21**, 3046 (2011).

33. F. Jiao, A.H. Hill, A. Harrison, A. Berko, A.V. Chadwick and P.G. Bruce: Synthesis of Ordered Mesoporous NiO with Crystalline Walls and a Bimodal Pore Size Distribution *J. Am. Chem. Soc.* **130**, 5262 (2008).

34. G.J. Kim and X.-F. Guo: Fabrication and application of highly ordered mesoporous Co_3O_4, NiO, and their metals *J. Phys. Chem. Solids.* **71**, 612 (2010).

35. W. Yue and W. Zhou: Synthesis of Porous Single Crystals of Metal Oxides via a Solid-Liquid Route *Chem. Mater.* **19**, 2359 (2007).

36. K.H. Gayer and A.B. Garrett: The Equilibria of Nickel Hydroxide, $Ni(OH)_2$, in Solutions of Hydrocholic Acid and Sodium Hydroxide at 25^o *J. Am. Chem. Soc.* **71**(9), 2973 (1949).

37. F.M. Sayler, A.J. Grano, S. Wiedmer, J.-H. Smått and M.G. Bakker: Application of 3-D Hierarchically Porous Silver, Cobalt Oxide and Zinc Oxide Monoliths to Chromatographic Separations, in MRS Symposium Proceedings, (Cambridge Journals Online, City, 2012), pp. g03.

38. H. Yen, Y. Seo, R. Guillet-Nicolas, S. Kaliaguinec and F. Kleitz: One-step-impregnation hard templating synthesis of high-surface-area nanostructured mixed metal oxides ($NiFe_2O_4$, $CuFe_2O_4$ and Cu/CeO_2) *Chem. Comm.* **47**, 10473 (2011).

39. M. Pourbaix: Atlas of Electrochemical Equilibria in Aqueous Solutions (National Association of Corrosion Engineers, City, 1974).

4.9 Supplemental Figures

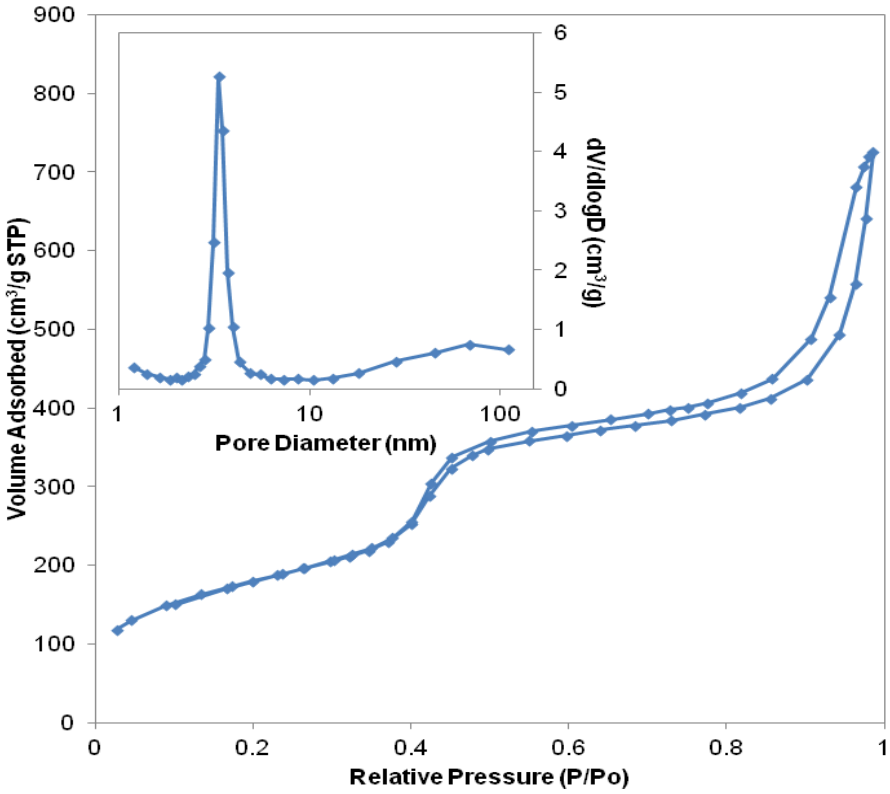

Figure 4.S1: Parent silica monolith nitrogen physisorption isotherm and BJH pore size distribution

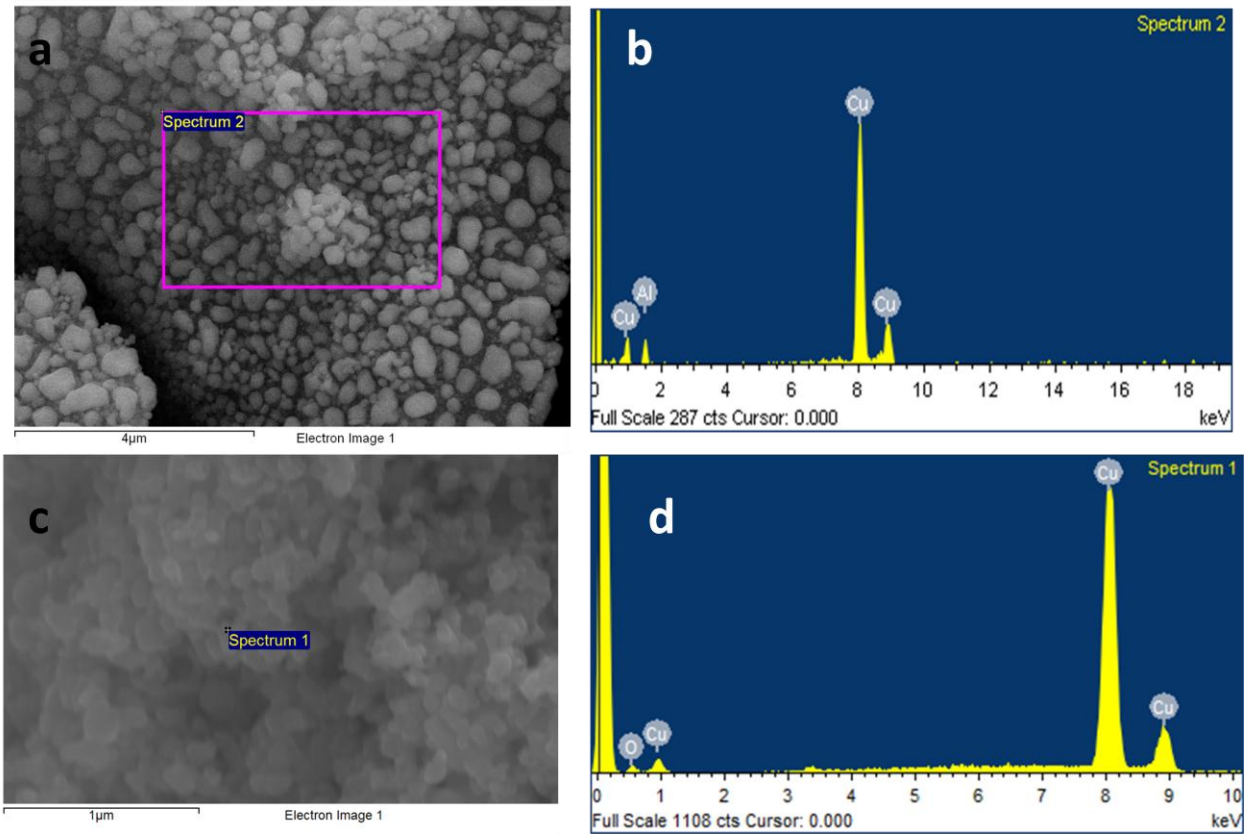

Figure 4.S2: a)SEM image of Cu-v copper, b) EDS spectra of Cu-v copper, c) SEM image of Cu-m, and d) EDS of Cu-m

CHAPTER 5

X-RAY AND FIB TOMOGRAPHY OF EXTREMELY HIGH SURFACE AREA NANOSTRUCTURED HOLLOW FIBER MEMBRANES

5.1 Abstract

Hierarchically porous materials are of interest in a wide range of applications. If the materials are electronic, or ionic conductors, such materials are of interest as electrodes for use in fuel cells. Using hierarchically porous silica as templates, we have demonstrated the formation of hierarchically porous metal and metal oxide structures. Through the control of the synthesis conditions, we have produced partial replicas ca. 1 cubic centimeter in volume, in which two macroporous networks are separated by a nanoporous membrane. The macroporous network in the silica template is known to be bicontinuous. Our underlying model predicts that the second, induced, macroporous network should be similarly bicontinuous.

Micrometer resolution X-ray tomography of the whole sample confirms that the synthesis produces one bicontinuous macroporous network, and is consistent with the existence of a second set of macropores. Preliminary experiments were carried out using FIB/SEM serial tomography to image the second macropore network, however, the length scale of the structures is such that this approach it is unable to firmly establish that the second macropore network is bicontinuous throughout the entire sample volume.

5.2 Introduction

Hierarchically porous materials are of interest in a wide range of applications. If the surface is catalytic, such materials are of interest for flow-through catalysis or flow-through

microreactors[1,2]. If the materials are electronic or ionic conductors, such materials are of interest as electrodes for use in fuel cells. Silica is a particularly useful starting point as sol-gel based syntheses incorporating high molecular weight polymers combined with surfactants or low molecular weight block copolymers, readily yield silica monoliths with porosity at micrometer and nanometer length scales.[3,4] These monoliths can in turn be used as hard templates for the formation of hierarchically porous, carbon[5], metal oxide[6,7] and metal monoliths. This is carried out by solution infiltration of a suitable precursor, followed by processing of the precursor, and removal of the silica to leave a free-standing replica. Typically, replication produces a negative replica of the nanometer pores and a positive replica of the micrometer scale pores. These pores are generally referred to as "macropores" to distinguish them from pores on the 3-50 nm scale which are referred to as "mesopores". Under some conditions, the replication appears to be only partial, which suggests that the ligaments are hollow. This structure, would correspond to a hollow fiber membrane, and if the internal network could be separately contacted would be of considerable potential utility as pervaporation membranes[8], contactors[9] and separations membranes[10]. SEM images of the these structures are shown in Figure 5.1a (cobalt oxide) and

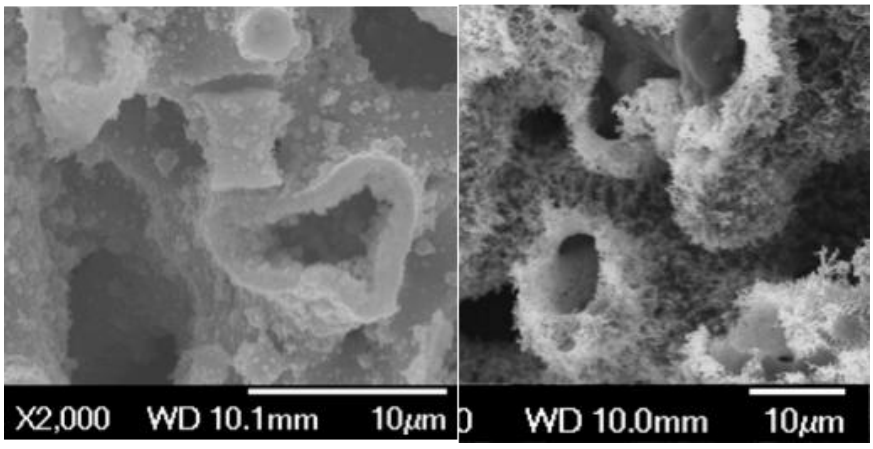

Figure 5.1. SEM images of a) Co_3O_4 and b) Nickel/nickel oxide showing macropore networks

Figure 5.1b (nickel/nickel oxide). The overall structure of these materials can be seen to be a network of ligaments defining a network of macropores. The apparently "hollow" nature of the ligaments can be seen in both the cobalt oxide and nickel/nickel oxide samples. Imaging the internal macropore network within such samples represents an interesting challenge. Preliminary experiments were conducted using Focused Ion Beam serial slice: in which a series of SEM images are collected by using the FIB to remove material between the images. Unfortunately at the length scale of our samples it would take weeks of instrument time to characterize a representative volume. It is possible that a microtome could be used to generate a stack of images that would produce a suitable 3-dimensional representation, however the resolution required presents a challenge for such methods. We have therefore been exploring the use of x-ray tomography to obtain the necessary information.

5.3 Experimental

Nickel and cobalt oxide samples were prepared by nanocasting of nickel and cobalt oxide respectively into hierarchically porous silica monoliths using the previously published procedures[6,7]. The hollow fiber geometry was produced by limiting the time the sample was exposed to the nitrate solution so only partial replication of the porous silica template occurred. The silica template was removed by dissolving in 3 M potassium hydroxide solution.

3D x-ray tomography images of cobalt oxide monoliths were taken at the micrometer scale was carried out on an Xradia (Pleasanton, CA) μCT instrument. Nanometer scale imaging of the sample from a nickel/nickel oxide monolith was carried out using the Transmission X-ray Microscope (TXM) at the Advanced Photon Source. Voxel size was 25 nm. Visualization of the data was carried out within the IDL programming environment. For both cobalt oxide and nickel/nickel oxide samples the sample preparation did not allow retention of any sample

orientation information.

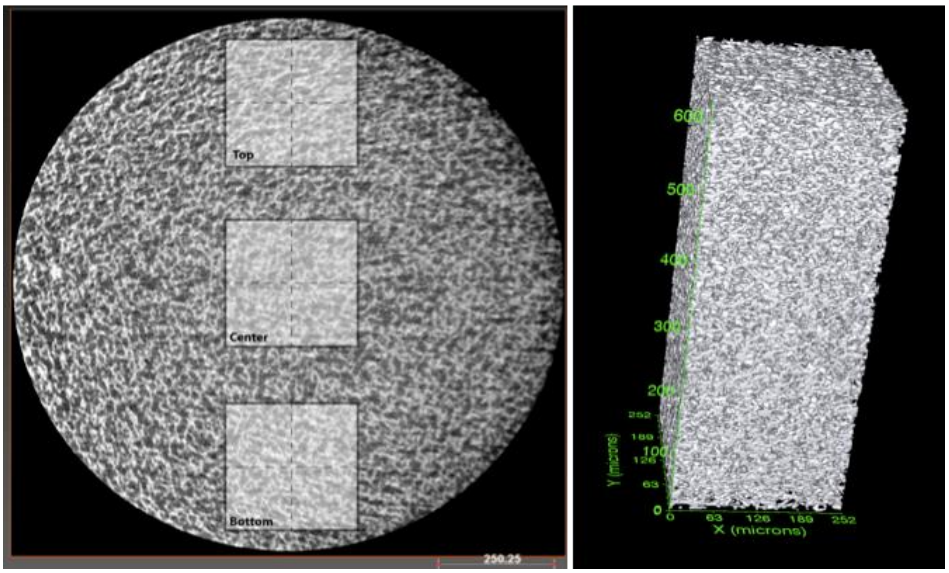

Figure 5.2. X-ray tomography images of cobalt oxide monolith. a) A reconstructed slice and b) full 3D rendering. Regions used in subsequent processing shown shaded. b) one such region.

5.4 Results

5.4.1 Microtomography

Figure 5.2a shows an example reconstructed slice taken from the end of a cobalt oxide monolith. This monolith has completely filled ligaments rather than the hollow fiber geometry shown in Figure 5.1a, and so constitutes a baseline for comparison to the hollow fiber replicates. In order to provide a statistically significant sampling of the data set, X-Y data consisting of 200 x 200 pixels was taken from within each of the three regions, top, center and bottom shown on Figure 5.2a. Three subsections were then extracted from each highlighted region and each subsection was then further subdivided into four subregions as shown in 5.2b, to give a total of 36 subsections of 100 x 100 x 100 pixels, corresponding to a volume of 125 x 125 x 125 micrometers^3. Within each region the volume occupied by cobalt oxide was determined as a fraction, f_S, of the total volume. A typical rendering of one subsection is shown in Figure 5.3a.

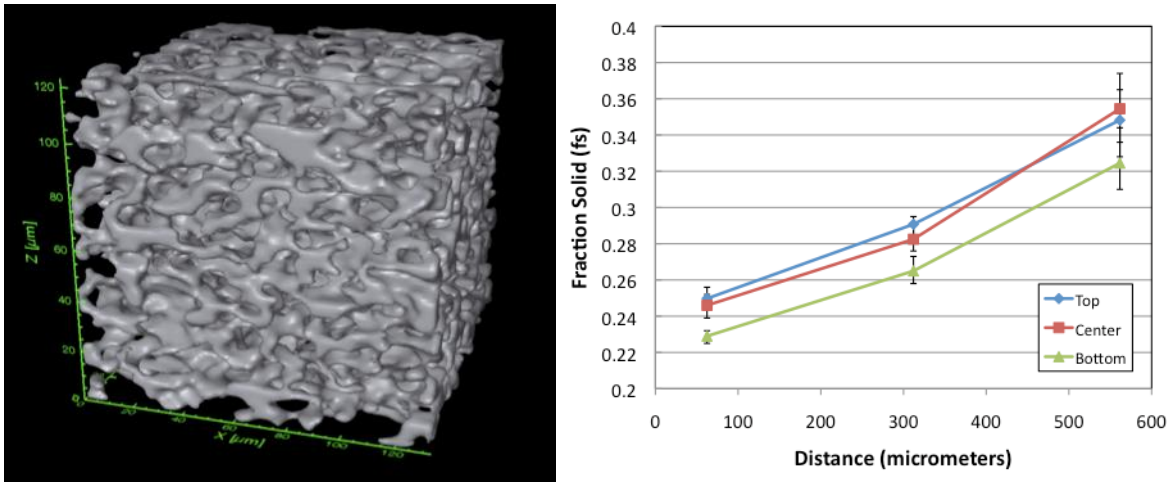

Figure 5.3. (a) Left: Rendering of one sub-region with solid interfaces selected. (b) Right: Plot of solid volume fractions for different regions of the dataset.

Averages from each of the 4 samples in a region are plotted in Figure 5.3b, which plots the data for the nine different positions within the dataset. There are clear differences between the volume fractions down the column from back to front, with a suggestion of possible (smaller) differences in going from top to bottom within the sample.

5.4.2 Nanotomography

An X-ray nano CT dataset was collected at APS on a small volume of the sample shown in Figure 5.1b. The sample as prepared consisted of nickel, however after some months stored in air we believe that some nickel has converted to nickel oxide, which have lead to the whiskers seen in Figure 5.1b. A series of images at different angles from this dataset are shown in Figures 5.4a & 5. 4b. Slices horizontal to the images in Figure 5.4a & b are shown in Figure 5.4c & d. Our interest in this sample is in determining the nature of the internal pore network that can be seen in Figure 5.1b. The nanotomography images in Figure 5.4a & b show the presence of thin nanoparticle-like features, some of them apparently unconnected to the remainder of the sample. This may reflect the threshold used, or that the nanostructures are at the resolution limit. Or possibly a combination of both. The X-ray energy was set just above the nickel adsorption edge,

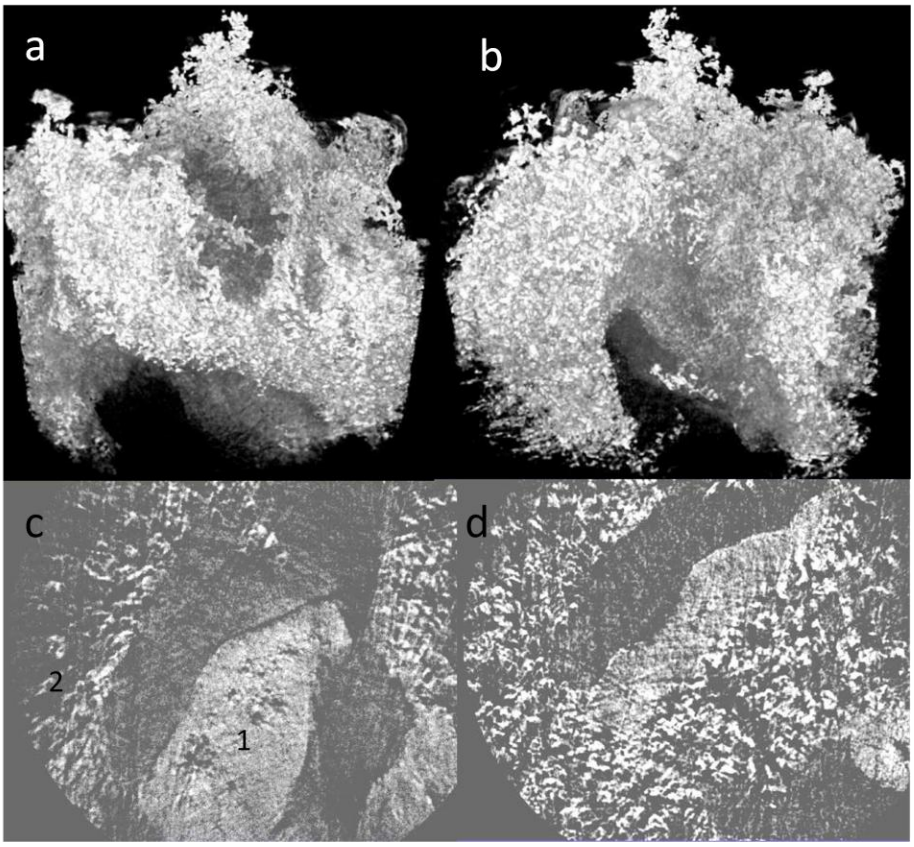

Figure 5.4. Higher resolution synchrotron x-ray CT of hollow nickel/nickel oxide. Image is 25 µm across. (a) and (b) 3D rendering, and (c) and (d) reconstructed slices, highlighting dense nickel region marked “1” on (c) and nickel oxide filaments marked “2” in (c)

and the lower density of the nickel oxide nanowires could well cause some parts of a nanowire to fall below the threshold selected. The cross-sections of Figure 5.4c & d show areas which are dense and continuous as indicated by "1", as well as other lower density areas which appear more granular, an example is indicated by "2" in Figure 5.4c. It is possible that this is granular texture is an artifact resulting from an insufficient number of attenuation images for the reconstruction. It is also possible that the apparent differences in density reflect parts of the sample being converted to lower density nickel oxide, and again falling below the threshold used. The cross-sectional images of Figure 5.4c & d do show the presence of two void regions; one that corresponds to the macropore network seen in Figure 5.3, and a second which corresponds to the internal region of a ligament. The data set of figure 5.4 is unfortunately not sufficiently large to

allow a large section of the internal macropore network to be traced and so further work will be required to confirm that this macropore network is also bicontinuous throughout the sample.

5.5 Discussion

The spatial inhomogeneities observed in the preliminary analysis of micrometer scale data raise an interesting question as to the possible cause of such inhomogeneities. We have not yet ruled out all possible artifacts in taking and processing the data, however, the differences we have found certainly appear statistically valid. We have also not yet determined the average macropore dimensions. It is possible that the parent silica monolith itself may have been spatially inhomogeneous. However, recently published x-ray tomography of similarly prepared silica monoliths[2] shows no indication of such heterogeneity. We believe that the differences we have observed could well reflect the nature of the replication process that converts the silica to cobalt oxide which utilizes solution processing. This solution processing involves infiltration of the solution into the silica monolith and could well be susceptible to mass transport effects that would result in less cobalt oxide being delivered to the center of the monolith, which may well be the case here. Work is on-going to study the parent silica monoliths and determine how the replicated structure varies with the precise position within a monolith.

5.6 Conclusions

Micrometer scale x-ray tomography data of cobalt oxide porous monoliths shows the presence of a bicontinuous macropore network consistent with the SEM images. Preliminary analysis of the data shows the presence of spatial inhomogeneities in the cobalt oxide that defines the pore network. These inhomogeneities were found in the fraction of the volume occupied by cobalt oxide, where different volume fractions were found for samples selected from different parts of the sample. Nanometer scale x-ray tomography of "hollow fiber" nickel/nickel

oxide monoliths is consistent with the presence of two macropore networks within the monolith, but that data are not sufficient to determine if this network is bicontinuous throughout the material.

5.7 Acknowledgements

Primary support for this work was provided by NSF CHE-0719398 (MGB), and by an REU position (KLG) provided by CHE 1004098. Electron microscopy was carried out in the Central Analytical Facility at The University of Alabama.

5.8 References

1. A. El Kadib; R. Chimenton; A. Sachse; F. O. Fajula; A. Galarneau; B. Coq "Functionalized Inorganic Monolithic Microreactors for High Productivity in Fine Chemicals Catalytic Synthesis", *Angew. Chem. Int. Ed.*, **121**, 5069 –5072 (2009).

2. A. Sachse; A. Galarneau; F. O. Fajula; F. Di Renzo; P. Creux; B. Coq "Functional silica monoliths with hierarchical uniform porosity as continuous flow catalytic reactors", *Micro. Meso. Mater.*, **140**, 58-68 (2011).

3. K. Nakanishi "Pore Structure Control of Silica Gels Based on Phase Separation", *J. Porous. Mat.*, **4**, 67-112 (1997).

4. J.-H. Smått; S. Schunk; M. Lindén "Versatile Double-Templating Synthesis Route to Silica Monoliths Exhibiting a Multimodal Hierarchical Porosity", *Chem. Mater.*, **15**, 2354-2361 (2003).

5. A. Taguchi; J.-H. Smatt; M. Linden "Carbon Monoliths Possessing a Hierarchical, Fully Interconnected Porosity", *Adv. Mat.*, **15**, 1209-1211 (2003).

6. J.-H. Smått; B. Spliethoff; J. B. Rosenholm; M. Lindén "Hierachically porous nanocrystalline cobalt oxide monoliths through nanocasting", *Chem. Comm.*, 2188-2189 (2004).

7. J.-H. Smått; C. Weidenthaler; J. B. Rosenholm; M. Lindén "Hierarchically Porous Metal Oxide Monoliths Prepared by the Nanocasting Route", *Chem. Mater.*, **18**, 1443-1450 (2006).

8. X. Feng; R. Y. M. Huang "Liquid Separation by Membrane Pervaporation: A Review", *Ind. Eng. Chem. Res.*, **36**, 1048-1066 (1997).

9. A. Gabelman; S.-T. Hwang "Hollow Fiber Membrane Contactors", *J. Membrane Sci.*, **159**, 61-106 (1999).

10. J. Lee; H. K. Lee; K. E. Rasmussen; S. Pedersen-Bjergaard "Environmental and bioanalytical applications of hollow fiber membrane liquid-phase microextraction: A review", *Anal. Chim. Acta.*, **624**, 253–268 (2008)

CHAPTER 6
CONCLUSIONS AND FUTURE WORK

6.1 Conclusions

In chapter 2, the expansion of the field of nanocasting to include monolithic materials with an ordered mesopore network is reported. Using an ordered system provides many advantages over a disordered system, including the ability to quantify the degree of replication seen in the final monolith. These monoliths with an ordered pore system have also been used as catalyst supports, in which effective degradation of methyl orange was demonstrated. They are also included in a pending patent. Chapter 3 reports the use of this ordered system to prove that there can in fact be destruction of the silica matrix during sintering of metal nanoparticles. In chapter 4, two new etching methods are demonstrated for use in removal of the silica during the process of nanocasting. These new approaches allow materials, which have previously been unattainable due to an absence of appropriate means to remove the template, to be synthesized by nanocasting. These etching methods can be expanded to include other materials that may not be stable under previously used etching methods. All of these achievements have added significantly to the body of knowledge in the nanocasting field, and developed promising new architectures for use in the field of catalysis. Finally, another unique geometry, the hollow fiber membrane, has been identified. An attempt to prove that this hollow fiber nature of the material exists throughout the entire monolith has been carried out via X-ray tomography. The X-ray tomography data did not allow this determination to be made, and it was concluded that X-ray optics with a wider field of view and higher resolution would need to be utilized.

6.2 Future Work

6.2.1 Ordered Monoliths

Ordered monoliths were first synthesized in carbon, cobalt oxide, and nickel oxide because those are the materials that were best understood. These ordered materials could now be used to elucidate which steps of the nanocasting process result the poor replication of zinc oxide and copper. The ordered nature of the silica allows easier interpretation of the TEM images as to whether the copper and zinc oxide replicate the silica mesopores.

6.2.2 Environmental TEM

Environmental transmission electron microscopy (ETEM) allows real time observation of nanomaterials under different temperature and chemical environments. This has been a great advancement for the development of catalysts, as gas phase and liquid phase reactions can be observed as they occur at the catalyst surface. This could be incredibly useful to continue understanding the factors responsible for good or poor replication during nanocasting. It is known that such factors as atmosphere and temperature of reduction can have an impact on the final structure of a material, but it is still debated as to the exact mechanism that causes these differences.

ETEM would allow the observation of the decomposition/reduction of the metal salts in the TEM. One could study at exactly what temperature and composition the movement from inside the mesopores to outside occurs. For example, it is known that cobalt nitrate hexahydrate decomposes at a lower temperature in mesoporous silica than in bulk, and that the atmosphere under which it is decomposed has an effect on final particle size. A temperature dependant ETEM study of the decomposition of cobalt nitrate in mesoporous silica under air, nitrogen, argon, and nitrous oxide would give insight into the temperature at which cobalt oxide particle

growth occurs. Comparison with nickel nitrate hexahydrate decomposition under comparable conditions would allow for direct comparison and provide a basis for explaining why cobalt oxide replicates so much better than nickel oxide. If hydrogen gas or other reductant is present, nanocasting of metals can be followed.

ETEM studies would also allow studies of the materials as catalysts, exemplified in chapter 2, in their working state. Gas phase catalysis, as well as liquid phase catalysis reactions, can be performed within the TEM holder. Observing the catalyst in its working state, as well as any reconstruction of the surface, would give information about the reusability of the catalyst. While it is possible to run TEM characterization of a catalyst before and after use, use of an ETEM removes any questions that might arise, for example, if surface reconstruction occurred during sample handling.

6.2.3 Plasma Focused Ion Beam

The plasma focused ion beam (FIB) is new technology that has been released within the past year. This uses an inductively coupled plasma ion source with the traditional ion column to achieve a much faster milling rate. This would be extremely useful in studying the hollow fiber monoliths. As discussed in chapter 5, x-ray tomography does not have a sufficiently wide field of view with the resolution needed to image the inside of the ligaments. Similarly, current FIB serial slicing cannot be done in a cost effective manner. Using a plasma FIB would produce much faster etching rates, and allow the removal of material sufficiently rapidly to enable the experiment to be done within a manageable time span.

6.2.4 Catalysis

We have shown that cobalt oxide, nickel oxide, and carbon monoliths can be used as supports for the reduction of methyl orange by silver particles as proof of concept. The data in

chapter 2 was collected at a borohydride concentration such that the reaction was over within the minimum experimental length. This meant that no support effect on catalytic activity could be discerned. Decreasing the concentration of borohydride would be expected to slow the reaction sufficiently to discern if there were any differences between the rate of reaction for silver nanoparticles on silica supports vs. metal oxide supports. TEM observation of the silver nanoparticles would also be necessary to determine the exact size of the particles (confirming, or otherwise, that the silver nanoparticles are the same size on all supports). TEM analysis after catalysis has been performed will determine if the particles are stable during the reaction on all supports.

Silver nanoparticle catalyzed decomposition of methyl orange was chosen as a proof of concept reaction due to the ease of implementation. There are more real world catalysis reactions that can be evaluated. The oxide and carbon monoliths can be used as supports for other precious metals, such as platinum, palladium, and gold. These combinations are used in a variety of organic synthesis reactions as well as flow through reactions. They can also be used as catalysts themselves. Cobalt oxide can be used as a catalyst for a ammonia oxidation in an industrial setting or carbon monoxide oxidation.

6.2.5 Dye Sensitized Solar Cells

There has been much research done on the incorporation of ZnO into the photoanode of DSSC. The zinc oxide reported in chapter 4 is relatively high surface area, but still significantly less than that of cobalt oxide produced by comparable methods. It is possible that by use of ordered mesoporous silica, a ZnO with an ordered mesopores structure and macropores could be obtained. These materials could be evaluated in DSSCs. The macropore network, in

combination with the nanostructure, could provide a novel material in the step towards more efficient solar cells.

APPENDIX

ADVANCED ENGINEERING MATERIALS

DOI: 10.1002/adem.201100355

Formation of Hierarchically Porous Metal Oxide and Metal Monoliths by Nanocasting into Silica Monoliths**

By Jan-Henrik Smått,* Franchessa M. Sayler, Amy J. Grano and Martin G. Bakker*

The formation of hierarchically porous metal and metal oxide monoliths by replication of hierarchically porous silica templates is reviewed. The various factors that impact the structure and properties of the synthesized materials are discussed and illustrated by the formation of new a-Fe_2O_3, ZrO_2, nickel, silver, and silver silicate porous monoliths. The impact of the atmosphere is addressed in the formation of Co_3O_4 and silver monoliths. For Co_3O_4, formation of the monolith under vacuum, air, argon, or nitrogen was found to dramatically change the structure of the final material. For silver, decomposition of the silver nitrate under air resulted in porous monoliths composed of silver silicates. Decomposition of silver nitrate under vacuum produced monoliths for which the chemical composition of the monolith was predominantly silver on the exterior of the monolith consisted of silver silicates in the interior of the monolith.

1. Introduction

Porous materials, particularly those with bicontinuous porosity, are central to a number of important application areas including heterogeneous catalysis[1,2] and separations.[3–6] When the material is electrically conducting or semiconducting such porous electrodes are central to electrochemical sensors, supercapacitors, electrocatalysis, and as electrodes in advanced batteries.[7–9] If the material displays ionic conduction rather than electronic conduction, these materials are a key component of fuel cells. All these applications require a large interfacial surface area, and efficient transport of reactants and products between the exterior and interior of the material. To meet these two requirements, a bicontinuous macropore network is needed. And this network needs to be either formed from mesopores or it could consist of a continuous skeleton covered with mesopores to generate the necessary high surface area. A number of synthetic approaches to preparing such structures have been developed. For instance, the group of Su et al. has developed a synthetic pathway where hierarchically porous metal oxides can spontaneously be formed using the self-assembly of nanoparticles around surfactant micelles.[10,11]

[*] Dr. J.-H Smått
Center for Functional Materials and
Laboratory of Physical Chemistry
Åbo Akademi University, Porthansgatan 3-5
FIN-20500, Turku, Finland
E-mail: jsmatt@abo.fi
F. M. Sayler, A. J. Grano, Prof. M. G. Bakker
Department of Chemistry, The University of Alabama
Tuscaloosa, AL 35487-0336, USA
E-mail: bakker@bama.ua.edu

[**] Support for this work was provided by NSF CHE-0719398 (MGB) and by the Academy of Finland 127919 (JHS). Electron microscopy was carried out in the Central Analytical Facility at The University of Alabama. Mika Lindén (University of Ulm) is gratefully acknowledged for valuable discussion, as are Mikael Järn (Åbo Akademi University) for SEM measurements (SiO_2 and ZrO_2) and Bernd Spliethoff (MPI, Mülheim an der Ruhr) for TEM measurements (SiO_2 and ZrO_2). Keana Graves (Fe_2O_3), Alison Hu (Ni and NiO), and Elizabeth Junkin (Co_3O_4) provided technical assistance with sample preparation. Supporting Information is available from the Wiley Online Library or from the authors.

However, this method has fairly poor morphology control and is not generally well suited for formation of large (mm–cm) pieces; often referred to as ''monoliths''. A number of groups have used colloidal crystal templating; self-assembly of polymer or silica beads to give a relatively hard template into which precursor solutions can be infiltrated to create a macroporous structure in metals, and metal oxide materials (also known as 3DOM materials).[12–15] Infiltration of a sol–gel precursor including a surfactant as template can be used to induce ordered mesopores in the macropore walls of these materials.[16] Major drawbacks of this approach are the expense of the polymeric beads for macroscopic pieces, and the presence of constrictions in the macropore network. A number of other methods of producing hierarchically porous materials have been developed using microemulsions,[17,18] bicontinuous polymer foams,[19] salt crystals,[20] bacteria,[21] butterfly wings,[22] cellulose,[23,24] sugars,[25] or ice[26] as templates for macro-structure, and foaming of the sol–gel silica.[27] These methods of forming macropores can be coupled with addition of surfactants or block copolymers to template mesopores. Liquid–solid phase separation induced by chemical reaction has also been used to produce bicontinuous silica macrostructures,[28] and extended to zirconia,[29] titania,[29,30] alumina,[31] and calcium, barium and strontium titanates.[32] This process is an example of spinodal decomposition, in which spontaneous fluctuations in local composition are amplified to produce phase separation at a number of length scales.

This paper focuses on the formation of sol–gel derived hierarchically porous monoliths prepared by such phase separation induced processes, and their conversion to other materials with related structures by ''nanocasting'': infiltration of various solution or gas phase precursors which react to produce other materials within the monolith. This approach has been used to make hierarchically porous MnO_2, Mn_2O_3, Co_3O_4, SnO_2,[33,34] and carbon[35,36] monoliths with well developed porosity at micrometer length scales and reasonable surface areas of up to 40 m^2 g^{-1} for metal oxides and >1000 m^2 g^{-1} for carbon. The template for these materials was one that did not include a surfactant. Such monoliths are referred to as being ''monomodal''. For silica monoliths containing surfactant mesopores (''bimodal'' monoliths) the surfactant mesopores provide higher surface areas, which if well replicated would result in higher surface area in the nanocast replicas. In this contribution we explore the use of bimodal rather monomodal silica templates and we (i) survey the various methods and materials developed for producing the original monoliths, (ii) outline the nanocasting approach when applied to monoliths, including a discussion of the various factors that impact the quality of nanocast material, and (iii) give representative examples of the approach to produce new materials including hierarchically porous iron oxide, zirconium oxide, nickel oxide, and the first reports of hierarchically porous metal and metal silicate monoliths formed by nanocasting.

1.1. Formation of Porous Silica and Metal Oxide Monoliths by Spinodal Decomposition

Various hierarchically porous silica and metal oxide monoliths can be formed by the use of sol–gel processes in which organic precursors react with water to produce monomeric forms of silica or the metal oxide. These monomeric forms condense to give oligomers which continue to grow and give solid material. The hydrolysis produces an alcohol as a by-product and this, together with the water, will phase separate from the growing inorganic component as the polymerization reaction proceeds. Often a high molecular weight polymer such as polyethylene oxide[37] or polyethylene glycol (PEG)[38] is added to improve the phase separation and to control the length scale of the macropore network. This approach has been used to form porous monoliths of titania,[39] zirconia,[29,30] aluminas,[31,40] and of mixed oxides of titania with barium, strontium, and calcium.[32] A related approach is to add a monomer such as furyl alcohol which will itself undergo polymerization as the phase separation occurs.[41] Including surfactants[38,42] or block copolymers [43] in the synthesis mixture can give silica monoliths that are macroporous and mesoporous with a narrow range of pore sizes. Whereas the addition of a cationic surfactant gives disordered networks of pores, the block copolymer templated materials can have highly ordered pores.[44,45] Scheme 1 shows images of porous silica monoliths that display the typical network of macropores. It can be seen that the macropore networks are generated by silica ligaments, where the ligaments are formed by agglomeration of smaller particles. The particles themselves can be mesoporous (having pores in the 3–10 nm) range, and the regions where the particles are in contact also generates voids on the 10–50 nm range depending upon the sizes of the particles. We will use the term ''surfactant'' mesopores to designate mesopores generated by an added charged or non-ionic surfactant, and ''textural'' mesopores to designate those mesopores generated by contact of silica particles. Typically the surfactant mesopores have a

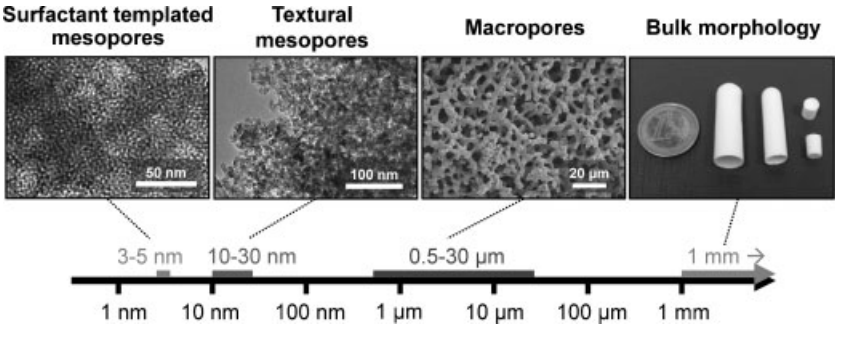

Scheme 1. The hierarchical nature of the monolithic silica templates used in this study.

ADVANCED ENGINEERING MATERIALS

constant diameter throughout a monolith, where the diameter of the mesopores is determined by the chain length of the hydrophobic portion of the surfactant, whereas the textural mesopores will have a broader range of diameters.

To summarize; these cationic surfactant templated hierarchically porous monoliths have controllable porosity of three different forms on three different length-scales: surfactant templated pores with 3–5 nm diameter, textural mesopores of 10–50 nm scale, and macropores controllable between 0.5 and 30 mm. Surface areas for these materials are typically 600–1100 m^2 g^{-1}, or, adjusting for the density of silica (2.2 g cm^{-3}), 1300–2500 m^2 cm^{-3}. These materials can be fabricated as large monolithic pieces, with dimensions of 1–20 cm.

Instead of a cationic surfactant, a non-ionic block copolymer can also be used.[44,46] Where cationic surfactants produce disordered arrays of pores, block copolymers can produce highly ordered arrays of mesopores with diameters in the range 6–9 nm. The resulting silica then also has micropores (<1 nm) that bridge the ordered mesopores. These porous materials therefore have porosity controllable on four length scales; <1 nm, 6–9 nm, 10–50 nm, and 500 nm–30 mm.

Although the block copolymer templated materials have considerable promise as templates for synthesis of large pieces of highly ordered nanomaterials, this is still a largely unexplored field, and so these materials will not be discussed further.

1.2. Nanocasting to Form Other Hierarchically Porous Materials

An overview of the replication process is given in Scheme 2: a solution of the precursor is added to a silica monolith, solvent is removed by evaporation/heating and the precursor is then decomposed to the metal oxide or metal. This process is repeated as often as necessary to build up the desired structure. Capillary forces generally favor filling of the smallest mesopores first, so that in some cases the textural mesopores are not filled. This process therefore forms a negative replica of the mesopores and a positive replica of the macropores. The details of the processing significantly impact the properties of the final product and will be discussed in the order in which the processes are carried out. Although the focus will be on monolithic materials, there is a large body of work on nanocasting into mesoporous silica particles[47–50] and such work will be discussed where it has potential impact on nanocasting into monoliths.

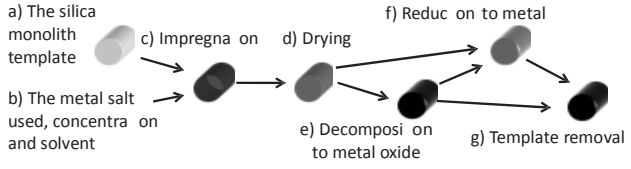

Scheme 2. An overview of the different steps that are involved in the nanocasting process.

Metal nitrate salts are widely used in nanocasting because of the high solubility in aqueous solution and the relatively easy decomposition to the metal oxide. Other metal salts including chlorides,[34,51–53] carbonate,[32] and acetates[54] have also been used, and we will discuss examples in which aqueous nickel acetate is used to produce nickel and in which aqueous zirconium sulfate is used as precursor to form zirconia. For monoliths, capillary forces will favor filling of the mesopores over the macropores, and so by adding a volume of solution that matches the volume of the mesopores, infiltration of solution can be limited to the mesopores. This approach is sometimes termed ''incipient wetness'' and is also used for nanocasting into mesoporous silica particles. A variation on this approach is to use a solution which is not saturated and then let evaporation concentrate the precursors into the mesopores since evaporation will occur preferentially from the macropores. This does require careful control of the starting concentration as salt deposition can occur into the macropores if the solution reaches saturation concentration while there is still solution in the macropores. This leads to significant filling of the macropores as seen in some of our earlier work on manganese oxides.[34] Because of the very significant differences in effective density between even the most concentrated aqueous solutions and the final metal oxide or metal, a number of infiltration cycles are necessary. For metal oxides this is typically 4–6 and for the metals it may be as high as 8–12.

A newer approach that can significantly decrease the number of infiltration cycles uses metal nitrate hydrate melts which have a significantly higher metal concentration than is attainable from saturated aqueous solutions. A number of metal nitrate hydrates have low melting points well below their decomposition temperatures, and so modest heating is sufficient to allow them to form a liquid that can penetrate into the mesopores. This process has recently been applied by a number of groups to nanocasting into mesoporous silica particles,[55–57] and we have also successfully applied it to nanocasting into silica monoliths.

The thermal decomposition of the precursor produces either a metal oxide or a metal depending upon the metal and on the atmosphere used. Transition metals decomposed under air, oxygen, or inert atmospheres typically give metal oxides. Decomposition under hydrogen can produce transition metals, particularly noble metals.[58] The high surface area of the resulting metal monoliths tends to make them very reactive, which can be advantageous for catalytic applications,[59] but also means that the material oxidizes rapidly in air. A detailed study of the impact of gas atmosphere is included below. The temperature at which the decomposition reaction is carried out and the length of time the sample spends at elevated temperatures both critically impact the structure and properties of the final material. This can be understood in context of the Tammann and Hü ttig temperatures and the wetting of the silica template by the metal oxide

or metal being formed. The Hüttig temperature is the temperature at which atoms at defects become mobile, and the Tammann temperature is the temperature at which atoms in the bulk become mobile.[60] The Hüttig temperature is estimated to be approximately one third the Kelvin melting point of the material, and the Tammann temperature approximately half the Kelvin melting point. If the metal or metal oxide wets the silica (i.e., adhesion is stronger than cohesion) the metal or metal oxide will spread across the silica giving good replication of the silica template structure. If on the other hand a metal or metal oxide does not wet silica, then Ostwald ripening will occur at temperatures for which the metal or metal oxide is mobile. This will tend to favor migration of the metal or metal oxides out of the smaller mesopores into the larger mesopores, and the macropores, resulting in a decrease in surface area and loss of the nanostructure. This can be seen clearly in Figure 1 which shows the growth of silver crystallites within the macropores. The wetting of the silica template by the metal oxide or metal can be evaluated from the contact angle between the metal oxide or metal and silica surface. Unfortunately most metals do not wet silica and so minimizing the time the sample spends at elevated temperature coupled with a slow decomposition will tend to give the best final structure. There is little data available on the contact angles between metal oxides and silica. Our experience indicates that most metal oxides can give reasonable replicas suggesting that they wet silica sufficiently well that Ostwald ripening is slow.

Despite the potentially negative impact on surface area and nanostructure replication of allowing significant migration of metal or metal oxide within the silica template, it may be desirable to allow such migration to improve the mechanical stability of the resulting monolithic material. If all the metal or metal oxide is confined to the surfactant mesopores and the smaller textural mesopores the replica may be continuous, but not sufficiently mechanically robust to survive subsequent processing and handling. The coefficients of thermal expansion of the largely amorphous silica template monolith and of the metal or metal oxide replica are likely to be significantly different, producing stresses in the materials as they cool. This often leads to fracturing of the material; sometimes in the parent silica monoliths, at other times after the silica is removed. A thermal annealing step may therefore be desirable to minimize these stresses.

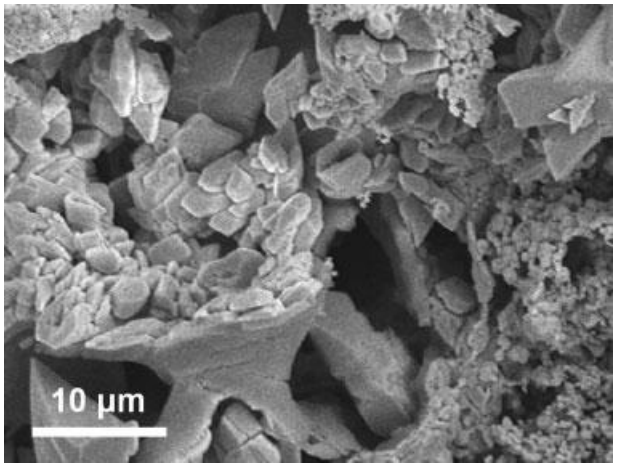

Fig. 1. SEM image of a silica monolith with silver crystallites in the macropore structure.

A further consideration in the thermal processing of the material results from interaction of the silica matrix with the incorporated metal or metal oxide. It is often tacitly assumed that the silica matrix is inert, playing no role other than acting as a mold. However, at elevated temperatures there is reason to believe that metals can be incorporated into the mesoporous silica walls to form metal silicates. This has been inferred for decomposition of cobalt acetate in mesoporous silica,[61] and a surface layer of silicon bonded to zirconium dioxide is inferred for nanocasting of ZrO_2 into mesoporous silica, based on FTIR spectra.[53] We report below observation of zirconium silicate and silver silicates.

Nanocasting into mesoporous silica is also a route to mixed metal oxides. The interest here is primarily in magnetic materials such as (1) ferrites: MFe_2O_4 where M ¼ zinc,[62] manganese,[63] nickel,[57,63,64] cobalt,[63–66] copper,[57,63] and magnesium,[64] (2) strontium hexaferrite,[67] (3) $NiCo_2O_4$ spinel,[68,69] and (4) copper doped cerium oxide[57] for solid oxide fuel cell applications.

After nanocasting the silica needs to be removed. This is done by etching away the silica with either an aqueous hydroxide solution or aqueous hydrogen fluoride. Both dissolve the silica. The hydroxide dissolution is more popular as there are significant safety concerns with the hydrogen fluoride process. The hydroxide etch is used in this work and detailed procedures are discussed in the Section 4. Not all nanocast materials are stable in aqueous hydroxide or aqueous hydrogen fluoride. For instance, zinc oxide is soluble in both etching solutions. One method of overcoming this limitation is to use a double nanocasting procedure involving first making a carbon replica of mesoporous silica particles, etching away the silica, and then nanocasting zinc oxide into the mesoporous carbon, followed by removal of the carbon to make mesoporous zinc oxide.[70,71] Other examples are copper oxide and copper which we have successfully nanocast into mesoporous silica monoliths, but again both dissolve on etching of the silica.

After etching of the silica to leave the mesoporous nanocast material, further transformations are possible with retention of structure if carried out carefully. Examples are reduction by glycol of particles of mesoporous Co_3O_4 to CoO[72] and the reduction by hydrogen of a-Fe_2O_3 to Fe_3O_4 and then oxidation under air to g-Fe_2O_3.[73] Again we are not aware of any examples of such transformations being carried out on monolithic materials. We report here on the first such example in which hierarchically porous nickel oxide monoliths are reduced to nickel.

ADVANCED ENGINEERING MATERIALS

2. Results and Discussion

2.1. SiO_2 Template Monoliths

In this study, we used hierarchically porous silica monoliths in the nanocasting process to form metal oxides and metals of similar structure. The starting monolithic pieces (cylinders of about 5 mm diameter and 10 mm length) were designed to all have interconnected macropores with pore diameters in the range of 1–15 mm (similar to the ones shown in Scheme 1).[74] Furthermore, as evident from the pore size distribution plot derived from nitrogen physisorption in Figure 2, the monoliths where only PEG was used as structure directing agent (samples SiO_2-M1 and SiO_2-M2), have only a monomodal textural porosity centered around 20 nm. When adding a surfactant (C_nTAB: $C_nH_{2n+1}N(CH_3)_3Br$) to the reaction mixture, another set of pores with a pore diameter close to 4 nm is induced in the final monoliths. The abundance and size of these surfactant templated mesopores can be controlled by the amount added and the chain length of the hydrocarbon moiety of C_nTAB, respectively. Thus, by changing the surfactant from $C_{16}TAB$ to $C_{18}TAB$, the size can be increased from 4.3 to 4.6 nm (Table 1). Both the textural and the surfactant templated mesopores are depicted in Scheme 1. The original isotherm data can be found in the Supporting Information, while the specific surface areas, pore volumes and pore sizes for these samples are summarized in Table 1.

2.2. Co_3O_4 Monoliths (Varying the Gas Atmosphere)

Figure 3 shows scanning electron microscopy (SEM) images of the macropore walls for nanocast cobalt oxide samples decomposed under vacuum and different gaseous atmospheres. The scale of all four images is the same, and it appears that the macropore structure is retained. The nature of the atmosphere does produce differences in sample morphology as can be seen clearly from comparison of the images. The most apparent difference is in the sample decomposed under vacuum, Co_3O_4-B1-Vac, in which the image is dominated by spherical structures of 400–500 nm in diameter. These structures are not replicas of the original silica template, and are much larger than the length scale of structures in the samples prepared under air, nitrogen, or argon. For these latter samples, the size of the features decreased in going from stagnant air (130 30 nm) to argon (100 15 nm), and to nitrogen (70 10 nm). A comparison with the SEM image of the parent silica monolith (Scheme 1) shows that the typical feature size is closer to 20 nm. The nitrogen adsorption data is summarized in Table 1, and the pore size distribution is given in Figure 4. The difference between the evacuated sample and the other three samples is striking. The surface area of sample Co_3O_4-vac is barely one third of the next lowest, and the pore size distribution shows only a single peak at approximately 20 nm. This peak is not from inter-particle pores produced by contact of the 400–500 nm aggregates seen in Figure 3, but instead is likely to be produced by replication of the textural mesopores present in the silica template. The other samples not only have much higher surface areas, but also have bimodal pore size distributions. A more detailed analysis of the pore size distributions shows clear differences in the other three samples, with the sample decomposed under stagnant air showing a lower surface area, a larger average mesopore size (10 nm) and a proportionately larger volume of pores in the 40 nm size region. The argon and nitrogen samples are more similar, with the sample decomposed under argon having a somewhat higher total surface area than the sample decomposed under nitrogen, more pores in the 4–10 nm range and proportionately fewer pores in the 20–100 nm range.

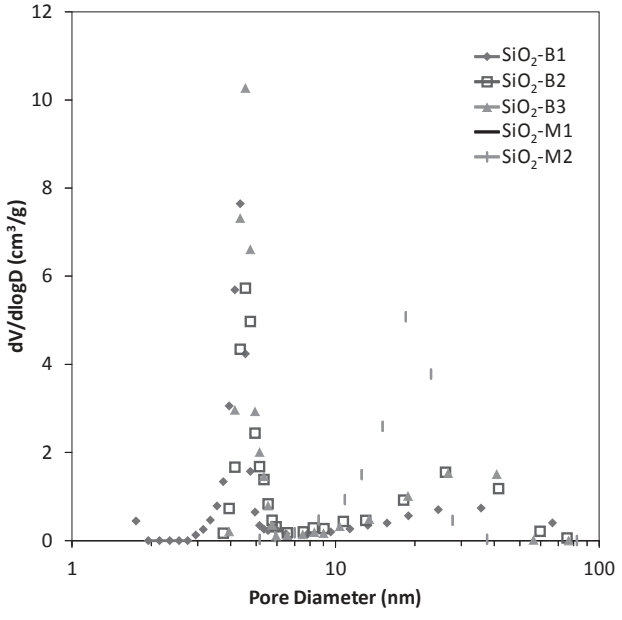

Fig. 2. Pore size distribution plots of the different silica monoliths used as templates in this study.

A bimodal pore size distribution in the replica monoliths is expected if the replication of the silica templates was perfect. However, even for the inert gas atmospheres, which give the smallest pores, the pore size distributions actually produced are on length scales that suggest that the replication was less than perfect.

In forming a replica, capillary forces will initially confine the solution to the smallest pores: the surfactant mesopores. If the replication process is prefect and controlled to replicate only the surfactant mesopores, then on removal of the silica template, the distribution of textural mesopores should be largely unchanged. The distribution of the surfactant mesopores on the other hand is expected to change. The surfactant mesopores have a narrow pore size distribution, but they are not ordered, and so the thickness of the silica walls is variable, leading to a broader pore size distribution, as is observed for carbon replicas.[75] The differences in the pore size distributions of both the textural mesopores, and the mesopores resulting from replication of the surfactant mesopores can best be explained by a number of physico-chemical phenomena. Firstly by differences in mobility of the

Table 1. Summary of textural properties of the starting silica monoliths and the different replica samples.

Silica template monoliths

Sample	BET surface	BET surface	Mesopore	Mesopore	Mesopore diameter		Crystal/particle diameter	
	Area [m^2 g^{-1}]	Area [m^2 cm^{-3}] [a]	Volume [cm^3 g^{-1}]	Volume [cm^3 cm^{-3}] [a]	Surf [nm]	Text [nm]	XRD [nm] [b]	N_2 [nm] [c]
SiO_2-B1	833	1830	0.95	2.09	4.3 [d]	30 [e]	–	3.3
SiO_2-B2	643	1410	1.31	2.88	4.5 [d]	30 [e]	–	4.2
SiO_2-B3	742	1630	1.43	3.14	4.6 [d]	30 [e]	–	3.7
SiO_2-M1	264	581	1.13	2.49	–	19	–	10.3
SiO_2-M2	267	587	1.16	2.55	–	19	–	10.2

Replica monoliths

Sample	BET surface	BET surface	Mesopore	Mesopore	Mesopore diameter		Crystal/particle diameter	
	Area [m^2 g^{-1}]	Area [m^2 cm^{-3}] [a]	Volume [cm^3 g^{-1}]	Volume [cm^3 cm^{-3}] [a]	Small [nm]	Large [nm]	XRD [nm] [b]	N_2 [nm] [c]
Co_3O_4-B1-Stag	68.8	420	0.2	1.22	10	40 [e]	28	14
Co_3O_4-B1-N_2	89.5	547	0.19	1.17	7.2	40 [e]	25	11
Co_3O_4-B1-Ar	95.4	583	0.19	1.15	6.4	40 [e]	18	10
Co_3O_4-B1-Vac	25.1	153	0.12	0.73	–	19	36	39
Fe_2O_3-B2	65.3	342	0.12	0.61	11	–	17.1	18
SiO_2/ZrO_2-M1	133	–	0.3	–	6.7	15	–	
ZrO_2-M1	97	551	0.22	1.26	8.5	–	–	11
ZrO_2-M2	84	477	0.21	1.19	8.5	–	12.5	13
Ag-B3-Air	17.9	–	0.09	–	–	30 [e]	–	–
Ag-B3-Vac	94.7	–	0.34	–	–	23	28 [f]	–
NiO-B1	37.7	182	0.09	0.44	–	20	–	24
Ni-B1-post-H_2	10.7	95	0.07	0.62	–	40 [e]	21.5	60
Ni-B2-H_2	21.8	194	0.08	0.71	–	30 [e]	–	31

[a] The surface areas and the pore volume values have been adjusted for the bulk densities: 2.2 g cm^{-3} for SiO_2, 6.11 g cm^{-3} for Co_3O_4, 5.24 g cm^{-3} for Fe_2O_3, 5.68 g cm^{-3} for ZrO_2, 6.67 g cm^{-3} for NiO, and 8.91 g cm^{-3} for Ni. The bulk densities for the SiO_2/ZrO_2 composite and the silver samples are uncertain and so a meaningful mesopore volume cannot be calculated;
[b] Crystallite size estimated from XRD using the Scherrer equation;
[c] The particle size diameter determined from the BET areas was calculated using the formula: $d = 6/(A_{BET} \cdot d)$, where d is the bulk density;
[d] NL-DFT pore size distribution (adsorption model for cylindrical pores);
[e] Gas adsorption is less sensitive for mesopores above 20 nm, and so these pore diameters are only approximate;
[f] Measured on the Ag metal peaks.

cobalt nitrate, cobalt nitrate decomposition products and cobalt oxide during the decomposition process and secondly by possible differences in interactions with the silica template. If the energy of adhesion of nanocast materials to silica is lower than the cohesive energy of the material then the enthalpy of the system can be minimized by particle growth leading to Ostwald ripening. This provides a natural driving force for material to move from the surfactant mesopores to the larger textural mesopores and then into the macropores. Little information is available on the nature of the interactions between nitrate salts, their decomposition products, and transition metal oxides and silica. Empirical evidence from nanocasting of a range of metal and metal oxide systems[34,76] is consistent with neither metals nor metal oxides wetting silica particularly well. Extended periods above the Hüttig temperature of cobalt oxide will therefore provide greater opportunity for migration of the cobalt oxide from the surfactant mesopores into the textural mesopores, and for migration within the textural mesopores to decrease the surface curvature.

The nature of the atmosphere can impact the replication process at multiple steps. Decomposition of nickel nitrate under an atmosphere of NO is reported[77,78] to significantly impact the surface area of nickel catalyst by altering the decomposition mechanism. Under oxygen atmosphere sintering of the nickel oxide is reported, with migration of the nickel oxide from within mesoporous silica particles to the exterior surface. These authors[77,78] advocate keeping the concentrations of oxygen and NO_2 gas, a decomposition product, at low levels. The observation of lower surface area and larger pore sizes for stagnant air compared to flowing nitrogen and argon are very consistent with this result. However this does not explain the result for decomposition under vacuum in which the concentration of oxygen and the other decomposition products would also be very low. This sample was decomposed at 150 °C under vacuum, but calcined under stagnant

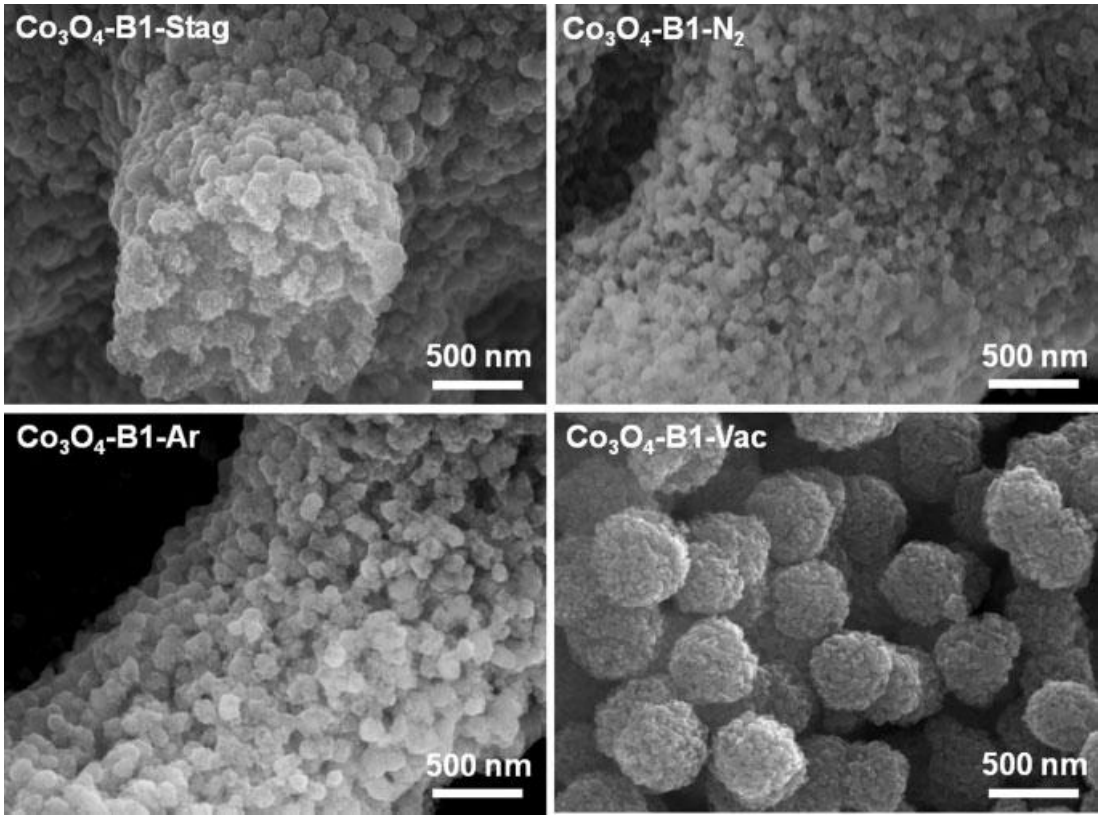

Fig. 3. SEM images showing the influence of the morphology of the Co_3O_4 macropore walls by different gas atmospheres (stagnant air, N_2 flow, Ar flow, and vacuum).

air at 550 8C to improve the mechanical stability of the monolith. The large difference in structure between this sample and that decomposed only under stagnant air indicates that the key effect here is the absence of gas during the decomposition process rather than the absence during the higher temperature calcination step. Since even the presence of chemically inert gases has a considerable impact this cannot be a purely chemical effect. One possible mechanism is a purely physical one. During the decomposition considerable gas evolution occurs. This gas must move out of the mesopores where the bulk of the material is located out into the macropores. Under vacuum there is a larger pressure difference providing more impetus to move un-decomposed cobalt nitrate as well as already formed cobalt oxide. A second possibility is that the presence of a gaseous atmosphere shifts the decomposition equilibria, slowing them down and giving more time for the gas evolved to slowly diffuse out into the macropores, or favoring the formation of decomposition products which are less mobile at 150 8C. The use of vacuum during the decomposition of silver nitrate (below) produces substantial changes in the nature of the final product, suggesting that shifts in chemical equilibria are distinctly possible.

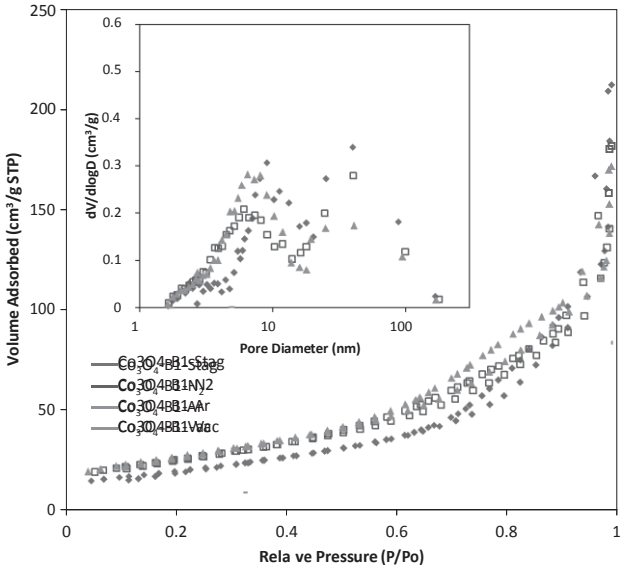

Fig. 4. Nitrogen physisorption isotherms of Co_3O_4 replicas prepared under different gas atmospheres. Inset: the corresponding BJH pore size distribution plots (desorption branch).

2.3. Fe_2O_3 Monoliths

Figure 5 shows SEM images from the iron oxide monolith Fe_2O_3-B2 prepared by nanocasting using iron nitrate. The macrostructure is clearly well replicated, and the presence of features on the 100 nm length scale on the surface of the macropore walls indicates that the growth of iron oxide in this system is consistent with what is seen for cobalt oxide synthesized under air. X-ray diffraction (XRD) (Figure 6) shows clearly peaks from a-Fe_2O_3 with no significant peaks

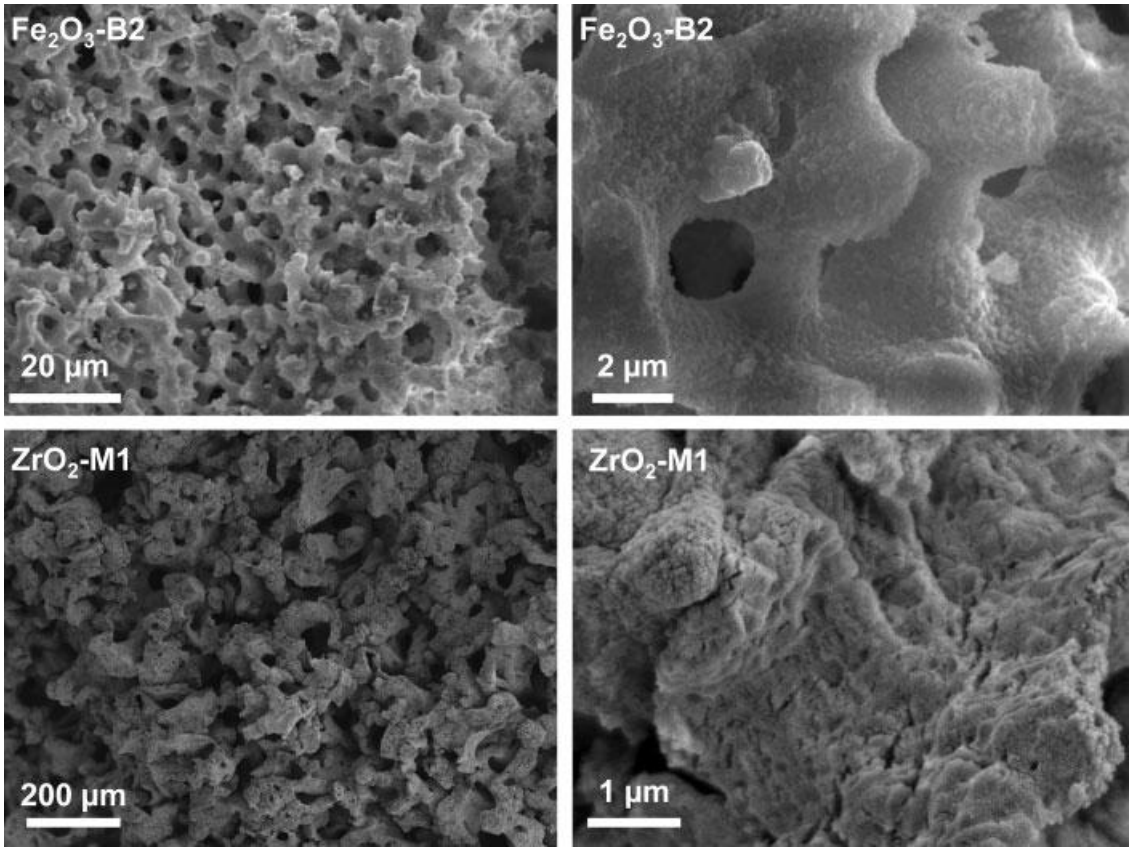

Fig. 5. SEM images of samples Fe_2O_3-B2 and ZrO_2-M1.

from other crystalline phases. The broad background observed in Figure 6 results from X-ray luminescence from the copper X-ray source used. The average crystallite size is 17 nm, which is significantly larger than the 4.5 nm pore diameter of the mesopores in the parent silica monolith. The pore size distribution in Figure 7 shows a peak at approximately 10 nm which is similar to that observed for nickel oxide using the same template (below), but significantly larger than that observed for cobalt oxide. The surface area to volume ratio is lower than that for cobalt oxide and zirconia but higher than observed for nickel oxide.

We believe that these results are consistent with significant migration of the iron oxide out of the surfactant mesopores into the textural mesopores. The melting point of a-Fe_2O_3 is 1565 8C, giving a Tammann temperature of 646 8C. This is significantly higher than 550 8C the temperature at which the sample was calcined. But 550 8C is higher than the Hü ttig temperature, so we would expect some migration to occur. The Tammann and Hü ttig temperatures for Fe_2O_3 are higher than those of Co_3O_4, so other factors such as wetting and extent of pore filling must also be contributing to the lower surface area compared to Co_3O_4.

2.4. ZrO_2 Monoliths

Hierarchically porous ZrO_2 monoliths with stable monolithic structures could be prepared by using $Zr(SO_4)_2$ $4H_2O$ as precursor salt, which is evident from Figure 8. Previous attempts to use aqueous solutions of $ZrOCl_2$ or $ZrO(NO_3)_2$ as ZrO_2 precursors lead to severe cracking of the monolith structure during the impregnation/drying/calcination stages, which may result from faster reaction kinetics and a strong interaction between the Zr species and the SiO_2 template. These effects can also be observed (although to a lesser degree) for the ZrO_2 monoliths prepared with the zirconium sulfate salt as the silica template is removed by chemical etching in NaOH. After being etched, the ZrO_2 monoliths shrink to some extent upon the final drying step (for sample M1 5.0% and for M2 3.8%), due to the removal of the rigid silica scaffold. The improved mechanical strength of the composites when using zirconium sulfate as precursor can probably be ascribed to the high decomposition temperature needed before the oxide is formed (720 8C for the pure salt). In addition, when calcining $Zr(SO_4)_2$ at 750 8C, the ZrO_2 formed is more dense and has a more rigid structure that can withstand shrinkage better. Several repeated impregnation steps also help to improve the mechanical stability of the zirconia replica.

From the SEM images in Figure 5, it is evident that the macropore structure of the ZrO_2 replica is not as well defined as in the starting silica monoliths, although one can clearly see that the structure is made up of interconnected macropores. The flow characteristics of these materials are still expected to be suitable for applications in catalysis.[79]

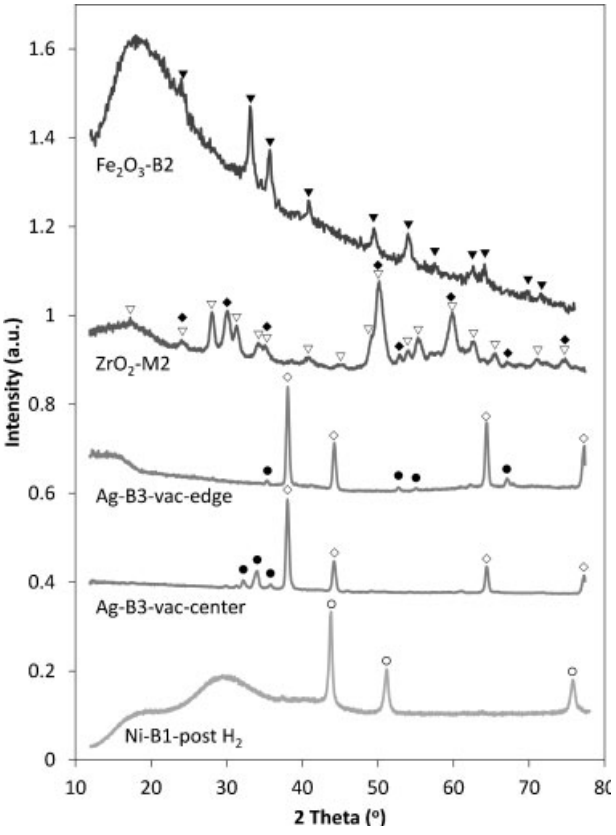

Fig. 6. XRD measurements of Fe_2O_3, ZrO_2, Ag, and Ni monoliths. The symbol ! indicates reflections from a-Fe_2O_3 (hematite), while in sample ZrO_2-M2 both monoclinic ZrO_2 (5) and orthorhombic or tetragonal ZrO_2 (^) phase can be seen. Mainly metallic Ag peaks (^) can be seen at the edge of the Ag-B3-vac monoliths, while at the center additional silver silicate peaks can be seen ( ). For the Ni-B1-post-H_2, the peaks seen are from metallic nickel (*). The broad peaks below 408 are from the sample holder.

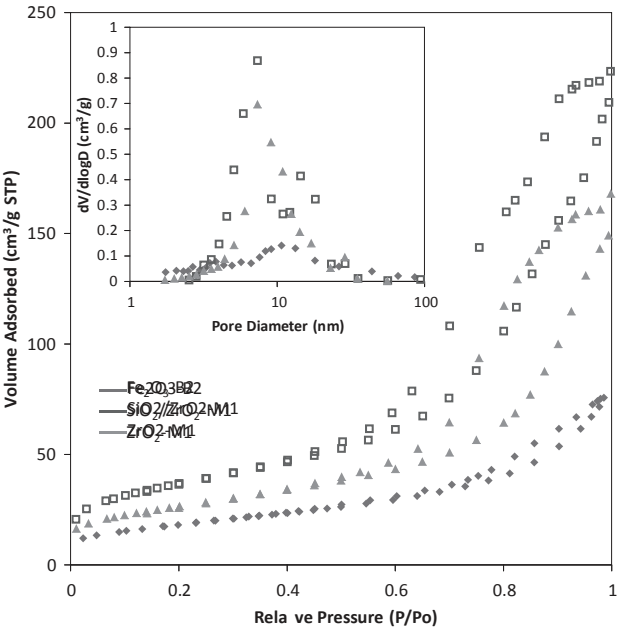

Fig. 7. Nitrogen physisorption measurements on the Fe_2O_3-B2 replica, the SiO_2/ZrO_2-M1 composite and the ZrO_2-M1 replica monoliths.

Nitrogen physisorption isotherms of the SiO_2/ZrO_2 composite and the ZrO_2 replica are shown in Figure 7, while the extracted textural properties are listed in Table 1. The original silica monolith shows a narrow pore size distribution around 20 nm (Figure 2), which is still present to a lesser extent in the composite monolith. Interestingly, a new set of pores appears in this sample at around 8 nm. The precise origin of these pores is still unclear. The ZrO_2 replica also shows a BET surface area close to that of the silica template (551 m^2 cm^{-3} vs. 581 m^2 cm^{-3}). Generally nanocast replicas have lower surface areas than the parent silica templates, which suggests that the induced pores do contribute significantly to the total surface area. The BET surface area of the ZrO_2 monoliths can also be used to estimate the grain size assuming that the sample would consist of spherical particles with a specific density similar to that of bulk ZrO_2 (Table 1). For sample ZrO_2-M2, the BET surface area corresponds to a particle size of about 13 nm.

The structure on the nanometer length scale was further investigated by transmission electron microscopy (TEM) (Figure 9). From these images it is clear the macropore walls are built up of loosely aggregated particles (11 2 nm) that appear to be single crystallites based on the crystal fringes that can be observed at higher magnifications. No internal particle porosity can be observed suggesting that the introduced porosity observed in the nitrogen physisorption data probably originates from the interparticle voids seen in the TEM images.

In order to shed some light on the chemical composition of the ZrO_2 replica monoliths various characterization techniques were used, for instance electron dispersive spectroscopy (EDS) to estimate the remaining Si content in the replica monoliths (results not shown). From these measurements it was clear that the replicas still contain fairly high concentrations of silicon: 7 at-% Si in ZrO_2-M1 and 8 at-% in ZrO_2-M2. The silicon that remains is not associated with undissolved template, as the dissolution times used were sufficient to completely dissolve the silica template in all the

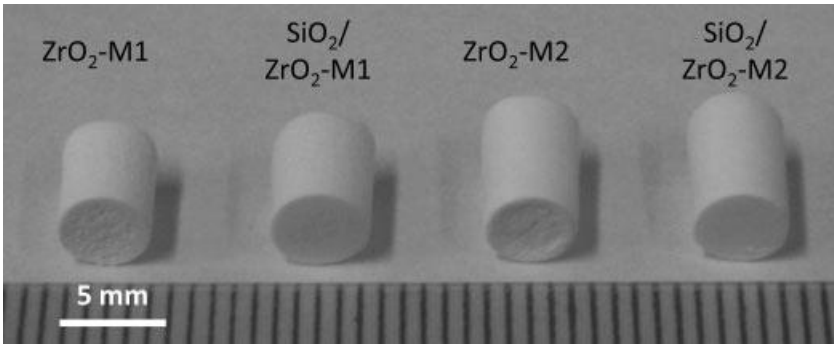

Fig. 8. Photograph showing etched (ZrO_2) and non-etched (ZrO_2/SiO_2) composites.

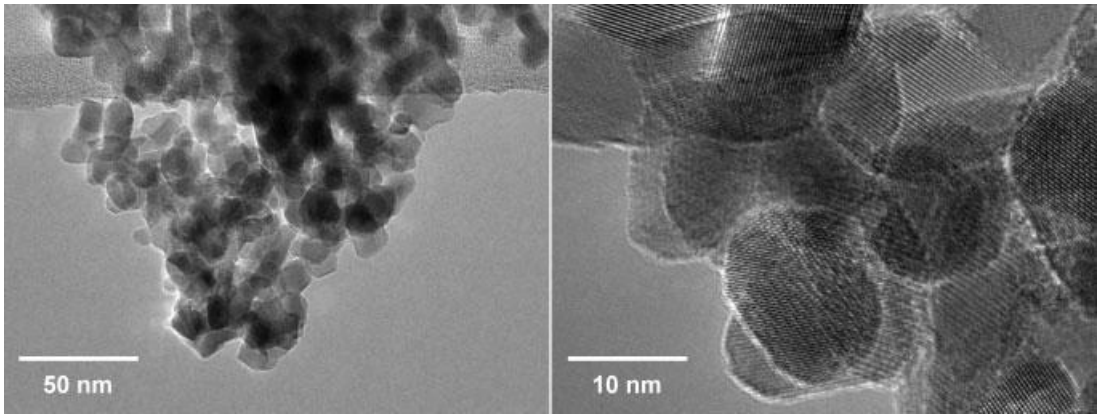

Fig. 9. TEM images of sample ZrO_2-M2 at different magnifications showing the particles and the crystal fringes.

other samples. Liu and Baker reported the formation of zirconium silicate when they nanocast zirconia into mesoporous silica particles,[53] which suggests that this could also be the cause for the retained silicon. This is consistent also with our observation of the formation of silver silicates (below).

The XRD plot in Figure 6 shows that the replica structure consists of a mixture of monoclinic ZrO_2 and tetragonal ZrO_2 (or orthorhombic ZrO_2 which would give almost the same peaks). However, there is no evidence of any crystalline phases of mixed Si Zr oxides (for instance $ZrSiO_4$ ¼ zircon), although a broad diffraction peak between 10 and 208 2u would indicate an amorphous phase. The monoclinic ZrO_2 peak at 288 2u was used to determine the crystallite size by the Scherrer equation and the size was estimated to be 12.5 nm which corresponds quite well to the TEM images.

FT-Raman spectroscopy gave further information about the crystalline structure of the ZrO_2 replica monoliths (Figure 10). Here again the conclusion was that the samples are mixtures of monoclinic and tetragonal ZrO_2, while no peak from zirconium silicate can be detected. The presence of both m-ZrO_2 and t-ZrO_2 is typical for calcinations at temperatures between 400 and 800 8C, where the transition from the tetragonal to the monoclinic form is evident with increasing temperature.[80,81] The peak at 1063 cm ^{1} typically appears for

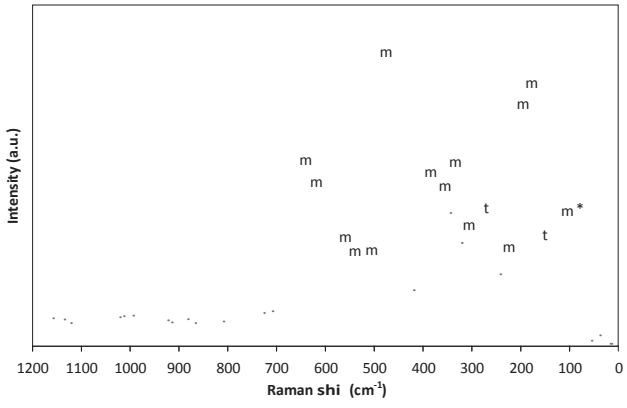

Fig. 10. FT-Raman measurement of sample ZrO_2-M2 showing both monoclinic (m) and tetragonal (t) peaks (previously observed ambiguity).

small crystallites or grain sizes (<20 nm) and the ratio between the S_{1063} and C_{475} peaks can be used to estimate the grain size. In this case it is about 15 nm which corresponds well with both the XRD and TEM results, as well as the size estimated from the surface area.

The absence of peaks from zirconium silicate in the XRD is not particularly surprising as XRD requires that there be some minimum crystallinity in the material. Liu and Baker in their work on nanocasting of zirconia into mesoporous silica particles[53] were also not able to detect any XRD peaks due to scattering from the zirconium silicate. They believed this was because the zirconium silicate was formed only at the surface of the silica and that this was not a bulk phase. In the absence of XRD peaks for $ZrSiO_4$ they relied on careful comparison of the Raman spectrum of their silica matrix in the presence and absence of added zirconia to identify the zirconium silicate phase. From their work it is clear that the peaks for zirconium silicate would be undetectable in our Raman spectrum (Figure 10) as they would be masked by the zirconia peaks.

2.5. Ag Monoliths

The silver monoliths produced by decomposition of silver nitrate under vacuum and under air were both a flat gray color on the exterior. Visual inspection of the interior however showed significant differences between the two samples. The sample prepared under vacuum, Ag-B3-vac was spatially inhomogeneous. A cross-section showed that the flat gray color extended only ca. 1 mm into the monolith. The center 2 mm of the sample was a dark pink/orangey red in color. The samples impregnated under air appeared homogeneous under visual inspection of cross-sections. Figure 1 and 11 show SEM images taken from the exterior region of the monolith decomposed under vacuum. The EDS (shown in Supporting Information) gives a composition which is 80 at.% silver. The XRD (Figure 6) also shows that the dominant peaks for this region are from metallic silver. The morphology of the material (Figure 1 and 11) is consistent with that of agglomerated silver. The decomposition was carried out at 450 8C. This exceeded the Hü ttig temperature for silver, and so

ADVANCED ENGINEERING MATERIALS

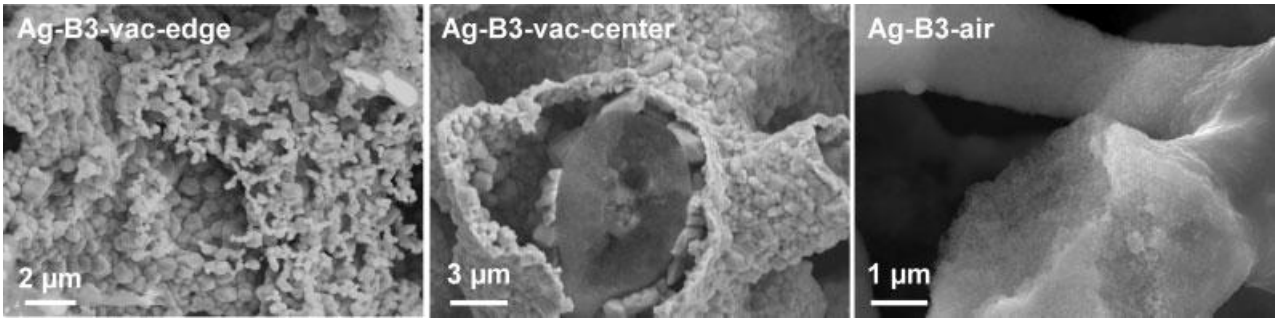

Fig. 11. SEM images (from left to right) from the center portion of Ag-B3-vacuum, the exterior portion of Ag-B3-vacuum, and Ag-B3-air.

sintering and particle growth of the silver crystallites are expected. The XRD for the center of sample Ag-B3-vac is quite different from that of the exterior of the monolith. Peaks due to metallic silver are clearly present, however there are also a number of other peaks, a set of which agree well with a silver silicate of composition $Ag_{10}Si_4O_{13}$. The inhomogeneous nature of the sample in this area is clearly seen in Figure 11, which shows a cross-section of a ligament displaying two very different morphologies, a very smooth central core surrounded by a shell of material with coarser structures. The composition of these two phases from EDS is significantly different (Supporting Information) with the shell having an atomic composition: Ag 10%:Si 26%:O 64%, and the core having a composition: Ag 66%:Si 6%:O 28%.

Figure 11 also shows a typical SEM image of the sample decomposed under air, sample Ag-B3-air. The observed morphology is relatively smooth at the micrometer length scale and consists of smaller features more typical of other nanocast samples such as Fe_2O_3 above. This morphology is consistent throughout sample Ag-B3-air. The XRD data for this sample does show the presence of metallic silver, but also shows the presence of a number of other peaks. The composition estimated by EDS varies from 8 to 15% silver and 10 to 21% silicon. The surface area of the two monoliths is also very different. Sample Ag-B3-vac has a surface area of 94.7 m^2 g^{-1} compared to 17.9 m^2 g^{-1} for sample Ag-B3-air, with a mesopore volume three times higher.

To the best of our knowledge the formation of silver silicates from mesoporous silica has not been previously reported. The formation of Ag_2SiO_3 is reported to be thermodynamically unfavorable for bulk materials, but becomes favorable for mixtures of silver and silica nanoparticles with diameters less than 20 nm.[82] Similarly the formation of $Ag_6Si_2O_7$ is reported to occur at the interface between silica nanoparticles and amorphous silica.[83] The formation of silver silicates within our mesoporous silica templates is consistent with both these reports.

We believe that the spatial variations in composition, and the impact of atmosphere can be explained by assuming that the decomposition of the silver nitrate to silver and growth of silver nanoparticles is in competition with formation of silver silicates. The presence of air could well modify the decomposition pathway for the silver nitrate, as is known to occur for other metal nitrates.[78] Under vacuum the decomposition products would be more quickly carried away and so the reduction would occur more rapidly. The data from the sample decomposed under vacuum suggests that in the core of the monolith the transport of decomposition products is too slow to produce complete conversion to the metallic silver. Although these types of spatially heterogeneous structures have not previously been reported in silica monoliths, a comparable effect has been recently reported for nanocasting of iron oxide into mesoporous silica particles.[84] In this report the shape of the container was observed to impact the size and morphology of the resulting mesoporous iron oxide particles.[84] This model is also broadly consistent with the impact of different gas atmospheres on Co_3O_4 monolith formation discussed above, although the exact chemical pathways must be significantly different given the formation of silicates in the case of silver but not cobalt.

2.6. Nickel Oxide and Nickel Monoliths

Figure 12 shows an SEM image of a nickel oxide monolith (sample NiO-B1) after removal of the silica template. This sample (NiO-B1) was produced by decomposition of nickel acetate. The reduction of this sample by hydrogen gas leads to the nickel monolith Ni-B1-post-H_2 with the SEM image shown in Figure 12. XRD shows (Figure 6) that the reduction is largely complete, although EDS data from the sample indicates that surface oxidation occurs relatively quickly. A comparison of the SEM images at multiple length scales indicates that the reduction retains the structure down to a length scale of 50–100 nm, however comparison of the nitrogen adsorption isotherms suggests that there is some loss of structure on reduction as indicated by the drop in surface area/volume from 182 m^2 cm^{-3} for the nickel oxide sample NiO-B1 to 95 m^2 cm^{-3} in the resulting nickel sample Ni-B1-post-H_2. This is also reflected in the pore size distribution where the nickel oxide has a peak in the pore size distribution at around 20 nm, this peak shifts and broadens in the nickel (Figure 13). This is not surprising as we would expect that the elevated temperatures associated with the hydrogen reduction would allow for some migration of the nickel, resulting in smoothing out of the highest curvature surfaces and a resultant decrease in surface area. The 0.5–1 mm voids that can be seen in the SEM

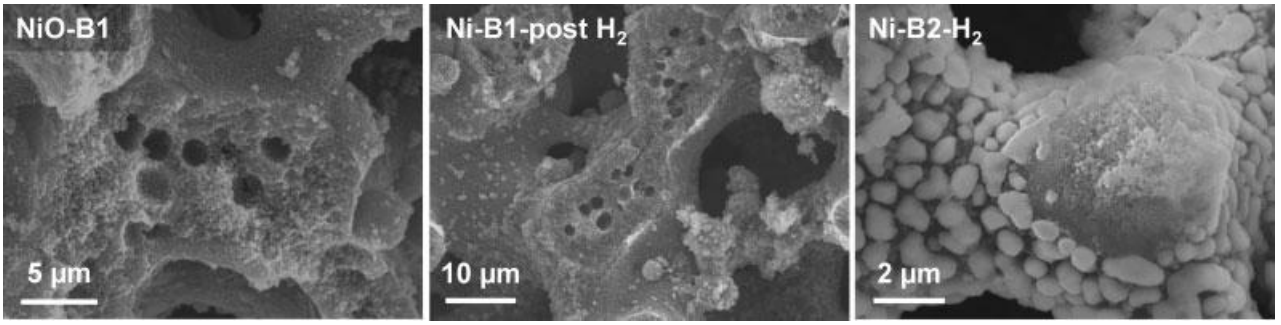

Fig. 12. SEM images from left to right of nickel oxide sample NiO-B1, nickel sample Ni-B1-post-H_2, and nickel sample Ni-B2-H_2.

images of NiO-B1 and Ni-B1-post-H_2 are almost certainly a result of similar voids that were present in the parent silica monolith. We believe that these voids are the result of air bubbles present during the sol–gel processing that produced the silica monoliths.

Figure 12 shows an SEM image of nickel (Ni-B2-H_2) made by an alternative route using a different template that does not contain voids in the ligament. This sample was synthesized from aqueous nickel nitrate solution, with the decomposition at each step being carried out under hydrogen. Hydrogen is believed to reduce the mobility of the nickel during the decomposition of nickel nitrate by scavenging the oxygen formed in the reaction. Oxygen can be catalytic in nitrate decomposition and so scavenging the oxygen slows the decomposition.[78] Formation of nickel under hydrogen leads to a surface/volume ratio which is significantly higher than decomposition under air and postreduction. The pore size distribution is also centered at a slightly lower pore diameter. Although it is tempting to conclude that the in situ hydrogen reduction did result in better retention of structure, the two samples were produced from different monoliths using different precursors and different procedures. Sample SiO_2-B1 used a lower concentration of a shorter chain surfactant, leading to smaller pores (4.3 nm for SiO_2-B1 cf. 4.5 nm for SiO_2-B2) and a smaller mesopore volume (2.09 cm^3 cm^{-3} for SiO_2-B1 cf. 2.88 cm^3 cm^{-3} for SiO_2-B2). Sample Ni-B1-post-H_2 was made by ''incipient wetness'' in air using an acetate precursor. This means that only enough solution was added to completely fill the surfactant mesopores. Sample Ni-B2-H_2 was made using nickel nitrate under vacuum infiltration. We believe this method leads to faster filling of the surfactant mesopores.

Overall the use of bimodal rather than monomodal silica templates does appear to produce an enhancement in the surface area of the nanocast metal oxides, but the extensive migration of materials from the surfactant mesopores into the textural mesopores is such that the potentially accessible surface area is not fully realized.

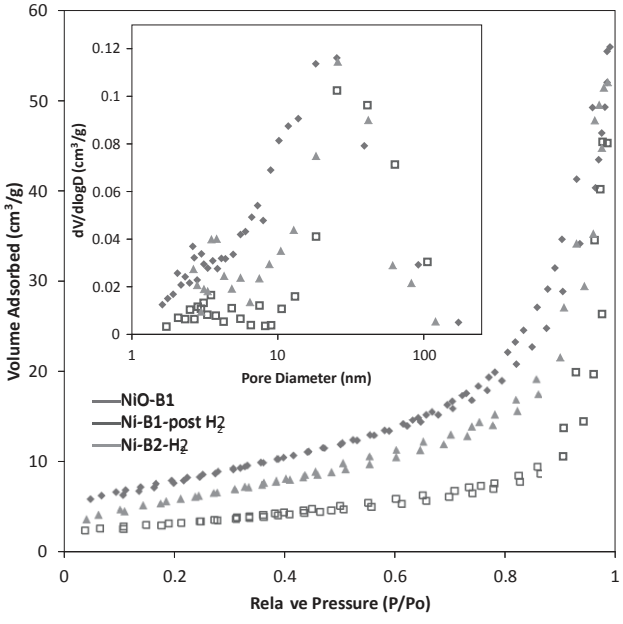

Fig. 13. Nitrogen physisorption of nickel oxide and nickel monoliths (a) nickel oxide, (b) nickel sample Ni-B2-post-H_2, and (c) nickel sample Ni-B2-H_2.

2.7. Impact of Monolith Type

The greater surface area available from the bimodal monoliths SiO_2-B1, SiO_2-B2, and SiO_2-B3 would be expected to be translated into a similarly higher surface area in the nanocast replicas. Although there are no direct comparisons in this work between the same material nanocast into monomodal and bimodal templates, comparison with our previously published work[34] and the results in Table 1 does allow some observations to be made. The different specific bulk densities of the different nanocast material make comparison of the surface area/gram misleading. Surface area per volume of nanocast material (m^2 cm^{-3}) is a more meaningful comparison. On this basis the previously reported[34] surface area for Co_3O_4 from a monomodal template would have a value of 247 m^2 cm^{-3} (based on a density of Co_3O_4 of 6.11 g cm^{-3}). This is less than half the best value in Table 1. This difference is inline with results from SnO_2 (based on a density of SnO_2 of 6.95 g cm^{-3}) which increases from 250 m^2 cm^{-3} for a monomodal template to 490 m^2 cm^{-3} for a bimodal template.[34] It is more difficult to discern any trends in the results as a function of metal oxide, as the values for ZrO_2 nanocast in monomodal templates are comparable to those for Co_3O_4 from bimodal templates and

ADVANCED ENGINEERING MATERIALS

significantly higher than that observed for Fe_2O_3 and NiO. However, considerable zirconium silicate formation at the interface between the zirconia and the silica template occurred in this sample, and so the higher surface area may well reflect this phenomenon. Silver monoliths on the other hand do not show a similarly high surface area, but in this case bulk silver silicate formation is believed to have occurred, implying large scale movement of materials which would allow considerable Ostwald ripening to have occurred.

3. Conclusions

The use of hierarchically porous silica as templates for nanocasting to produce hierarchically porous metals and metal oxides as a general method to make these classes of materials has been demonstrated by synthesis of nickel oxide, a-Fe_2O_3, ZrO_2, nickel, and silver monoliths. The details of the processes used in converting the silica template to the replica monolith have a significant impact on the structure and properties of the final material. This was illustrated by the effect of carrying out the processes under vacuum or under different gases on Co_3O_4 and silver monoliths. In the case of the silver monoliths the atmosphere impacts not simply the structure of the material, but also the composition of the material, and the composition as a function of location in the monolith. We have also demonstrated that metal silicates can be formed at relatively modest temperatures within mesoporous silica templates, which appears to have received little attention within the nanocasting field.

4. Experimental

4.1. Preparation of Hierarchically Porous Silica Monoliths

Hierarchically porous silica monoliths were prepared according to previously described procedures [28,38]. In the preparation of monoliths with a monomodal mesopore size distribution, PEG (MW: 35 000 g/mol) was used to induce the macroporosity [38]. These samples are denoted SiO_2-M1 and SiO_2-M2 depending on the PEG amount (4.7 and 5.3 wt%, respectively). Monoliths with a bimodal mesoporosity were produced by using a combination of PEG and hexadecyltrimethylammonium bromide (C_{16}TAB) or PEG and octadecyltrimethylammonium bromide (C_{18}TAB) as structure directing agents [38]. These samples are denoted SiO_2-B1 (9 wt% C_{16}TAB), SiO_2-B2 (7 wt% C_{18}TAB), and SiO_2-B3 (9 wt% C_{18}TAB). A more detailed description can be found in the Supporting Information.

4.2. Preparation of Co_3O_4 Monoliths (Varying the Gas Atmosphere)

Silica monoliths with a bimodal mesopore size distribution (SiO_2-B1) were used as templates for Co_3O_4 monoliths. The silica monoliths were impregnated with a 58 wt% aqueous solution of $Co(NO_3)_2$ $6H_2O$ (98%, Fluka) under vacuum. After soaking for 1 h, the monoliths were rolled on copier paper to remove excess solution. Impregnated monoliths were then heated to 150 8C at a rate of 2 8C min ^{1} and held at 150 8C for 10 h under stagnant air, argon flow, nitrogen flow, or vacuum. These steps were repeated twice. The monoliths were then calcined at 550 8C for 6 h under the mentioned atmospheres with a ramp rate of 1 8C min ^{1}, except for the vacuum sample which was calcined under stagnant air. The silica template was removed with 4 M aqueous NaOH (2 24 h treatments at 90 8C). Co_3O_4 monoliths were then rinsed with deionized water and dried at 90 8C.

4.3. Preparation of Fe_2O_3

Silica monoliths with bimodal mesopore size distribution (SiO_2-B2) were used as templates for Fe_2O_3 monoliths. Silica monoliths were soaked in a 87 wt% aqueous solution of $Fe(NO_3)_3$ $9H_2O$ (98 þ %, Alfa Aesar) at 75 8C until they appeared translucent, approximately 24 h. Excess solution was removed and the monoliths were dried and the salt decomposed in air at 150 8C for 10 h. Impregnation of iron nitrate and decomposition was repeated twice for these samples. The sample was then calcined in air at 550 8C for 6 h with a ramp rate of 1 8C min ^{1}. The silica was removed by etching in 3 M KOH overnight. Monoliths were then rinsed with deionized water and dried at 90 8C.

4.4. Preparation of ZrO_2 Monoliths

Silica monoliths with monomodal mesopore size distribution (SiO_2-M1 and SiO_2-M2 described above) were used as templates in the preparation of hierarchically porous ZrO_2 monoliths. The monoliths were impregnated with a 50 wt% aqueous solution of $Zr(SO_4)_2$ $4H_2O$ (98þ%, Alfa Aesar) under vacuum. After soaking for 1 h, the monoliths were carefully wiped with a paper tissue to remove excess solution and dried at 40 8C for 24 h. The impregnation and drying procedure was repeated once, after which the samples were calcined in air 2 h at 750 8C (heating ramp 1 8C min ^{1}) to fully decompose the sulfate to the oxide (which occurs at 720 8C for the pure salt). In order to obtain a mechanically stable ZrO_2 replica the impregnation-drying-impregnation-drying-calcination cycle was carried out 4 times in total. In a final step, the silica template was removed by etching the composite monoliths in 1 M aqueous NaOH solution (24 h at 90 8C). The monoliths were then washed thoroughly with water and acetone and finally dried at 40 8C for more than 24 h.

4.5. Preparation of Ag Monoliths

Silica monoliths with a bimodal mesopore size distribution (SiO_2-B3) were soaked in melted $AgNO_3$ (99.9%, Alfa Aesar) at 400 8C until the salt had visibly wet the entire monolith, approximately 1 h. Excess salt was removed and the monoliths were heated to 450 8C and held for 1 h in either air or under vacuum to decompose the salt. The composite was cooled and the silica was removed with 3 M aqueous KOH solution overnight. Monoliths were then rinsed with deionized water and dried at 80 8C under vacuum.

4.6. Preparation of NiO and Ni Monoliths

Silica monoliths with a bimodal (B1) mesopore size distribution were used as templates for the preparation of nickel oxide monoliths. The monoliths were impregnated with 0.7 M aqueous nickel acetate (98%, Aldrich). After drying, the monoliths were heated under air to 400 8C for 5 h to decompose the salt. This procedure was repeated eight times to obtain a stable replica. The silica template was then removed with 4 M NaOH for 48 h, rinsed with water to remove excess salt, and then dried at 40 8C. The nickel oxide replicas were then heated under a reducing atmosphere (5% H_2 in N_2) to 240 8C, at a ramp

of 1 8C min ^{1} to reduce the monoliths to nickel metal. These samples are designated Ni-B1-post-H_2.

In situ reduction under hydrogen was also carried out. Silica monoliths possessing a bimodal pore size distribution (SiO_2-B2) were impregnated with a 57 wt% $Ni(NO_3)_2$ $6H_2O$ (98%, Alfa Aesar) solution under vacuum. Excess solution was removed and monoliths were heated at 150 8C for 10 h, ramped to 350 8C at a rate of 2 8C min ^{1}, and held at 350 8C for 5 h under 5% hydrogen in nitrogen flow. Samples were cooled and infiltration and reduction cycles were repeated four times. Samples were etched with aqueous 3 M KOH, rinsed with deionized water, and dried at 80 8C under vacuum. These samples are designated Ni-B2-H_2.

4.7. Characterization Methods

SEM/EDS measurements were carried out on a JEOL 7000 SEM or a Jeol JSM-6335F equipped with Oxford EDS detectors, while the transmission electron microscope images were taken with a Hitachi HF2000 TEM instrument, equipped with a cold field emission gun. Nitrogen physisorption measurements were conducted on a Nova 2200e or an Autosorb-1 instrument (both from Quantachrome), as well as an ASAP 2010 instrument (from Micromeritics). In the pore size calculations the BJH model based on the desorption branch was generally used. For the silica monoliths, the NL-DFT method was used for pores smaller than 6 nm (kernel for cylindrical pores using the adsorption branch). XRD patterns were measured on either a Bruker D2 Phaser system or a Bruker AXS D8 Discover instrument (both using X-ray copper sources). Crystallite sizes were estimated from the XRD measurements by applying the Scherrer equation [85] using the Topas software provided from Bruker. FT-Raman spectroscopy was carried out on a Bruker FRA 106 instrument using a Nd:YAG laser (wavelength: 1060 nm).

Received: December 25, 2011
Final Version: April 19, 2012
Published online: May 23, 2012

[1] A. El Kadib, R. Chimenton, A. Sachse, Fo. Fajula, A. Galarneau, B. Coq, Angew. Chem., Int. Ed. 2009, 121, 5069.
[2] A. Sachse, A. Galarneau, Fo. Fajula, F. Di Renzo, P. Creux, B. Coq, Microporous Mesoporous Mater. 2011, 140, 58.
[3] Z. Jiang, N. W. Smith, Z. Liu, J. Chromatogr., A 2011, 1218, 2350.
[4] S. Miller, Anal. Chem. 2004, 76, 99A.
[5] K. K. Unger, R. Skudas, M. M. Schulte, J. Chromatogr., A 2008, 1184, 393.
[6] G. Guiochon, J. Chromatogr., A 2007, 1168, 101.
[7] M. Winter, R. J. Brodd, Chem. Rev. 2004, 104, 4245.
[8] J. W. Long, B. Dunn, D. R. Rolison, H. S. White, Chem. Rev. 2004, 104, 4463.
[9] D. R. Rolison, J. W. Long, J. C. Lytle, A. E. Fischer, C. P. Rhodes, T. M. McEvoy, M. E. Bourg, A. M. Lubers, Chem. Soc. Rev. 2009, 38, 226.
[10] Z.-Y. Yuan, T.-Z. Ren, A. Vantomme, B.-L. Su, Chem. Mater. 2004, 16, 5096.
[11] A. Vantomme, A. Leonard, Z.-Y. Yuan, B.-L. Su, Colloids Surf., A 2007, 300, 70.
[12] J. C. Lytle, A. Stein, in Annual Review of Nano Research, Vol. 1 (Eds: G. Cao, C. J. Brinker), World Scientific, River Edge, NJ, USA 2006, p. 1.
[13] A. Stein, F. Li, N. R. Denny, Chem. Mater. 2008, 20, 649.
[14] N. V. Dziomkina, G. J. Vancso, Soft Matter 2005, 1, 265.
[15] M. Antonietti, B. Berton, C. Goltner, H.-P. Hentze, Adv. Mater. 1998, 10, 154.
[16] F. Li, Z. Wang, N. S. Ergang, C. A. Fyfe, A. Stein, Langmuir 2007, 23, 3996.
[17] F. Carn, A. Colin, M.-F. Achard, H. Deleuze, E. Sellier, M. Birot, R. Backov, J. Mater. Chem. 2004, 14, 1370.
[18] J. J. Chui, D. J. Pine, S. T. Bishop, B. F. Chmelka, J. Catal. 2004, 221, 400.
[19] H. Maekawa, J. Esquena, S. Bishop, C. Solans, B. F. Chmelka, Adv. Mater. 2003, 15, 591.
[20] D. Zhao, P. Yang, B. F. Chmelka, G. D. Stucky, Chem. Mater. 1999, 11, 1174.
[21] S. A. Davis, S. L. Burkett, N. H. Mendelson, S. Mann, Nature 1997, 385, 420.
[22] C. Mille, E. C. Tyrode, R. W. Corkery, Chem. Commun. 2011, 47, 9873.
[23] R. A. Caruso, M. Antonietti, Adv. Funct. Mater. 2002, 12, 307.
[24] R. A. Caruso, J. H. Schattka, Adv. Mater. 2000, 12, 1921.
[25] D. Walsh, L. Arcelli, T. Ikoma, J. Tanaka, S. Mann, Nat. Mater. 2003, 2, 386.
[26] H. Nishihara, S. R. Mukai, D. Yamashita, H. Tamon, Chem. Mater. 2005, 17, 683.
[27] K. Suzuki, K. Ikari, H. Imai, J. Mater. Chem. 2003, 13, 1812.
[28] K. Nakanishi, J. Porous Mater. 1997, 4, 67.
[29] J. Konishi, K. Fujita, S. Oiwa, K. Nakanishi, K. Hirao, Chem. Mater. 2008, 20, 2165.
[30] J. Konishi, K. Fujita, K. Nakanishi, K. Hirao, Chem. Mater. 2006, 18, 864.
[31] Y. Tokudome, K. Fujita, K. Nakanishi, K. Miura, K. Hirao, Chem. Mater. 2007, 19, 3393.
[32] O. Ruzimuradov, G. Hasegawa, K. Kanamori, K. Nakanishi, J. Am. Ceram. Soc. 2011, 94, 3335.
[33] J.-H. Smått, B. Spliethoff, J. B. Rosenholm, M. Lindé n, Chem. Commun. 2004, 2188.
[34] J.-H. Smått, C. Weidenthaler, J. B. Rosenholm, M. Lindén, Chem. Mater. 2006, 18, 1443.
[35] A. Taguchi, J.-H. Smått, M. Lindé n, Adv. Mater. 2003, 15, 1209.
[36] A.-H. Lu, J.-H. Smått, M. Lindé n, Adv. Funct. Mater. 2005, 15, 865.
[37] K. Nakanishi, H. Komura, R. Takahashi, N. Soga, Bull. Chem. Soc. Jpn. 1994, 67, 1327.
[38] J.-H. Smått, S. Schunk, M. Lindé n, Chem. Mater. 2003, 15, 2354.
[39] J. Konishi, K. Fujita, K. Nakanishi, K. Hirao, Chem. Mater. 2006, 18, 6069.

[40] S. Murai, K. Fujita, K. Iwata, K. Tanaka, J. Phys. Chem. C 2011, 115, 17676.
[41] G. L. Drisko, Ae. Zelcer, V. Luca, R. A. Caruso, G. J. de A. A. Soler-Illia, Chem. Mater. 2010, 22, 4379.
[42] K. Nakanishi, Y. Sato, Y. Ruyat, K. Hirao, J. Sol-Gel Sci. Technol. 2003, 26, 567.
[43] Y. Sato, K. Nakanishi, K. Hirao, H. Jinnai, M. Shibayama, Y. B. Melnichenko, G. D. Wignall, Colloids Surf., A 2001, 187, 117.
[44] T. Amatani, K. Nakanishi, K. Hirao, T. Kodaira, Chem. Mater. 2005, 17, 2114.
[45] H. Zhong, G. Zhu, P. Wang, J. Liu, J. Yang, Q. Yang, J. Chromatogr., A 2008, 1190, 232.
[46] D. Brandhuber, V. Torma, C. Raab, H. Peterlik, A. Kulak, N. Hüsing, Chem. Mater. 2005, 17, 4262.
[47] A.-H. Lu, D. Zhao, Y. Wan, Nanocasting: A Versatile Strategy for Creating Nanostructured Porous Materials, Vol. 11, Royal Society of Chemistry, Cambridge 2010.
[48] A.-H. Lu, F. Schüth, Adv. Mater. 2006, 18, 1793.
[49] H. Yang, D. Zhao, J. Mater. Chem. 2005, 15, 1217.
[50] M. Tiemann, Chem. Mater. 2008, 20, 961.
[51] R. Bao, K. Jiao, H. He, J. Zhuang, B. Yue, Stud. Surf. Sci. Catal. 2007, 165, 267.
[52] B. G. So, J. K. Shon, J. A. Yu, O.-S. Joo, J. M. Kim, in Recent Progress in Mesostructured Materials (Eds: D. Zhao, S. Qui, Y. Tang, C. Yu), Elsevier, Amsterdam 2007, p. 309.
[53] B. Liu, R. Thornton Baker, J. Mater. Chem. 2008, 18, 5200.
[54] Y. M. Wang, Z. Y. Wu, H. J. Wang, J. H. Zhu, Adv. Funct. Mater. 2006, 16, 2374.
[55] W. Yue, W. Zhou, Chem. Mater. 2007, 19, 2359.
[56] W. B. Yue, W. Z. Zhou, Stud. Surf. Sci. Catal. 2007, 170, 1755.
[57] H. Yen, Y. Seo, R. Guillet-Nicolas, S. Kaliaguinec, F. Kleitz, Chem. Commun. 2011, 47, 10473.
[58] M. G. Bakker, V. Warke, in Nanowire Research Progress (Ed: X. Xue), Nova Science Publishers, Hauppauge, NY 2008, p. 15.
[59] F. M. Sayler, A. J. Grano, W. Scogin, P. Sanders, J.-H. Smått, K. Shaughnessy, M. G. Bakker, in MRS Symposium Proceedings, Cambridge University Press, Cambridge 2012, 1389, G01-08.
[60] J. A. Moulijn, A. E. van Diepen, F. Kapteijn, Appl. Catal., A 2001, 212, 3.
[61] A. Martinez, C. Lopez, F. Marquez, I. Diaz, J. Catal. 2003, 220, 486.
[62] S. Liu, B. Yue, K. Jiao, Y. Zhou, H. He, Mater. Lett. 2006, 60, 154.
[63] T. Valdes-Solis, P. Tartaj, G. Marban, A. B. Fuertes, Nanotechnology 2007, 18, 145603.
[64] M. Gu, B. Yue, R. Bao, H. He, Mater. Res. Bull. 2009, 44, 1422.
[65] H. Tuysuz, C. W. Lehmann, H. Bongard, B. Tesche, R. Schmidt, F. Schüth, J. Am. Chem. Soc. 2008, 130, 11510.
[66] S. M. El-Sheikh, F. A. Harraz, M. M. Hessien, Mater. Res. Chem. Phys. 2010, 123, 254.
[67] A. A. Eliseev, D. F. Gorozhankina, D. D. Zaitseva, A. V. Lukashina, A. V. Knotkoa, Y. D. Tretyakova, P. Görnert, J. Magn. Magn. Mater. 2005, 290–291, 106.
[68] Me. Cabo, E. Pellicer, E. Rossinyol, O. Castell, S. Surinach, M. D. Baro, Cryst. Growth Des. 2009, 9, 4814.
[69] M. Cabo, E. Pellicer, E. Rossinyol, M. Estrader, A. Lopez-Ortega, J. Nogues, O. Castell, S. Surinach, M. D. Baro, J. Mater. Chem. 2010, 20, 7021.
[70] S. Polarz, A. V. Orlov, F. Schüth, A.-H. Lu, Chem. Eur. J. 2007, 13, 592.
[71] T. Waitz, M. Tiemann, P. J. Klar, J. Sann, J. Stehr, B. K. Meyer, Appl. Phys. Lett. 2007, 90, 123108.
[72] H. Tuysuz, Y. Liu, C. Weidenthaler, F. Schüth, J. Am. Chem. Soc. 2008, 130, 14108.
[73] F. Jiao, J.-C. Jumas, M. Womes, A. V. Chadwick, A. Harrison, P. G. Bruce, J. Am. Chem. Soc. 2006, 128, 12905.
[74] J.-H. Smått, S. A. Schunk, M. Lindén, Chem. Mater. 2003, 15, 2354.
[75] A.-H. Lu, J.-H. Smått, S. Backlund, M. Lindén, Microporous Mesoporous Mater. 2004, 72, 59.
[76] S. Haffer, T. Waitz, M. Tiemann, J. Phys. Chem. C 2010, 114, 2075.
[77] J. R. A. Sietsma, H. Friedrich, A. Broersma, M. Versluijs-Helder, A. J. van Dillen, P. E. de Jongh, K. P. de Jong, J. Catal. 2008, 260, 227.
[78] J. R. A. Sietsma, J. D. Meeldijk, M. Versluijs-Helder, A. Broersma, A. J. van Dillen, P. E. de Jongh, K. P. de Jong, Chem. Mater. 2008, 20, 2921.
[79] H. L. Tidahy, S. Siffert, J.-F. Lamonier, E. A. Zhilinskaya, A. Aboukais, Z.-Y. Yuan, A. Vantomme, B.-L. Su, X. Canet, G. De Weireld, M. Frere, T. B. N'Guyen, J.-M. Giraudon, G. Leclercq, Appl. Catal., A 2006, 310, 61.
[80] C. Li, M. Li, J. Raman Spectrosc. 2002, 33, 301.
[81] G. G. Siu, M. J. Stokes, Y. Liu, Phys. Rev. B 1999, 59, 3173.
[82] J. De, A. M. Umarji, K. Chattopadhyay, Mater. Sci. Eng. 2007, 449–451, 1062.
[83] W. Cai, L. Zhang, Appl. Phys. A 1998, 66, 419.
[84] X. Sun, Y. Shi, P. Zhang, C. Zheng, X. Zheng, F. Zhang, Y. Zhang, N. Guan, D. Zhao, G. D. Stucky, J. Am. Chem. Soc. 2011, 133, 14542.
[85] J. I. Langford, A. J. C. Wilson, J. Appl. Crystallogr. 1978, 11, 102.

APPLICATION

FOR

UNITED STATES LETTERS PATENT

FOR

METHODS FOR PREPARING AND USING METAL AND/OR METAL OXIDE POROUS MATERIALS

BY

MARTIN BAKKER, a citizen of the United States of America residing at Tuscaloosa, Alabama, USA; **FRANCHESSA SAYLER**, a citizen of the United States of America residing at Tuscaloosa, Alabama, USA; **AMY GRANO**, a citizen of the United States of America residing at Tuscaloosa, Alabama, USA; and **JAN-HENRIK SMÅTT**, a citizen of Finland residing at Turku, Finland.

METHODS FOR PREPARING AND USING METAL AND/OR METAL OXIDE POROUS MATERIALS

CROSS REFERENCE TO RELATED APPLICATIONS

This application claims the benefit of priority to U.S. Provisional Application No. 61/447,072, filed February 27, 2011, which is incorporated by reference herein in its entirety.

FIELD

The subject matter disclosed herein relates to methods for producing metal and/or metal oxide porous materials. Metal and/or metal oxide porous materials and methods of using them are also disclosed herein.

BACKGROUND

A number of methods have been advanced to produce controlled porosity on micrometer and millimeter length scales. Principal among these methods is the use of colloidal templating in which micrometer sized beads of silica or polymers such as polystyrene are used as template for sol-gel mixtures, primarily silica. The sol-gel mixture may or may not include a structure directing agent to give porosity on the nanometer scale. After the removal of the polymer and nanostructure directing agent by dissolution or combustion, a three dimensional replica is produced. These replicas have regular, highly ordered micropore networks, are typically not mechanically very strong, and are difficult to produce in large bodies. The need for polymer or silica beads increases the cost of this synthesis and limits the range of structures available. The need for infiltration of the sol-gel precursor through the material also limits the applicability of this approach. The material formed by this approach has been used as a template for the formation of metal oxide and metals. Such materials have low surface areas.

Other methods for producing porous metal materials known as metal foams include bubbling gas through molten metal, generating gas during an exothermic reaction that melts the metal or that reduces and melts the metal, and generating gas during electrodeposition of the metal. Such processes generally produce large pore size distributions, are not compatible with the simultaneous formation of nanopores, are typically not very mechanically robust, and often have significant amounts of organic impurities. Other methods of making metal foams involve electrodeposition or metal condensation onto carbon skeletons. These approaches typically are not capable of generating small pore diameters and large bodies.

Other methods have been developed for producing porous metal oxide particles. Yue *et al.* ("Synthesis of Porous Single Crystals of Metal Oxides via a Solid-Liquid Route",*Chem. Mater.* 19:2359, 2007, and "Mesoporous metal oxides templated by FDU-12 using a new convenient method", *Studies Surf. Sci. Catal* , 170:1755, 2007)**,** disclose that metal nitrates can be introduced into mesoporous silica particles by grinding the metal nitrate and mesoporous silica particles in a crucible and then heating the material at a rate of 1 ^{o}C/min to 500 ^{o}C where the temperature is maintained for 5 hours. Yue *et al.* teach that the metal nitrate melted and entered the pores of the silica. They disclose images of small (<150 nm) sized particles. Yue *et al.*'s disclosure demonstrates a limitation of that method for preparing larger bodies. For example, the grinding step reduces the size of the mesoporous silica particles limiting the size of replica particle that can be produced. The grinding step would result in the destruction of a larger body. The heating ramp used also constitutes a limit on the size of replica that can be achieved as it provides insufficient time for transport of materials within the mesopores. As such, these methods have not been applied to larger porous bodies.

Moreover, while the decomposition of metal nitrates has been much studied, the results have been contradictory. As the temperature of a nitrate melt is raised towards the decomposition temperature of the nitrate, water of hydration can be lost producing compounds that may either be a liquid or a solid and so may or may not be able to move within a mesopore. The loss of water is determined by the pressure of any ambient atmosphere and by the rate of transport of the water vapor through the mesopores. This can be illustrated by considering the nickel nitrate system which is among the most studied metal nitrates. Heating nickel nitrate is reported to go through a series of dehydration steps (Brockner *et al.*, "Thermal decomposition of nickel nitrate hexahydrate, $Ni(NO_3)_2 \cdot 6H_2O$, in comparison to $Co(NO_3)_2 \cdot 6H_2O$ and $Ca(NO_3)_2 \cdot 4H_2O$", *Thermochim. Acta* 456:64, 2007; Llewellyn *et al.*, "Preparation of reactive nickel oxide by the controlled thermolysis of hexahydrated nickel nitrate", *Solid State Ionics* 101:1293, 1997; Mansour, "Spectroscopic and microscopic investigations of the thermal decomposition of nickel oxysalts. Part 2. Nickel nitrate hexahydrate", *Thermochim. Acta* 228:173, 1993; Paulik *et al.*, "Investigation of the Phase Diagram for the System $Ni(NO_3)_2$-H_2O and Examination of the Decomposition of $Ni(NO_3)_2$ $6H_2O$ ", *Thermochim. Acta* 121:137, 1987; and Estelle *et al.*, "Comparative study of the morphology and surface properties of nickel oxide prepared from different precursors", *Solid State Ionics*, 156:233, 2003). Various mechanisms of decomposition of the nickel nitrate to nickel oxides are reported. (Brockner *et al.*, *Thermochim. Acta* 456:64,

2007; Llewellyn *et al., Solid State Ionics* 101:1293, 1997; Sietsma *et al.*, "Ordered Mesoporous Silica to Study the Preparation of Ni/SiO_2 ex Nitrate Catalysts: Impregnation, Drying, and Thermal Treatments", *Chem. Mater.* 20:2921, 2008; and Sietsma *et al.*, "How nitric oxide affects the decomposition of supported nickel nitrate to arrive at highly dispersed catalysts", *J. Catal.* 260:227, 2008). Further, the products and the mechanism are both reported to depend upon the atmosphere under which the heating to decomposition takes place. Sun *et al.* ("Container Effect in Nanocasting Synthesis of Mesoporous Metal Oxides", *J. Am. Chem. Soc.* 133:14542, 2011) teach that even the shape of the container in which an amount of porous silica particles containing a metal nitrate melt is heated can change the structure of the metal oxide formed within the porous silica particles. Seitsma *et al.*(*Chem. Mater.* 20:2921, 2008 and *J. Catal.* 260:227, 2008) teach that carrying out heating of nickel nitrate under different atmospheres can affect the extent of migration of the nickel oxide product from the mesopores in silica particles onto the exterior of the particle. The affect of such variability in the decomposition and migration of metal nitrates has meant that these techniques have only been applied to particles, where the effects, though present, are more manageable and have less effect on the small scales seen with particle products. Such methods have not been applied for the preparation of larger porous materials.

Accordingly, there are no known methods for generating porous metal and/or metal oxide materials in which the spatial distribution of different metals and metal oxides within one material can be controlled. The methods disclosed herein can produce metal and/or metal oxide porous materials (*e.g.*, bodies) having precisely controlled microstructure and nanostructure that includes control over the spatial distribution of a number of metal and metal oxides within the same material. The disclosed porous materials can be used in a variety of applications and can also incorporate carbon or silica present in some templates.

SUMMARY

In accordance with the purposes of the disclosed materials, compounds, compositions, articles, devices, and methods, as embodied and broadly described herein, the disclosed subject matter, in one aspect, relates to methods for producing metal and/or metal oxide porous materials. Metal and/or metal oxide porous materials, with or without a template, are also disclosed, as are methods of using the disclosed materials.

Additional advantages of the subject matter described herein will be set forth in part in the description that follows, and in part will be obvious from the description, or can be learned by practice of the aspects described below. The advantages described below will be

realized and attained by means of the elements and combinations particularly pointed out in the appended claims. It is to be understood that both the foregoing general description and the following detailed description are exemplary and explanatory only and are not restrictive.

BRIEF DESCRIPTION OF THE FIGURES

The accompanying Figures, which are incorporated in and constitute a part of this specification, illustrate several aspects of the invention and together with the description serve to explain the principles of the invention.

Figure 1(a) is a cartoon of a porous material prepared by the methods disclosed herein. The porous material has a bimacroporous, "hollow" system in which two bicontinuous macroporous networks (**10**) are separated by a 100-500 nanometer thick membrane (**11**) (the membrane can also be referred to as a "wall" of the macropore). This membrane can be mesoporous and/or microporous or can be continuous (*i.e.*, without porosity). The membrane can be metal, metal oxide, silica, carbon, or other material (*e.g.*, sulfides). If the membrane is porous then the porous material has utility as "hollow fiber" membranes also known as contactors. If the membrane is not porous but is, for example, all metal, it can have utility as a heat exchanger, or if, for example, it comprises various metal oxides, which are oxygen permeable (generally as oxide) it can be used as an oxygen filter membrane. **Figure 1(b)** is an empirical, schematic representation of a bicontinuous structure.

Figure 2 is a SEM image of macropores in cobalt metal monolith.

Figure 3 is a SEM image of macropores in copper metal monolith.

Figure 4 is a SEM image of macropores in sterling silver monolith.

Figure 5 is a SEM image of macropores in nickel oxide monolith.

Figure 6 is a SEM image of hollow fiber cobalt monolith with two separate macroporous networks.

Figure 7 is a SEM image of macropores in nickel metal monolith.

Figure 8 is a group of SEM and TEM images of cobalt oxide monolith macropores (5 micrometer scale bar image) and highly ordered mesopores (100 and 10 nm scale bar images).

DETAILED DESCRIPTION

The materials, compounds, compositions, articles, devices, and methods described herein may be understood more readily by reference to the following detailed description of

specific aspects of the disclosed subject matter and the Examples and Figures included therein.

Before the present materials, compounds, compositions, and methods are disclosed and described, it is to be understood that the aspects described below are not limited to specific synthetic methods or specific reagents, as such may, of course, vary. It is also to be understood that the terminology used herein is for the purpose of describing particular aspects only and is not intended to be limiting.

Also, throughout this specification, various publications are referenced. The disclosures of these publications in their entireties are hereby incorporated by reference into this application in order to more fully describe the state of the art to which the disclosed matter pertains. The references disclosed are also individually and specifically incorporated by reference herein for the material contained in them that is discussed in the sentence in which the reference is relied upon.

General Definitions

In this specification and in the claims that follow, reference will be made to a number of terms, which shall be defined to have the following meanings:

Throughout the description and claims of this specification the word "comprise" and other forms of the word, such as "comprising" and "comprises," means including but not limited to, and is not intended to exclude, for example, other additives, components, integers, or steps.

As used in the description and the appended claims, the singular forms "a," "an," and "the" include plural referents unless the context clearly dictates otherwise. Thus, for example, reference to "a metal salt" includes mixtures of two or more such metal salts, reference to "an agent" includes mixtures of two or more such agents, reference to "the porous material" includes mixtures of two or more such porous materials, and the like.

"Optional" or "optionally" means that the subsequently described event or circumstance can or cannot occur, and that the description includes instances where the event or circumstance occurs and instances where it does not.

Ranges can be expressed herein as from "about" one particular value, and/or to "about" another particular value. When such a range is expressed, another aspect includes from the one particular value and/or to the other particular value. Similarly, when values are expressed as approximations, by use of the antecedent "about," it will be understood that the particular value forms another aspect. It will be further understood that the endpoints of each of the ranges are significant both in relation to the other endpoint, and independently

of the other endpoint.

References in the specification and concluding claims to parts by weight of a particular element or component in a composition denotes the weight relationship between the element or component and any other elements or components in the composition or article for which a part by weight is expressed. Thus, in a compound containing 2 parts by weight of component X and 5 parts by weight component Y, X and Y are present at a weight ratio of 2:5, and are present in such ratio regardless of whether additional components are contained in the compound.

A weight percent (wt. %) of a component, unless specifically stated to the contrary, is based on the total weight of the formulation or composition in which the component is included.

By "continuous" is meant a phase such that all points within the phase are directly connected, so that for any two points within a continuous phase there exists a path which connects the two points and does not leave the phase. A "phase" in this context can refer to a pore, void, or a metal or metal oxide layer. A "bicontinuous" material contains two separate continuous phases such that each phase is continuous, and in which the two phases are interpenetrating as shown schematically in **Figure 1(b)**. It is impossible to separate the two structures without tearing one of the structures. Another example of a system with this property is the gyroid phase of block copolymers (Bates, "Block Copolymers - Designer Soft Materials", *Physics Today* February, 32, 1999, which is incororated by reference herein for its description of a bicontinuous material structure.)

By "tortuous" is meant when phases have only short straight line distances so that moving within the phase requires continuing changes in direction.

By "hollow" is meant when two continuous (void) network phases completely separated by a third continuous phase that prevents any direct contact between the two continuous void network phases. In a large body, material cannot travel from one continuous void phase to the other continuous void phase without passing through the third continuous separating phase.

By "hierarchical pores" and other forms of the phrase like "heirarchiacally porous material" is meant having pores that span a number of different length scales. As used herein materials with hierarchial pores have pores that span two or more length scales. Typically, there will be a distribution of pore diameters at each length scale, where often the distribution of pore diameters are sufficiently narrow that there is little or no overlap between the pore size distributions; there are some pore sizes for which few or no pores are

present in such a hierarchically porous material.

By "constant diameter" is meant when the smallest distance across a continuous phase is constant, i.e., less than one standard deviation.

By the word "body" is meant a macroscopic, single piece of solid material typically with dimensions (length, width, and/or hight) exceeding about 1 mm. A body is distinguished from a particle, where the dimensions of the material are typically much less than that for a body.

By "partial infiltration" is meant that the metal salt or carbon precursor infiltrates and contacts less than all of the volume of the porous template. Generally, partial infiltration is when from about 10 to about 90, from about 25 to about 75, or about 50 % of the template is filled with the metal salt or carbon precursor.

Also, disclosed herein are materials, compounds, compositions, and components that can be used for, can be used in conjunction with, can be used in preparation for, or are products of the disclosed methods and compositions. These and other materials are disclosed herein, and it is understood that when combinations, subsets, interactions, groups, etc. of these materials are disclosed that while specific reference of each various individual and collective combinations and permutation of these compounds may not be explicitly disclosed, each is specifically contemplated and described herein. For example, if a composition is disclosed and a number of modifications that can be made to a number of components of the composition are discussed, each and every combination and permutation that are possible are specifically contemplated unless specifically indicated to the contrary. Thus, if a class of components A, B, and C are disclosed as well as a class of components D, E, and F and an example of a composition A-D is disclosed, then even if each is not individually recited, each is individually and collectively contemplated. Thus, in this example, each of the combinations A-E, A-F, B-D, B-E, B-F, C-D, C-E, and C-F are specifically contemplated and should be considered disclosed from disclosure of A, B, and C; D, E, and F; and the example combination A-D. Likewise, any subset or combination of these is also specifically contemplated and disclosed. Thus, for example, the sub-group of A-E, B-F, and C-E are specifically contemplated and should be considered disclosed from disclosure of A, B, and C; D, E, and F; and the example combination A-D. This concept applies to all aspects of this disclosure including, but not limited to, steps in methods of making and using the disclosed compositions. Thus, if there are a variety of additional steps that can be performed it is understood that each of these additional steps can be performed with any specific aspect or combination of aspects of the disclosed methods, and

that each such combination is specifically contemplated and should be considered disclosed.

Reference will now be made in detail to specific aspects of the disclosed materials, compounds, compositions, articles, and methods, examples of which are illustrated in the accompanying Examples and Figures.

Methods

The methods disclosed herein relate, in certain aspects, to the production of metal and/or metal oxide porous materials (*e.g.*, bodies) by a single or repeated introduction of one or more metal salts into a porous template, and controlled thermal decomposition of the metal salt under reducing conditions or to convert the metal salt to metal. In another aspect, disclosed herein are methods for the production of metal and/or metal oxide porous materials by a single or repeated introduction of one or more metal salts into a porous template, and controlled heating of a metal nitrate under in an inert or oxidizing atmosphere, followed by thermal decomposition or reduction to convert the metal salt or metal oxide, respectively, to metal. These methods can also be used to produce metal and/or metal oxide nanowires. Generally, the disclosed methods comprise combining a composition comprising a metal salt (*e.g.*, a neat metal salt, metal salt hydrate, metal salt solution, or melt) with a porous template to form a mixture; maintaining the mixture at below the decomposition temperature of the metal salt until a desired spatial distribution of the metal salt in the template is obtained; and then heating the mixture to above the decomposition temperature of the metal salt in the presence of a reducing agent or inert atmosphere to produce the metal and/or metal oxide porous material. These steps can optionally, be repeated with the same metal salt (*e.g.*, a neat metal salt, metal salt hydrate, metal salt solution, or melt) or with a different metal salt. These steps can also, optionally, be followed by removal of the template.

Alternatively, disclosed herein is a method that comprises combining a composition comprising a metal nitrate (*e.g.*, a neat metal nitrate, metal nitrate hydrate, or metal nitrate solution) with a porous template to form a mixture; maintaining the mixture at below the decomposition temperature of the metal nitrate until a desired spatial distribution of the metal nitrate in the template is obtained; and then heating the mixture to above the decomposition temperature of the metal nitrate in the presence of a reducing agent, inert atmosphere, or oxidizing atmosphere to produce the metal or metal oxide porous material. If the metal oxide is prepared the porous material the oxide can be reduced to prepare a metal porous material.

The disclosed methods involve the infiltration of metal salts as described herein into a suitable porous template to form a mixture. This occurs by contacting a composition comprising the metal salt with the porous template. The metal salt can be used in solution, hydrate or solvate form, or neat. When using a metal salt hydrate, solvate or neat salt, infiltration can be accomplished by contacting the porous template with the metal salt at above the salt's melt temperature, though below the salt's decomposition temperature. Alternatively, the metal salt can be part of a solution, *i.e.*, the composition can comprise the metal salt and a solvent. For convenience, reference to the "metal salt" means either a neat metal salt, metal salt hydrate, metal salt solvate, or a metal salt solution, unless the context clearly refers to one or the other. Contacting the metal salt with the porous template can be performed by, for example, adding the porous template to the metal salt or by adding the metal salt solution to the porous template. Contacting can also be performed by slowly mixing one component with the other or by drop-wise addition of one component into the other. Agitation (*e.g.*, stirring, shaking, or ultrasonic agitation) can be used to facilitate the contacting of the metal salt with the porous template.

The metal salts that are suitable for use in the disclosed methods can comprise one or more transition metals, alkaline metals, alkaline earth metals, or lanthanide metals. For example, a suitable metal salt can comprise a metal selected from the group consisting of of Li, Be, Na, Mg, Al, K, Ca, Sc, Ti, V, Cr, Mn, Fe, Co, Ni, Cu, Zn, Ga, Rb, Sr, Y, Zr, Nb, Mo, Tc, Ru, Rh, Pd, Ag, Cd, In, Sn, Sb, Cs, Ba, La, Ce, Pr, Nd, Pm, Sm, Eu, Gd, Tb, Dy, Ho, Er, Tm, Yb, Lu, Hf, Ta, W, Re, Os, Ir, Pt, Au, Tl, Pb, and Bi. The counterion of the metal salt can be a nitrate, acetate, sulfate, or chloride. Other suitable counterions can be organic or inorganic ions such as carbonate, nitrile, bromide, iodide, phosphate, sulfite, phosphite, nitrite, and the like. Some particularly preferred metal salts are transition metal, alkaline metal, alkaline earth metal, or lanthanide metal nitrate, acetate, sulfate, or chloride. Metal salts suitable for use herein can be readily obtained from commercial suppliers or synthesized by methods known in the art. Similarly metal salt hydrates and metal salt solutions can be prepared by methods known in the art or obtained from commercial sources.

Metal salts for use herein have a decomposition temperature and a melting temperature. When using a composition comprising the metal salt hydrate, solvate, or neat metal salt the composition is heated above the melt temperature of the metal salt, but below the decomposition temperature of the metal salt. When using a composition comprising a metal salt and a solvent, the solvent can be any suitable solvent that dissolves the particular

metal salt being used. In certain aspects, water is used as the solvent. Other aqueous solvents can be used, such as water/organic solvent mixtures. Suitable water/organic solvent mixtures contain water and an organic solvent that is at least partially miscible with water. For example, as aqueous alcohols, aqueous polyols, aqueous carboxylic acids, aqueous esters, aqueous aldehydes, aqueous ketones, and the like can be used. In other examples, carboxylic acids, alcohols, polyols, ketones, or aldehydes can be used and are advantageous solvents because they can also act as the reducing agent. The use of aqueous metal salt solutions is particularly advantageous as aqueous solutions effectively wet certain porous templates (*e.g.*, silica templates), producing good penetration of the metal salt solution into the porous template. When a solution of a metal salt is used, the weight or molar ratio of metal salt to solvent can be from about 1:10 to about 10:1. For example, the weight ratio of metal salt to solution can be from about 1:10, 2:10, 3:10, 4:10, 5:10, 6:10, 7:10, 8:10, 9:10, 10:9, 10:8, 10:7, 10:6, 10:5, 10:4, 10:3, 10:2, 10:1, or 1:1. In other examples, the molar ratio of metal salt to solution can be from about 1:10, 2:10, 3:10, 4:10, 5:10, 6:10, 7:10, 8:10, 9:10, 10:9, 10:8, 10:7, 10:6, 10:5, 10:4, 10:3, 10:2, 10:1, or 1:1. A neat metal salt can be used as well, *i.e.*, where there is no solvent. Further, metal salt hydrates and solvates can also be used. Such hydrates or solvates typically contain from 1 to 10 water or solvent molecules per metal center.

In a preferred aspect, a composition comprising an aqueous metal nitrate or metal nitrate hydrate is used. The use of the metal nitrate salts can be advantageous since such salts have high solubility in water. As metal nitrate hydrates, many metal nitrates also have a liquid range that allows for continued movement of the salt, improving the fidelity of the replication of the porous template, and increasing the surface area of the final product.

In preferred aspects, the composition comprising the metal salt is not a sol-gel or a metal foam.

The porous template can be a monolithic body. When the decomposition is under reducing conditions, the template can also be a particular template. The form and shape of the porous template used, as well as the amount and degree of infiltration of the metal salt into the porous template, affect the final form of the metal and/or metal oxide porous material. When using a monolithic form of porous template, the resulting metal and/or metal oxide porous material can be a bicontinuous monolithic body.

Suitable porous templates can be obtained commercially or can be prepared according to methods described in the art. For example, a number of groups have used colloidal crystal templating or self-assembly of polymer or silica beads to give a relatively

hard template into which the metal salts disclosed herein can be infiltrated to create the disclosed metal and/or metal oxide porous material. *See e.g.*, US Patent 6,911,192 and Nakanishi, "Pore Structure Control of Silica Gels Based on Phase Separation", *J. Porous. Mat.* 4:67, 1997. Infiltration of a sol-gel precursor including a surfactant as template can be used to induce ordered mesopores in the macropore walls of these materials (Li *et al.*, "Controlling the Shape and Alignment of Mesopores by Confinement in Colloidal Crystals: Designer Pathways to Silica Monoliths with Hierarchical Porosity", *Langmuir* 23:3996, 2007). The major drawback of this approach is the expense of the polymeric beads for macroscopic pieces. A number of other methods of producing suitable porous templates have been developed using microemulsions (Carn *et al.*, "Inorganic monoliths hierarchically textured via concentrated direct emulsion and micellar templates", *J. Mater. Chem.* 14:1370, 2004), bicontinuous polymer foams (Maekawa *et al.*, "Meso/Macroporous Inorganic Oxide Monoliths from Polymer Foams", *Adv. Mat.* 15:591, 2003), salt crystals (Zhao *et al.*, "Multiphase Assembly of Mesoporous-Macroporous Membranes", *Chem. Mater.* 11:1174, 1999), bacteria (Davis *et al.*, "Baterial templating of ordered macrostructures in silica and silica-surfactant mesophases", *Nature*, 385:420, 1997), cellulose (Caruso *et al.*, "Silica Films with Bimodal Pore Structure Prepared by Using Membranes as Templates and Amphiphiles as Porogens", *Adv. Functional Mater.* 12:307, 2002; Caruso *et al.*, "Cellulose Acetate Templates for Porous Inorganic Network Fabrication", *Adv. Mat.*, 12:1921, 2000), sugars (Walsh *et al.*, "Dextran templating for the synthesis of metallic and metal oxide sponges", *Nat. Mat.* 2:386, 2003), or ice (Nishihara *et al.*, "Ordered Macroporous Silica by Ice Templating", *Chem. Mater.* 17:683, 2005) as templates for macrostructure, and foaming of the sol-gel silica (Suzuki *et al.*, "Synthesis of mesoporous silica foams with hierarchical trimodal pore structures", *J. Mater. Chem.* 13:1812, 2003). Each of these articles is incorporated herein by reference for their teaching of processes for producing porous templates.

Suitable porous templates for use herein can comprise silica, carbon, metal, or metal oxide. In other examples, the porous template comprises a combination or composite of one or more of silica, carbon, metal, or metal oxide. In a preferred aspect, the porous template is a mesoporous and/or microporous silica. The use of a silica template is particularly advantageous since porous silica templates of controlled structure on the micrometer and nanometer scales are readily available.

A particularly suitable porous templates are hierarchically porous silica monoliths as prepared by the methods of Nakanishi *et al*. US Patent 6,911,192, and Smått *et. al.* (Smått,

et al. "Versatile Double-Templating Synthesis Route to Silica Monoliths Possessing a Multimodal Hierarchical Porosity", *Chem. Mater.* 15:2354, 2003), which are incorporated by reference herein for their teaching of templates and their method of preparation and use.

When using a metal salt solution with the porous template, a portion of the solvent can be removed. This is done to concentrate the metal salt solution, thus forming a concentrated mixture of the metal salt solution and porous template. All of the solvent should not be removed, however, as enough solvent should remain in the concentrated mixture for maintaining the metal salt solution as a liquid.

The mixture of the composition comprising a metal salt and the porous template can be maintained at below the decomposition temperature of the metal salt (and in the case of a metal salt hydrate, solvate or neat salt above the melt temperature of the metal salt) for a sufficient period of time to allow the infiltration of the metal salt into the porous template to proceed to the desired degree of distribution. The melt temperature and the decomposition temperature of a metal salt is a value that can readily be determined based on the particular metal salt used. By controlling the temperature the degree of infiltration can be controlled. Rapid heating ramps should be avoided in that the metal salt can decompose prematurely, before it has infiltrated the template to the desired degree.

The pressure of the system can also be controlled, as well as the equilibration time, to control the degree of penetration of the metal salts into the porous template. Thus by controlling the pressure and time, one can only partially replicate the porous template or fully replicate the porous template, whichever is desired. Partial replication of the porous template can produce a second set of voids on a micrometer length scale.

The use of vacuum (*e.g.*, from at or below about 1 Torr) to remove all air from the template and dissolved gases from the metal salt solution can produce an even spatial distribution of the metal salt and, consequently, metal and/or metal oxides in the porous template, because it prevents blockage of meso and micropores by air or dissolved gas. For example, the pressure can be at or below about 1 Torr, 0.1 Torr, 10^{-2} Torr, 10^{-3} Torr, 10^{-4} Torr, 10^{-5} Torr, or 10^{-6} Torr, where any of the stated values can form an upper or lower endpoint of a range. The use of reduced pressure therefore allows the metal salt to completely infiltrate the meso and/or micropores of the porous template. Increasing the time of contact and reducing the temperature during contact can also be used to achieve complete infiltration of the metal salt into the porous template.

When a vacuum is not applied at this step, or when pressure is increased, one can produce a metal and/or metal oxide porous material with a "hollow core" structure. A

hollow core structure is when the mesoporous and/or microporous membrane of a porous template is only partially infiltrated by the metal salt. Thus, infiltration of the metal salt occurs into only surface mesopores. In other words, when walls of the macropores themselves contain mesopores and/or macropores, infiltration of the metal salt can be controlled with weaker vacuum or increased pressure so that the metal salt does not go completely through the meso and/or micropore. This results in spaces along the mesopores and/or micropores with no metal and/or metal oxide. Partial infiltration to produce a hollow core structure can also be achieved by shortening the time of contact between the metal salt and the porous template or by increasing the temperature during contact. Such partial replication of only a portion of the porous template can be used to produce useful and unique structures.

Once the desired spatial distribution of the metal salt in the porous template is attained, the mixture of the metal salt and porous template can then be heated to above the decomposition temperature of the metal salt under appropriate reducing conditions to convert the metal salt to a metal or metal oxide. Heating under reducing conditions can involve heating the mixture in the presence of a reducing agent. The reducing agent can be added to the mixture by any method known in the art or described herein. Suitable reducing agents can be hydrogen gas or alcohols, *e.g.*, methanol, ethanol, and ethylene glycol, carboxylic acids (*e.g.*, acetic acid), aldehydes, hydrazine, hydrides, ketones, boranes, and the like.

Decomposition should be carried out at the lowest temperature possible to prevent migration of the metal or metal oxide from nanometer sized pores into larger pores. Carrying out the decomposition under an atmosphere of hydrogen can convert the metal salt into metal. The presence of the hydrogen can assist in decreasing the mobility of the metal oxide and metal oxynitride intermediates produced in the reaction. This can improve the fidelity of the replication and increases the surface area of the final product. The use of reductants allows the decomposition of the metal salt to be carried out at lower temperature, improving the fidelity of replication and alleviating the use of hydrogen gas which in some cases can represent a safety concern. The resulting porous material can be cooled after the decomposition step under nitrogen, and then stored under nitrogen or degassed water or similar solvent. This can prevent reaction with oxygen to form the oxide.

The decomposition step can also be conducted under inert or oxidizing atmosphere. An inert atmosphere can be helium or argon. An oxidizing atmosphere can be synthesis gas or CO_2. This can produce a metal porous material or metal oxide porous material,

respectively. Metal oxide porous materials can be reduced to metal porous materials by addition of a suitable reducing agent. The reducing agent can be added to the mixture by any method known in the art or described herein. Suitable reducing agents can be hydrogen gas or alcohols, *e.g.*, methanol, ethanol, and ethylene glycol, carboxylic acids (*e.g.*, acetic acid), aldehydes, hydrazine, hydrides, ketones, boranes, and the like.

The steps of the disclosed methods can optionally be repeated one or more times in order to control the nature of the microstructure and nanostructure of the porous material. This allows the production of mechanically robust metal and/or metal oxide porous materials with high surface area. The material can be kept under a chemically inert atmosphere or degassed solvent between steps or, alternatively, the material can be kept under air between steps.

In certain aspects, one or more of the steps disclosed herein can be performed under inert atmosphere, under air, at reduced pressure, at atmospheric pressure, or at about atmospheric pressure. Also, different metal salts can be used at each repetition cycle to produce different distributions of different metals and/or metal oxides in the final material. Also, when the desired degree of replication is achieved the template can optionally be removed.

As another additional and optional step, the disclosed methods can include adding an additional metal to the metal and/or metal oxide porous materials by electrodeposition, electroless deposition, or by displacement deposition.

The disclosed methods involving metal salt infiltration into a porous template, thermal decomposition of the metal salt under reducing condition, and removal of the template, can result in metal and/or metal oxide porous materials (*e.g.*, porous particles or porous body). The disclosed methods can, with high fidelity, replicate the porous template's structure with metal and/or metal oxide. The resulting metal and/or metal oxide porous material is thus a high surface area metal and/or metal oxide composition.

Similar procedures to those disclosed herein for making metal and/or metal oxide porous materials can be used to produce porous carbon materials with similar structures and useful properties. There are a number of procedures known in the art for introducing carbon precursors into mesoporous silica templates and hierarchically porous silica templates (*see e.g.*, Ryoo *et al.*, "Ordered Mesoporous Carbons", *Adv. Mat.* 13,:677, 2001, Lu *et al.*, "Synthesis of Polyacrylonitrile-Based Ordered Mesoporous Carbon with Tunable Pore Structures", *Chem. Mater.* 16:100, 2004, Yang, *et al.* "Synthesis of replica mesostructures by the nanocasting strategy", *J. Mater. Chem.* 15:1217, 2005, and Hu *et al.*, "Synthesis of

Hierarchically Porous Carbon Monoliths with Highly Ordered Microstructure and Their Application in Rechargeable Lithium Batteries with High-Rate Capability", *Adv. Functional Mater.* 17:1873, 2007), which are incorporated herein for their teaching of carbon precursors, silica templates, and methods of using thereof. In general they involve infiltration of a carbon precursor such as a polymer precursor, where polymerization is thermally initiated. Subsequent pyrolysis under an inert atmosphere converts the polymer into carbon. The resultant replica can be produced in one infiltration cycle and has very significant microporosity. The electrical conductivity of the replica is dependent upon the temperature, with temperatures of 800-1000 °C being necessary to produce highly conducting carbon. These methods do not produce the hollow hierarchically porous structures as are disclosed herein. Such hierarchically porous carbon structures are produced by the methods disclosed herein and involve increasing the viscosity of the infiltrating carbon precursor solution, and by increasing the rate at which the polymerization of the carbon precursor occurs.

Disclosed herein is a method for producing a hollow, carbon porous material that comprises contacting a porous template, such as those disclosed herein, in particular a hierarchical porous template, and a polymerizable carbon precursor to form a mixture. This contacting step is performed such that the precursor does not infiltrate through the entire template and is referred to herein as partial infiltration. Then the mixture is heated to polymerize the precursor. Further heating is then performed to pyrolize the polymerized precursor, thereby producing a carbon porous material. These steps can be repeated with the same carbon precursor or with a different precursor. The disclosed process can be used to prepare hollow carbon porous materials.

In these methods, particular infiltration can be accomplished by varying the time of contact, rate of polymerization, and viscosity of the precursor. The carbon precursor can be of increased viscosity so that it does not penetrate as far or as quickly as a low viscosity precursor. Specifying the exact viscosity of the carbon precursor is not possible since the desirable viscosity will depend on the size and type of template, the type of carbon precursor (which affects the rate of polymerization), the time the precursor is contacted with the template, and the desired level of infiltration. More viscous precursors allowed to contact the template for a longer period of time can produce similar structures as a less viscous precursor allowed to contact the template for a shorter period of time. Thus, the practitioner can determine a sufficient viscosity for a given precursor by simple experimentation, raising or lowering the viscosity or time of contact with the template as

needed to obtain the desired level of infiltration. If more viscous precursors are needed, additives such as sugars, alcohols, glycols, and alkanes can be added. Other suitable methods for increasing the viscosity include allowing the carbon precursor to undergo some polymerization prior to introduction to the hierarchically porous silica template.

Further, the rate of polymerization of the precursor can be varied to provide a desired level of infiltration. More rapid polymerization means that the polymerizable carbon precursor would not infiltrate as far as a slower polymerization rate. Suitable methods for increasing the rate of the polymerization of the precursor prior to introduction to the porous template include, but are not limited to addition of crosslinking agents or polymerization initiators.

The carbon precursor can be for example, furfuryl alcohol, poly(furfuryl alcohol), formaldehyde, resourcinol, phenol, 1,2,3-trihydroxybenzene, 1,5-dihydroxynaphthalene, polyvinyl chloride-acrylate terpolymer, phenol resin, acrylonitrile-methyl methacrylate copolymer, polyimide, polypyrrolone, polyaromatic resin, polydivinylbenzene, sucrose, or mixtures thereof. Further examples of suitable carbon precursors are disclosed in Lu *etal.* chapters 2 and 3, *Nanocasting: A Versatile Strategy for Creating Nanostructured Porous Materials*; Royal Society of Chemistry: Cambridge, 2010, which is incorporated by reference herein for its teachings of carbon precursors, templates and nanocasting techniques.

The use of silica templates, for the metal, metal oxide, or carbon based methods disclosed herein, allows for the use of well defined chemistry to remove the template. For example, the porous material can be immersed in concentrated aqueous hydroxide solution at from about 25 °C to about 110 °C. For example, the material can be immersed for a period of about 4 to about 12 hours in 1-3 M aqueous sodium or potassium hydroxide solution. Alternatively, the material can be immersed in hydrofluoric acid. For metals such as copper and metal oxides such as zinc oxide, which are dissolved or corroded by exposure to aqueous hydroxide or hydrofluoric acid, the metal and/or metal oxide porous material can be immersed in a solution of basic alcohol such as a solution of sodium hydroxide or potassium hydroxide in dry methyl alcohol or ethyl alcohol in order to remove a silica template. In one example with copper, the corrosion of copper by aqueous potassium hydroxide solutions can be prevented by applying a small (0.3-3.0 Volt) anodic potential to the copper during the dissolution of the silica. However, the use of alcoholic base as described herein is more convenient and bypasses difficulties with contacting the copper.

Compositions

The metal and/or metal oxide porous materials produced according to the methods disclosed herein are porous. Similarly the carbon materials produced according to the methods disclosed herein are porous. The term "porous" as used herein means a material having a plurality of pores, holes, and/or channels, each of which may or may not extend throughout the entire length of the material. However, the pores can interconnect, resulting in a network of pores or voids that spans the material, permitting the flow of liquid or gas into and through the material, *i.e.*, a continuous phase of pores or voids.

The disclosed materials can have two or more continuous phases, *e.g.*, a bicontinuous structure. By "bicontinuous" is meant that both the voids/pores phase and the metal, metal oxide or carbon phase are continuous throughout the material. In other words, for a metal the metal surface is continuous and the materials can thus be electrically conductive. Similarly, the voids or pores are continuous so that a fluid (gas or liquid) can pass through the porous material. Bicontinuous can also refer to different porous networks, *e.g.*, two or more continuous pore/void phases. This occurs when there are, for example, a macroporous network and a mesoporous network, both of which are continuous. Thus the disclosed materials can be bicontinuous by reference to the various pore or void phases that are continuous.

The disclosed materials can also be hollow in that two continuous void phases are completely separated by a third continuous phase that prevents any direct contact between the two continuous phases. To illustrate this characteristic, the disclosed materials can have a continuous phase made up of a non-porous oxygen conducting ceramic where air would enter through one continuous void network, the oxygen would pass through the ceramic and exit through the other continuous void network, and would leave behind the other components of air. A second illustrative example is when the third continuous, separating phase, was itself porous on a much smaller scale, such that only ions or molecules less than a given size could penetrate the third continuous separating phase. A solution containing a mixture of ions or molecules of various sizes could then enter through one continuous void phase, the selected ions or molecules could travel through the third separating geometry and exit through the second continuous void phase. Such geometries can therefore serve as filters.

When the disclosed materials have a hollow geometry they can be even-walled. By "even-walled" is meant where a third continuous phase separates two continuous void phases and the shortest distance between one continuous void phase and the other

continuous void phase is constant. Equivalently, if the thickness of the third continuous separating phase is constant this material can be referred to as "even-walled". For filters and similar devices the property "even-walled" can be advantageous because it affects how fast material is transported across the third continuous phase, and it also impacts the pressure drop across this phase as material is transported through the phase. Materials with large variations in wall thickness, *i.e.*, those which are not "even-walled," can have significant differences in the rate at which materials transport through the third continuous phase at different positions, this can lead to decreased selectivity in filter applications.

The disclosed materials can also be said to have hierarchical pores. As noted above, a material with hierarchical pores has pores that span two or more length scales. For example, the material can have both macropores and mesopores, both macropores and micropores, both mesopores and micropores, or macropores, mesopores and micropores.

Thus, in certain examples, the materials disclosed herein can have a macroporous system. This means the porous material has a plurality of pores, holes, and/or channels greater than about 0.1 μm in diameter, *i.e.*, macropores. For example, the macropores can have a diameter of from about 0.5 μm to about 30 μm, from about 1 μm to about 20 μm, from about 5 μm to about 15 μm, from about 10 μm to about 30 μm, or from about 0.5 μm to about 15 μm in diameter.

The walls of the macropores (also termed the "membrane") can be from about 50 nm to about 15 μm, for example, from about 50 nm to about 600 nm, 100 nm to about 500 nm, from about 200 to about 400 nm, from about 50 to about 200, from about 300 to about 600 nm, from about 500 nm to about 5 μm, from about 5 μm to about 10 μm, or from about 5 μm to about 15 μm thick. In one aspect, the walls of the macropores are continuous, *i.e.*, without porosity. In another aspect, the walls of the macropores are themselves porous. These pores, holes, and/or channels within the macropore walls can be from about 2 nm to about 30 nm, from about 10 nm to about 20 nm, from about 15 nm to about 50 nm, or from about 2 nm to about 15 nm in diameter, *i.e.*, mesopores. Still further, the walls of the macropores can contain pores, holes, and/or channels that are less than about 2 nm, *i.e.*, micropores. In a preferred aspect, the porous materials disclosed herein have macropores as well as meso and/or micropores, which exist in the membrane or macropore wall. This presence of pores of more than one length scale in one material is characterized as a hierarchical pore structure. In one aspect, the macropores lying within the membrane are themselves continuous. Such materials are hollow, hierarchically porous structures. In this aspect the macroporous phase lying within the membrane is completely separated from the

macroporous phase lying outside the membrane. A cartoon showing a porous material as disclosed herein with both macropores and meso and/or micropores is shown in **Figure 1(a)**.

The structure of these hollow hierarchically porous bodies is such that the material is tortuous and contains three interpenetrating phases. All three phases are continuous. In certain aspects, two phases are voids and the third is solid and separates the two void phases such that any continuous path that joins any point in one void region to any point in the other void region must past through the third region. This geometry therefore functions as a filter or membrane.

Notably, this geometry is distinct from other porous materials and hierarchically porous materials. This is shown by comparing the disclosed materials to other types of porous materials:

Three dimensionally ordered materials (also known as 3-DOM, or colloid crystal templated materials) contain only two continuous phases, one solid the other void. Therefore, these structures are not hollow as that term is defined herein. These phases are tortuous and interpenetrating. But the absence of a third, continuous, separate void region means that these materials do not have the same features as the disclosed hollow hierarchically porous materials, which can be prepared by the methods disclosed herein. 3-DOM structures have distinctly different properties than the materials disclosed herein. The largest and smallest diameters of the void phase in 3-DOM materials are generally significantly different. As such, the disclosed materials can, in contrast to 3-DOM materials, have more than two continuous regions and narrow pore diameter distribution (*e.g.*, less than 1 standard deviation in diameter).

Aerogels, ambigels, and xerogels are classes of materials prepared by sol-gel chemistry with removal of the solvent in different manners. The structure of these materials typically contains an agglomeration of small particles. The distribution of pore sizes is typically broad with pores as small as 2-5 nm to as large as 400-4000 nm. The materials have no order, and they may not be completely or even largely bicontinuous. These materials also do not have the property of being hollow. The materials disclosed herein are not aerogels, ambigels, and xerogels because, unlike those structures, they are bicontinuous, hollow and have a narrow distribution of pore sizes.

Foams are typically of two forms. In closed-cell foams the regions of one material are completely enclosed within a continuous region of a second material. While an open-cell foam can be bicontinuous, the void network is disordered and the diameters of the void

network show a large range, with large spherical voids separated from each other by small windows. The materials disclosed herein are not foams.

The disclosed materials can, in certain examples, be described as tortuous, interpenetrating, and not hollow. Generally they have a smaller range of void network diameters than 3-DOM, foams, or aerogel materials, and have a narrower range of smallest dimensions across the solid material.

The disclosed porous materials can comprise one or more metals, metal oxides, or a combination thereof, wherein the metals are selected from the group consisting of Li, Be, Na, Mg, Al, K, Ca, Sc, Ti, V, Cr, Mn, Fe, Co, Ni, Cu, Zn, Ga, Rb, Sr, Y, Zr, Nb, Mo, Tc, Ru, Rh, Pd, Ag, Cd, In, Sn, Sb, Cs, Ba, La, Ce, Pr, Nd, Pm, Sm, Eu, Gd, Tb, Dy, Ho, Er, Tm, Yb, Lu, Hf, Ta, W, Re, Os, Ir, Pt, Au, Tl, Pb, and Bi. When magnetic metals or metal oxides are present in the disclosed materials, the material can be magnetic.

The disclosed porous materials can have very high surface area, approaching that of nanoparticles. For example, the surface area can be greater than about 5, 10, 15, 20, 25, 30, 35, 40, 45, 50, 55, 60, 65, 70, 75, 80, 85, 90, 95, or 100 m^2/g, where any of the stated values can form an upper or lower endpoint of a range. In some examples, porous materials with a surface area up to about 200 m^2/g are disclosed.

When the disclosed porous material is a carbon porous material the surface area can be even greater than that described for the metal and/or metal oxide porous materials. For example, in these materials the surface area can be greater than about 200, 400, 600, 800, 1000, 1200, or 1600 m^2/g, where any of the stated values can form an upper or lower endpoint of a range.

Further, the disclosed porous materials, in certain aspects, do not release nanoparticles of metal when used. This can be environmentally advantageous.

Additional components can be added to the disclosed metal and/or metal oxide porous materials, such as catalysts. The disclosed porous materials are not etch materials whereby ionizing radiation is used to form the pores. The disclosed materials can be substantially free (*i.e.*, having less than about 1 % by weight of the porous material) of surfactant. The disclosed materials can be substantially free (having less than about 1, 0.1, or 0.01 % by weight of the porous material) of silica.

Also disclosed herein are compositions that comprise the metal and/or metal oxide porous materials disclosed herein and a carbon nanotube.

Applications

The disclosed methods allow the control of the spatial distribution of different metals and/or metal oxides simultaneously within the same porous material, and formation of metal and/or metal oxide nanowires. The metal and/or metal oxide porous materials produced by the methods disclosed herein can be used as packing materials in chromatography, as catalysts, or as electrocatalysts. The disclosed materials can be used for chemical conversions such as combustion of liquid and gaseous fuels, conversion of liquid and gaseous fuels to electricity, and conversion of electricity to liquid and gaseous fuels. The disclosed materials can be used to assist heat transfer or to store and release electrical charge. The disclosed materials can be used to convert light to electric energy.

In particular, any process that uses a metal or metal oxide catalyst can be adapted by using the metal or metal oxide porous materials disclosed herein. For example, nickel is used as a reduction catalyst. A porous material as disclosed herein comprising nickel can be likewise used as a reduction catalyst in similar processes. Similarly, the disclosed metal and/or metal oxide porous materials can be used as catalysts in other reactions where traditional metal and metal oxide catalysts are used, such as hydrogenation of carbon-carbon and carbon-heteroatom pi bonds (alkenes, alkynes, nitriles, imines, carbonyls, etc.), reduction of carbon-nitrogen or carbon-oxygen pi bonds to give alcohols and amines, Fischer-Tropsch type chemistry to make hydrocarbons from CO/H_2, hydrogenolysis of alcohols, hydrogen production from biomass, Pauson-Khand reactions (alkyne + alkene + CO to give cyclopentanones), and dechlorination of aromatic compounds. Further, the disclosed porous materials would be advantageous over traditional heterogeneous catalysts given their high surface area, which would aid efficiency, and their monolithic structure, which would simplify separation of the catalyst and make continuous flow reactions an option.

In a preferred use, the disclosed materials can be used as starting materials for deposition of carbon nanotubes and other charge storage materials, and the like. The growth of carbon nanotubes on porous substrates is known. These processes can be adapted by using the metal and/or metal oxide porous materials disclosed herein as substrates for the carbon nanotubes. As such, disclosed herein are compositions that comprise the disclosed metal and/or metal porous materials and a carbon nanotube.

The disclosed materials can also be used in the production of metal and metal oxide nanowires for use in electrically and thermally conducting fabric, metal and metal oxide nanowires for use in catalysis and electrocatalysis, metal and metal oxide nanowires for use

in information storage and the like. By controlling the level of infiltration of the metal salt into a porous template, thermal decomposition of the metal under reducing conditions or inert atmosphere, and removal of the porous template, a nanowire can be formed. The disclosed process also allows one to form large quantities of nanowires. As such disclosed herein are charge storage materials, nanowires, conducting fabric, catalysts, and information storage media comprising the porous materials disclosed herein.

Certain aspects of the disclosed methods can also be applied to the formation of porous carbon materials. The disclosed methods can also be applied to the production of microstructured and nanostructured porous carbon materials as templates for other materials, microstructured and nanostructured porous carbon bodies as catalyst support, microstructured, and nanostructured porous carbon bodies as current collectors in capacitors and batteries, microstructured and nanostructured porous carbon bodies as filters, microstructured and nanostructured porous carbon bodies as combined catalyst support and filter.

In a preferred use, the disclosed materials can be used as filters. There are many situations in which it is desirable to be able to separate or analyze an analyte or target molecule from a given sample or to remove impurities from a sample. For example, in disease diagnoses there is often a particular analyte that is produced by or part of a pathogen, and physicians use the presence or absence of that analyte to determine whether the patient is infected with the pathogen.

Described herein are methods for separating one or more target molecules present in a sample. "Separating a target from a sample" means removing the target molecule from the sample. In one aspect, the method involves passing the sample through a porous material as disclosed herein. When the sample is passed through the porous material, the target molecules can be localized on or in the porous material. The porous materials disclosed herein can permit the flow of liquid through or into the material. In certain embodiments, the target molecules are reversibly localized and in other embodiments the localization is irreversible.

Often it is desirable to detect the target molecules that have been localized, by for example, viewing them directly or assaying for some type of label that has been associated with the target molecule. Once the target molecule has been localized near the surface of the porous material, further processing steps may be performed. The target molecules can also be, for example, amplified, detected, or isolated. For example, the target molecules can also be counted, correlated, purified, or collected. One way of categorizing target molecule

is by their size, relative to the pore size of the disclosed porous material used. For example, the target molecule can have a contour length or globular diameter at least 1.5 times, two times, three times, four times, six times, eight times, ten times, or twenty times the diameter of the pores in the porous material. Any target molecule that has the properties necessary for localization on the disclosed porous material can be targeted or manipulated. For example, the target molecule can be a protein, peptide, polypeptide (*e.g.*, antibody, enzyme), carbohydrate, sugar, nucleic acid, phospholipid, detergent, or surfactant or a combination thereof.

Similarly, it is possible to use the disclosed porous materials as filters to remove impurities from a sample. This can be done by contacting a sample with impurities to the disclosed porous materials. The impurities can be trapped, adsorbed, and/or degraded by the porous material, thus resulting in the removal of the impurities from the sample. This method can be used to separate gaseous impurities from gaseous or liquid samples. It can also be used to separate liquid impurities from gaseous or liquid samples. For example, the disclosed porous materials can be used a solid state oxygen filters, and gas/liquid separators.

The disclosed porous materials can also be used in chromatography, for example, gas, HPLC, flash, or thin-layer chromatography, as the stationary phase. The chromatography can also involve the use of applied potential to control localization of target molecules, such as in electrochemical chromatography and electromodulated or electrochemically modulated chromatography. Because the disclosed porous materials have such high surface area and can be conductive, they are particularly well suited for these uses.

In another aspect, the disclosed porous materials can be used in fuel cells as a fuel cell separator. Thus, fuel cells comprising the disclosed porous materials are also contemplated herein.

In still another aspect, the disclosed porous materials can be used in environmental remediation. For example, the metal surface of the porous materials can be an active site to decompose hazardous materials. This can be useful for general remediation or waste water filtration. The material is also beneficial in that it can be retrofit into existing filtration systems and incorporated into existing industrial processes.

In still other examples, the disclosed porous materials have such high surface areas that they can be used for heat dissipation applications. For example, they can be used in heat exchanges, heat sinks (*e.g.*, in computers and gaming consoles), thermal conduits, and the like. The disclosed porous material can be adapted to be positioned in a heat conducting

relationship with an electronic module to be cooled. As another example, the disclosed porous materials can be used in cookware.

EXAMPLES

The following examples are set forth below to illustrate the methods and results according to the disclosed subject matter. These examples are not intended to be inclusive of all aspects of the subject matter disclosed herein, but rather to illustrate representative methods and results. These examples are not intended to exclude equivalents and variations of the present invention which are apparent to one skilled in the art.

Efforts have been made to ensure accuracy with respect to numbers (*e.g.*, amounts, temperature, etc.) but some errors and deviations should be accounted for. Unless indicated otherwise, parts are parts by weight, temperature is in °C or is at ambient temperature, and pressure is at or near atmospheric. There are numerous variations and combinations of reaction conditions, *e.g.*, component concentrations, temperatures, pressures, and other reaction ranges and conditions that can be used to optimize the product purity and yield obtained from the described process. Only reasonable and routine experimentation will be required to optimize such process conditions.

The silica monoliths used in these examples were produced using the methods disclosed by US Patent 6,911,192, Nakanishi, "Pore Structure Control of Silica Gels Based on Phase Separation", *J. Porous. Mat.* 4:67, 1997 and Smått, *et al.* "Versatile Double-Templating Synthesis Route to Silica Monoliths Possessing a Multimodal Hierarchical Porosity", *Chem. Mater.* 15:2354, 2003).

In a typical synthesis tetraethylorthosilicate (TCI America), 30% nitric acid, deionized water, polyethylene glycol MW = 35,000 g/mol (Sigma-Aldrich), and OTAB (Alfa Aesar) were mixed in the following molar ratios, 1:0.25:14.7:0.43:0.1, respectively. The solution was transferred into a template and allowed to gel for 72 hours at 40 °C. Monoliths were then aged in 1 M ammonium hydroxide at 90 °C overnight followed by neutralization in 0.1 M nitric acid, rinsing three times with deionized water, three times with acetone, and dried at 40 °C for 72 hours. Finally, the silica monoliths were calcined at 550 °C for 5 hours with a ramp rate of 1 °C/min.

Example 1

A concentrated solution comprising 77.7 g of $Co(NO_3)_2 \cdot 6H_2O$ dissolved in 59.0 g of de-ionized water (4.5 mol/ kg solvent) was prepared. Silica monoliths containing large pores, 1-5 μm in diameter, and much smaller pores, 4.5 nm in diameter, were dried under vacuum for 20 minutes and filled with the solution above. Monoliths became translucent

and excess solution was removed from the outside. Filled monoliths were heated at 150 °C for 10 hours and then heated up to 400 °C over 4 hours and held at 400 °C for 30 hours while flowing 5 % H_2 in N_2. The filling and heating steps were repeated 4 times. The silica was removed by soaking the composite in an aqueous potassium hydroxide solution (3 mol/ liter water) overnight. This resulted in a free standing, porous cobalt metal monolith.

Electron microscopy confirmed positive replication of the large pores and can be seen in **Figure 2**. X-ray Diffraction confirmed the presence of cobalt metal. Replication of the small pores was confirmed by nitrogen adsorption measurements where the porosity, before removal of the silica, at 4.5 nm was nearly absent and after silica removal pores larger than 20 nm in diameter remain. The resulting specific surface area of this material was no less than 40 m^2/g.

Example 2

In the same manner as Example 1, a concentrated solution consisting of 137.8 g of $Cu(NO_3)_2 \cdot 3H_2O$ diluted to 100 mL with de-ionized water (5.7 mol/ liter solution) was prepared and used to fill the pores of the silica monolith. Filled monoliths were dried under nitrogen atmosphere at 150 °C for 10 hours, and then heated up to 310 °C for an hour under a flow of nitrogen bubbled through methanol. The filling and heating cycles were repeated 3 times. The silica was removed by soaking the composite in a solution of potassium hydroxide (3 mol/liter) in dry methanol at 80 °C overnight. This resulted in a free standing, porous copper metal monolith. The same characterization methods were used as in Example 1. The resulting monolith gave a brilliant rose color and a SEM image can be seen in **Figure 3**. The specific surface area of the resulting material was 10 m^2/g or greater.

Example 3

In the same manner as Example 1, a solution of 23.5 g $AgNO_3$, 2.7 g $Cu(NO_3)_2 \cdot 3H_2O$, and 5 mL water was prepared and used to fill the pores of the silica monolith. Filled monoliths were dried at 150 °C for 10 hours, and then heated under an ethylene glycol atmosphere to reduce to the metal. The filling and heating cycle was done twice. The silica was removed by soaking the composite in an aqueous potassium hydroxide solution (3 mol/ liter water) for several hours. This resulted in a free standing, porous sterling silver monolith and the SEM image can be seen in **Figure 4**. The same characterization methods were used as in Example 1. The resulting specific surface area of this material was 2 m^2/g and greater.

Example 4

In the same manner as Example 1, a concentrated solution of 59.6 g $Ni(NO_3)_2 \cdot 6H_2O$ diluted to 50 mL with de-ionized water was prepared and used to fill the silica pores. Filled monoliths are heated at 150 °C for 10 hours, and then at 250 °C for four hours to ensure complete decomposition. The filling and heating cycle was done three times. The monoliths were then heated to 600 °C for 5 hours. The silica was removed by soaking the composite in a solution of potassium hydroxide (3 mol/liter) in dry methanol at 90 °C overnight. This resulted in a free standing, porous nickel oxide monolith. The monoliths were grayish green in color and a SEM image can be seen in **Figure 5**. The same characterization methods were used as in Example 1. The resulting specific surface area of this material was 32 m^2/g.

Example 5

A mixture of $Co(NO_3)_2 \cdot 6H_2O$ and water (16.5 M) was prepared. The mixture was then heated to 60 °C, which is above the melting point of the salt, and kept there. Silica monoliths containing large pores, 1-5 μm in diameter, and much smaller pores, 4.5 nm in diameter, were placed in the solution and allowed to soak overnight, and were translucent in color the next day. They monoliths were then removed from the solution, placed in a 60 °C furnace so that the salt would not crystallize in the monoliths, and excess solution was removed. The monoliths were then heated for 10 hours at 150 °C for 10 hours under flow of 5% H_2 in N_2, and then at 400 °C for 24 hours under the same atmosphere. This process was repeated twice. The silica was removed in the same manner as Example 1. This resulted in a free standing, porous cobalt monolith.

Electron microscopy was used to confirm replication. These monoliths exhibited the same positive replica of the large pores, but also contained hollow ligaments within the walls, as seen in **Figure 6**. This gave a specific surface area of 65 m^2/g.

Example 6

The solution from Example 4 was used and introduced into the silica as in Example 1. The filled monolith was heated at 150 °C for 10 hours under flow of 5% H_2 in N_2, and then at 350 °C for 10 hours under the same atmosphere. This process was repeated 4 times. However, great care was taken not to expose the samples to oxygen. They were kept under deoxygenated water or nitrogen gas the entire time. The silica was removed in deoxygenated potassium hydroxide solution (3 mol/L). The same characterization methods were used as in Example 1 and a SEM image of the nickel replica can be seen in **Figure 7**. The specific surface area of this nickel metal replica was 15 m^2/g or better.

Example 7

The solution from Example 1 was used and introduced into the silica as in Example 1. The silica monoliths contained large pores, 1-5 μm in diameter, and much smaller pores, about 8 nm in diameter, that are ordered in orientation. The filled monoliths were heated at 150 °C for 10 hours under N_2 flow and then at 250 °C for 1 hour under the same atmosphere. This process was repeated twice. The silica was removed in the same manner as in Example 1. This resulted in a free standing, porous cobalt oxide monolith containing ordered pores of about 4 nm. The same characterization methods were used as in Example 1 and electron microscope images of the ordered cobalt oxide replica can be seen in **Figure 8**. The specific surface area of this cobalt oxide replica was 120 m^2/g or better.

As described, according to the disclosed methods it is possible to produce porous bodies composed of metals and metal oxides and mixtures of various metals and metal oxides that have structure at a number of length scales, where the structure is determined by the template used and the precise procedure carried out. Applications of such materials include, but are not limited to chromatography and other separations methods, catalysis and electrocatalysis, energy storage and energy conversion.

Other advantages which are obvious and which are inherent to the invention will be evident to one skilled in the art. It will be understood that certain features and sub-combinations are of utility and may be employed without reference to other features and sub-combinations. This is contemplated by and is within the scope of the claims. Since many possible aspects may be made of the invention without departing from the scope thereof, it is to be understood that all matter herein set forth is to be interpreted as illustrative and not in a limiting sense.

CLAIMS

What is claimed is:

1. A bicontinuous porous body, comprising: a plurality of macropores having a diameter of from greater than about 0.1 μm, wherein the macropores interconnect, forming a continuous network of pores that spans the material, permitting the flow of liquid or gas into and through the material, and wherein the wall of the macropores comprise a continuous layer of metal and/or metal oxide.

2. The body of claim 1, wherein the macropores have a diameter of from about 0.5 μm to about 30 μm.

3. The body of claim 1, wherein the walls of the macropores are not porous.

4. The body of claim 1, wherein the walls of the macropores have a plurality of mesopores having a diameter of from about 2 nm to about 50 nm thereby resulting in a bicontinuous porous material with hierarchical pores.

5. The body of claim 1, wherein the walls of the macropores have a plurality of micropores having a diameter of from less than about 2 nm thereby resulting in a bicontinuous porous material with hierarchical pores.

6. The body of claim 1, wherein the body is a hollow body.

7. The body of claim 1, wherein the material comprises one or more metals, metal oxides, or a combination thereof, wherein the metals are selected from the group consisting of Li, Be, Na, Mg, Al, K, Ca, Sc, Ti, V, Cr, Mn, Fe, Co, Ni, Cu, Zn, Ga, Rb, Sr, Y, Zr, Nb, Mo, Tc, Ru, Rh, Pd, Ag, Cd, In, Sn, Sb, Cs, Ba, La, Ce, Pr, Nd, Pm, Sm, Eu, Gd, Tb, Dy, Ho, Er, Tm, Yb, Lu, Hf, Ta, W, Re, Os, Ir, Pt, Au, Tl, Pb, and Bi.

8. A method for producing a metal and/or metal oxide porous body, comprising:
   (i) contacting a porous template and a composition comprising a metal salt to form a mixture, wherein the metal salt has a decomposition temperature;
   (ii) maintaining the mixture below the decomposition temperature of the metal salt until a desired spatial distribution of the metal salt in the porous template is obtained; and then

(iii) heating the mixture to above the decomposition temperature of the metal salt in the presence of a reducing agent or inert atmosphere to produce the metal and/or metal oxide porous material; and

optionally repeating steps (i)-(iii) with the same metal salt or with a different metal salt.

9. The method of claim 8, wherein the metal salt comprises a metal selected from the group consisting of Li, Be, Na, Mg, Al, K, Ca, Sc, Ti, V, Cr, Fe, Cu, Ga, Rb, Sr, Y, Zr, Nb, Mo, Tc, Ru, Rh, Pd, Cd, In, Sb, Cs, Ba, La, Ce, Pr, Nd, Pm, Sm, Eu, Gd, Tb, Dy, Ho, Er, Tm, Yb, Lu, Hf, Ta, W, Re, Os, Ir, Pt, Au, Tl, Pb, and Bi.

10. The method of claim 8, wherein the metal salt comprises a metal selected from the group consisting of Ni, Co, Mn, Ag, Zn, and Sn.

11. The method of claim 8, wherein the composition comprising the metal salt is a neat metal salt or a metal salt hydrate.

12. The method of claim 8, wherein the composition comprising the metal salt further comprises a solvent.

13. The method of claim 12, wherein the solvent is water.

14. The method of claim 12, wherein the solvent is an aqueous alcohol, aqueous polyol, aqueous carboxylic acid, aqueous ester, or aqueous aldehyde.

15. The method of claim 12, wherein the ratio of metal salt to solvent in the composition is from 1:10 to 10:1.

16. The method of claim 8, wherein the composition comprising the metal salt comprises a metal nitrate hydrate or an aqueous metal nitrate.

17. The method of claim 8, wherein the porous template is monolithic or particulate.

18. The method of claim 8, wherein the porous template comprises a composite of one or more of silica, carbon, metal, or metal oxide.

19. The method of claim 8, wherein the porous template comprises silica.

20. The method of claim 8, wherein the porous template comprises macropores having a diameter of from greater than about 0.1 μm in diameter and mesopores having a diameter of from about 2 nm to about 30 nm.

21. The method of claim 8, wherein the reducing agent comprises hydrogen gas, alcohol, polyol, carboxylic acid, aldehyde, hydrazine, hydride, ketone, or borane.

22. The method of claim 8, further comprising removing the porous template.

23. The method of claim 22, wherein the porous template comprises silica and the silica is removed by immersing the porous material from step (iii) in an aqueous hydroxide solution at from about 25 °C to about 110 °C.

24. The method of claim 22, wherein the porous template comprises silica and the silica is removed by immersing the porous material from step (iii) in hydrofluoric acid.

25. The method of claim 22, wherein the porous template comprises silica and the silica is removed by immersing the porous material from step (iii) in a solution of basic alcohol.

26. The method of claim 8, further comprising adding an additional metal to the metal and/or metal oxide porous material by electrodeposition, by electroless deposition, or by displacement deposition.

ABSTRACT

Disclosed are methods for producing carbon, metal and/or metal oxide porous materials that have precisely controlled structures on the nanometer and micrometer scales. The methods involve the single or repeated infiltration of porous templates with metal salts at controlled temperatures, the controlled drying and decomposition of the metal salts under reducing conditions, and optionally the removal of the template. The carbon porous materials are involve the infiltration of a carbon precursor into a porous template, followed
by polymerization and pyrolysis. These porous materials have utility in separations, catalysis, among others.

FIGURE 1

(a)

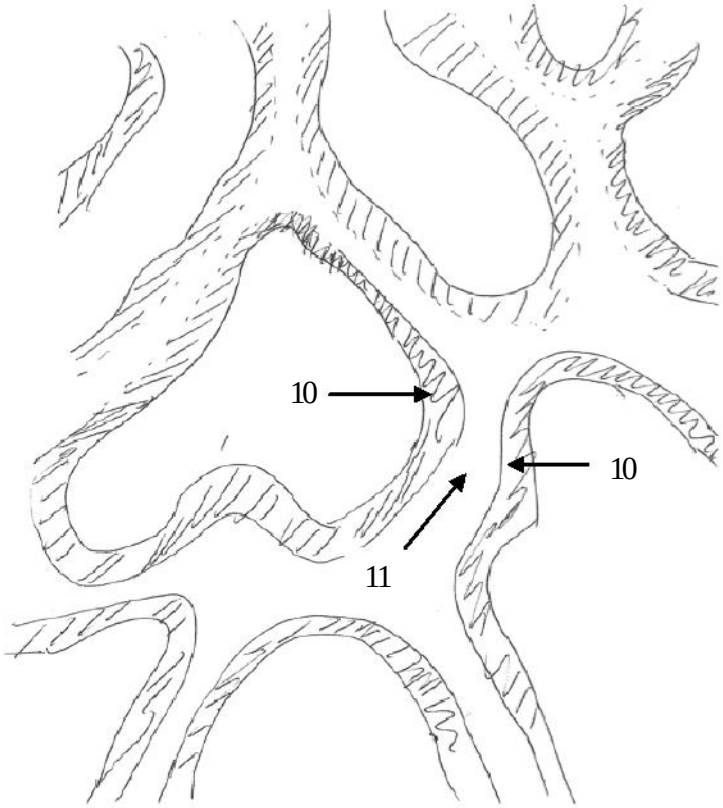

(b)

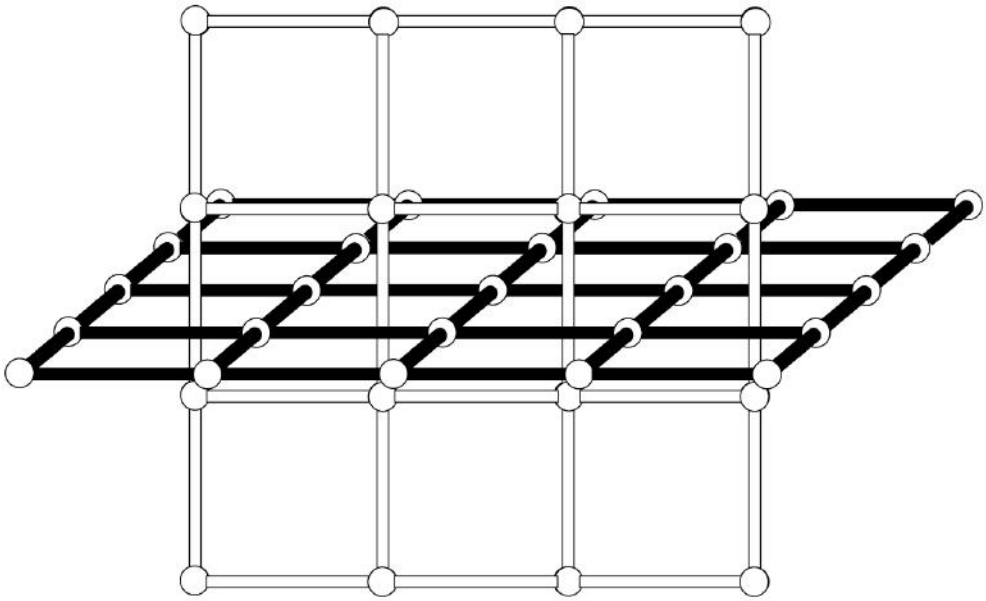

FIGURE 2

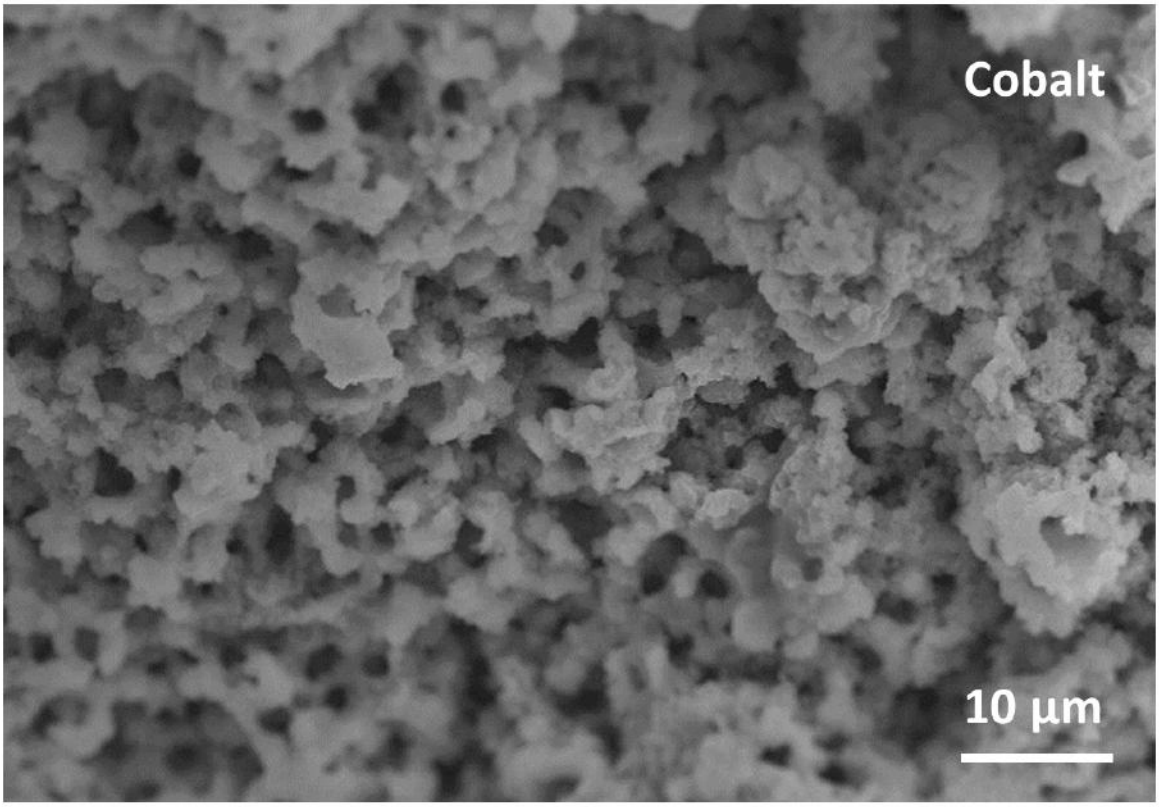

FIGURE 3

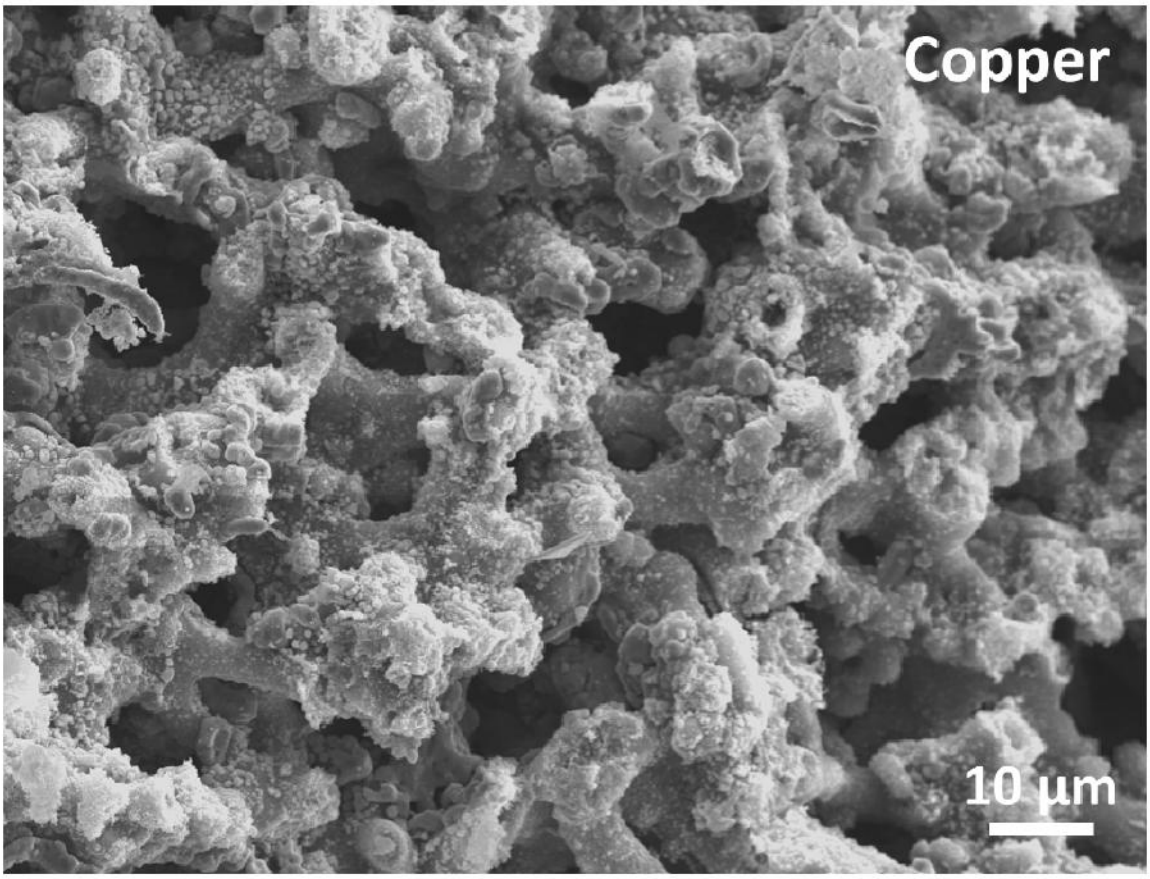

FIGURE 4

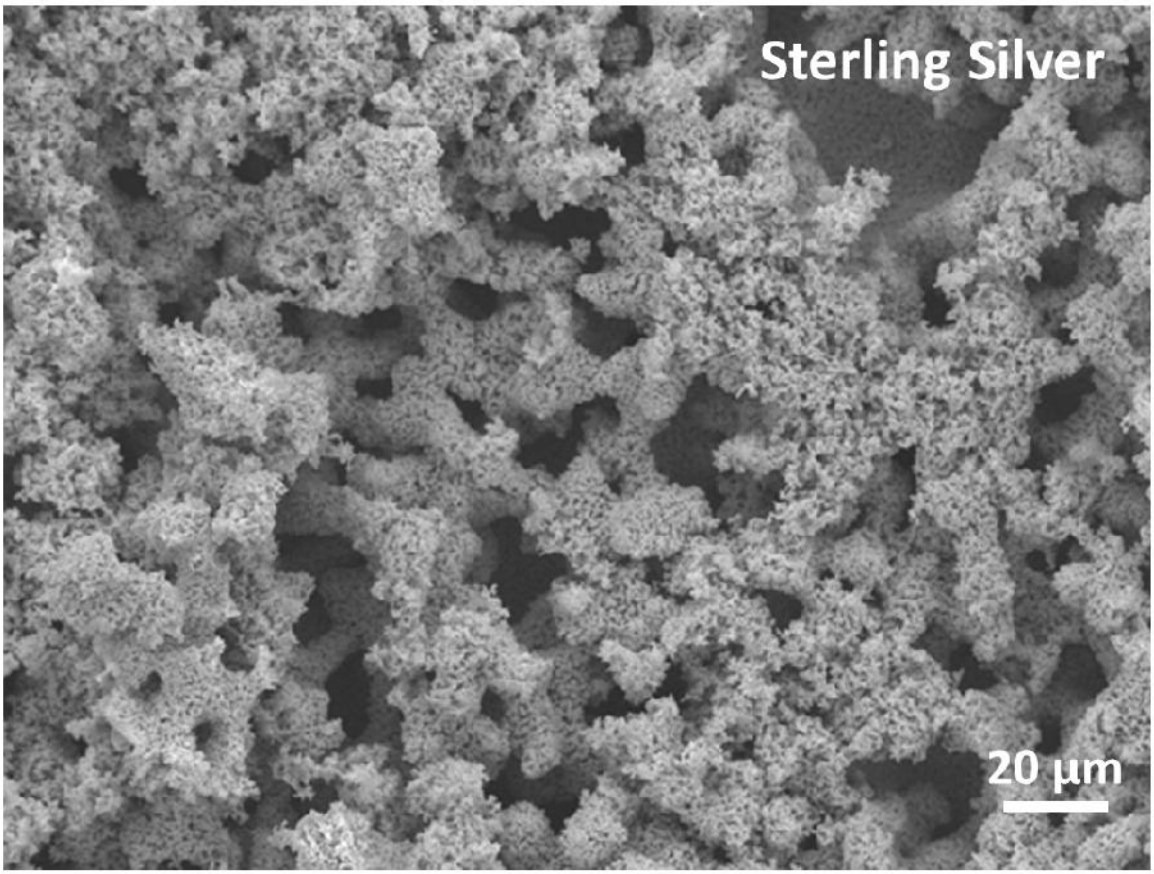

FIGURE 5

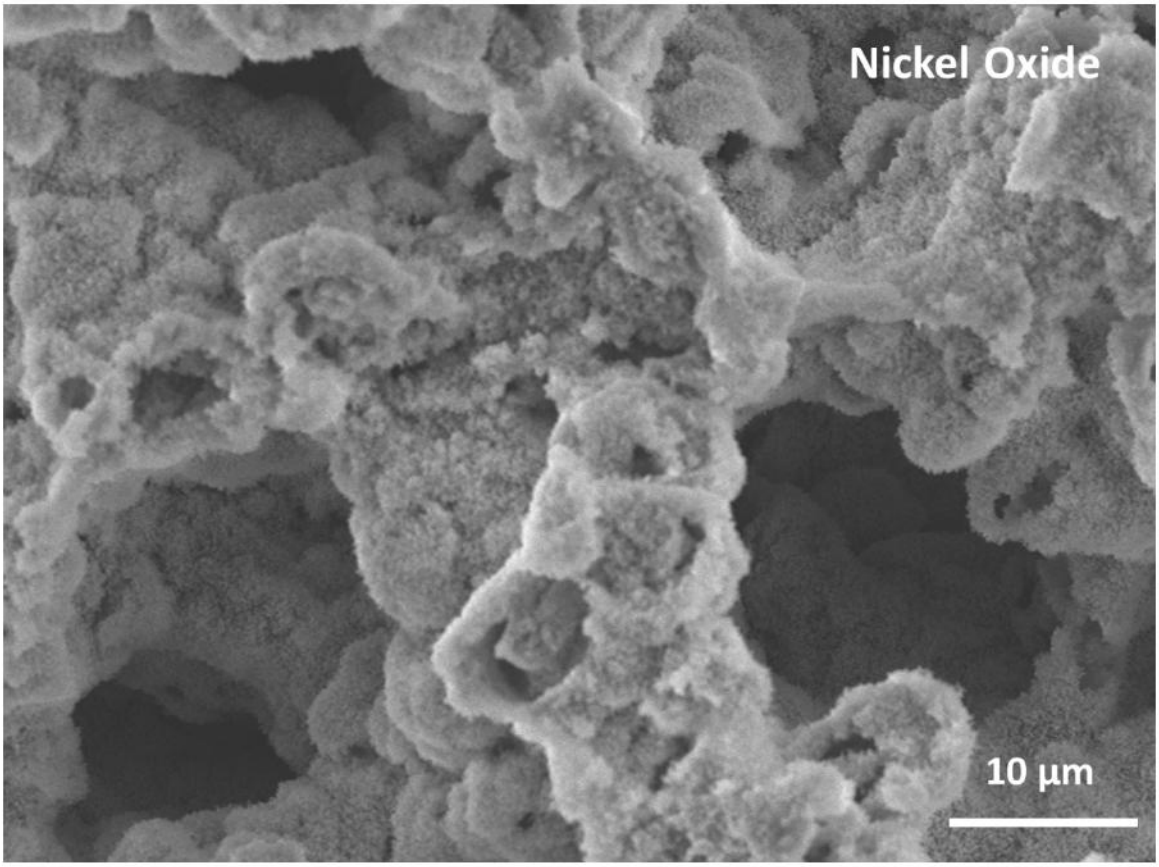

FIGURE 6

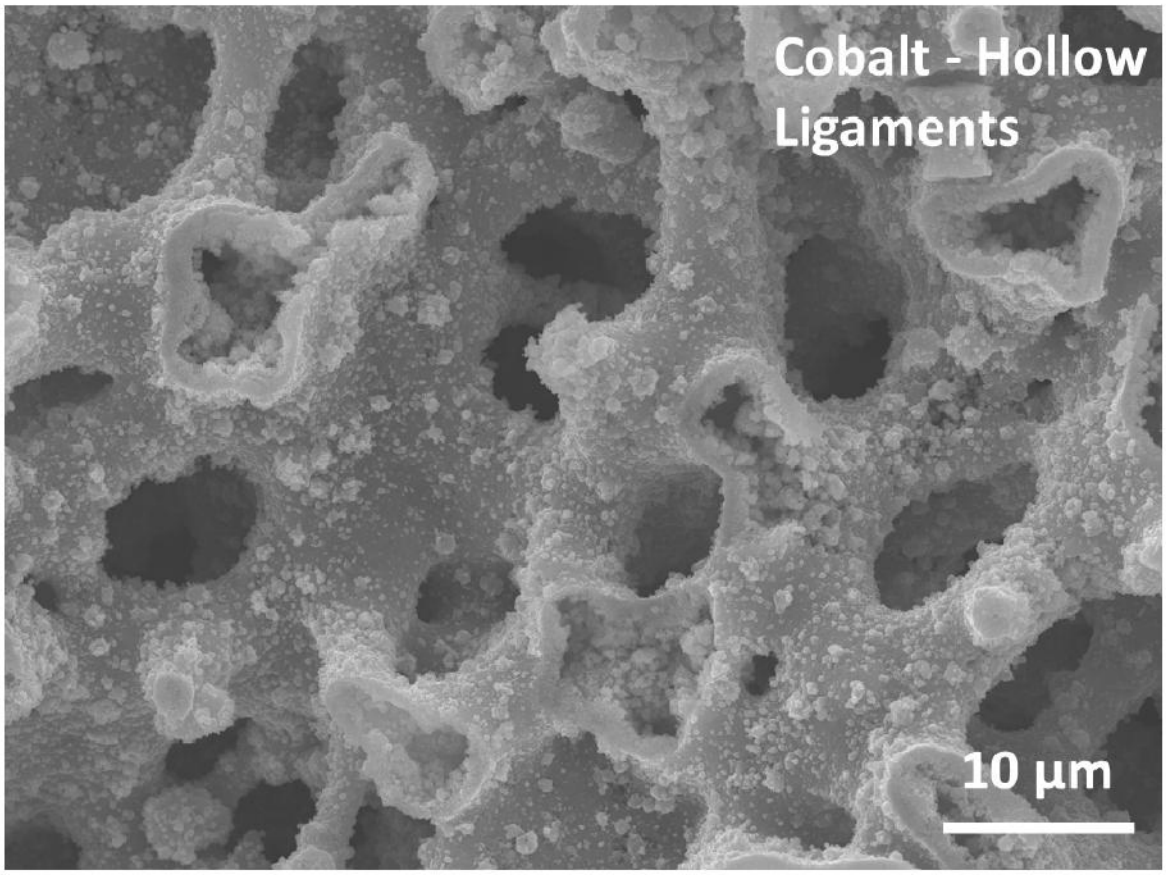

FIGURE 7

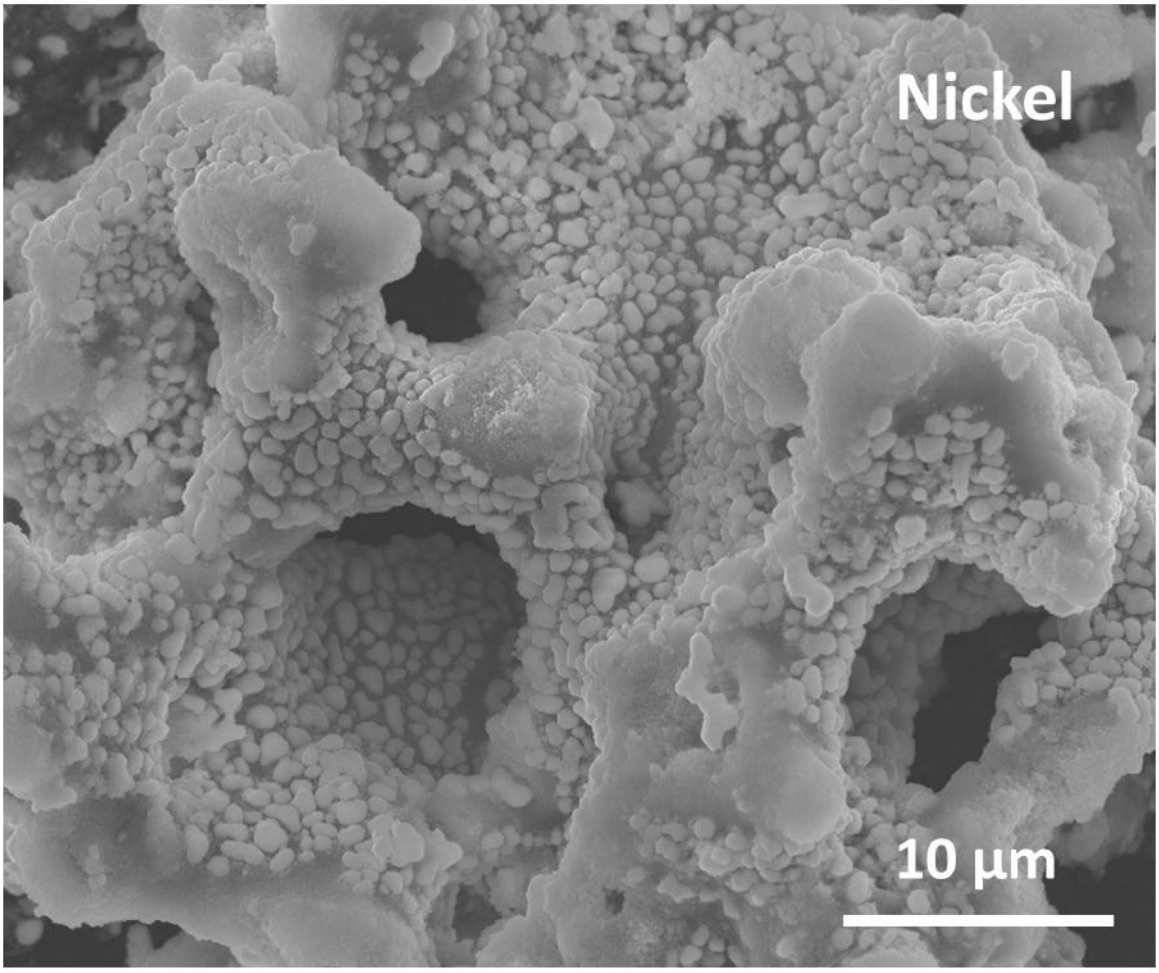

FIGURE 8

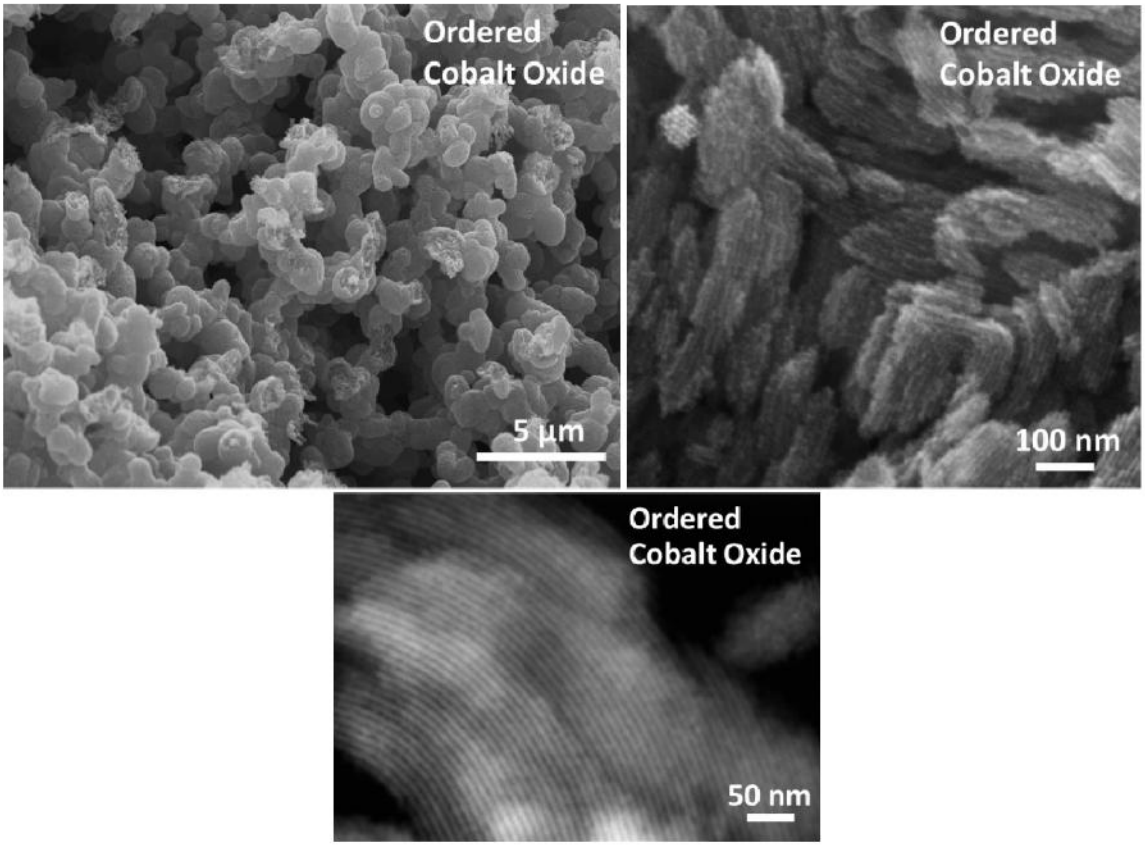
Ordered
Cobalt Oxide
5 µm
Ordered
Cobalt Oxide
100 nm
Ordered
Cobalt Oxide
50 nm